



**University of
Nottingham**

UK | CHINA | MALAYSIA

**Design, Preparation and Mechanism Study
of Lightweight Composite Materials for
Integration of Sound Absorption and
Structural Bearing**

By

Chenhao Dong

A Thesis Submitted to the University of Nottingham Ningbo China for the

Degree of

Doctor of Philosophy

Abstract

With the development of society, on the one hand, industrial and traffic noise pollution has become a serious problem, and on the other hand, people's demands for a high-quality living environment are also increasing. Thus, the issue of noise pollution, which significantly impacts life quality, is receiving increasing attention from researchers around the world. Recent advancements have seen sound absorption materials evolve from basic porous materials and micro perforated plates to sophisticated acoustic metamaterials, exhibiting progressively superior performance. However, these materials typically lack the desired combination of sound absorption performance and strength, as sound absorption capacity and mechanical robustness are often inversely related.

Therefore, this study first improved the micro perforated plate-honeycomb structure, utilizing the principle of hierarchical pore structure to greatly enhance sound absorption ability in the low frequency range without significantly changing the weight of the structure. Subsequently, a folded structure made of woven fabric composites was designed using the concept of origami. The results showed that the folded structure can maintain the sound absorption coefficient over 0.4 in the range of 400-6300 Hz, realizing broadband sound absorption. Finally, membrane metamaterials was combined with the folded structure to achieve the lightweight, high-strength, and high-efficiency sound absorption ability. The finite element model and theoretical model were established to analyze the sound absorption mechanisms of the structures. This research provides the theoretical basis and design ideas for lightweight and high-strength sound absorption composite materials. The resulting structure is not only functionally effective but also simple and easy to manufacture, indicating significant potential for engineering applications and scientific advancement.

Keywords: Sound absorption, multi-functional materials, composites materials.

Table of Contents

Design, Preparation and Mechanism Study of Lightweight Composite Materials for Integration of Sound Absorption and Structural Bearing	i
Abstract	ii
Table of Contents.....	iii
List of Figures	v
List of Tables	viii
Acknowledgment.....	ix
Abbreviations	x
Chapter 1 Introduction	1
1.1 Background	1
1.2 Motivations of the Research.....	2
1.3 Aims and Objectives.....	4
1.4 Thesis Outline.....	6
Chapter 2 Literature review	8
2.1 The Research about Sound Absorption Materials.....	8
2.2.1 Porous materials.....	9
2.2.2 Micro perforated plate structure	13
2.2.3 Acoustics metamaterials	15
2.2.4 The combination sound absorption structure	19
2.2 The Research about the Integration of Sound Absorption and Structural Bearing.....	21
2.2.1 The improvement of micro perforated plate structure	22
2.2.2 Metal foam.....	25
Chapter 3 Sound Absorption Performance of a Micro Perforated Sandwich Panel with Honeycomb-hierarchical Pore Structure Core.....	29
3.1 Experiment	29
3.1.1 Preparation.....	29
3.1.2 Sound absorption performance test.....	32
3.2 Analytical Model	37
3.2.1 Analytical model of micro perforated panel	40
3.2.2 Analytical model of the double porosity materials	41
3.2.3 Results of analytical modelling.....	44
3.3 Finite Element Analysis (FEA).....	46
3.3.1 Finite element model	46
3.3.2 Results of FEA	49
3.4 The Influence of the Parameters	52
3.5 Conclusion.....	54
Chapter 4 Sound Absorption Performance of Folded Structures Prepared from Woven Prepreg and Porous Materials Composites.....	56
4.1 Experiment	57
4.1.1 Materials and fabrication	57
4.1.2 Sound absorption test system.....	62
4.1.3 Experimental results	63

4.2 Theoretical Model.....	65
4.3 Parametric Investigation of Sound Absorption Performance	72
4.4 Conclusion.....	76
Chapter 5 A Novel Membrane-coupled Foldable Structure with Low Frequency Sound Absorption and Vibration Isolation Performance	79
5.1 Materials and Methods	81
5.1.1 <i>Materials</i>	81
5.1.2 <i>CAD models and 3D printing</i>	82
5.1.3 <i>Mechanical testing</i>	83
5.1.4 <i>Sound absorption testing</i>	84
5.1.5 <i>Vibration isolation testing</i>	84
5.1.6 <i>Finite element modeling</i>	85
5.2 Results and Discussion	86
5.2.1 <i>Sound absorption performance</i>	86
5.2.2 <i>Vibration isolation test results</i>	91
5.2.3 <i>Mechanical performance</i>	93
5.3 Conclusion.....	100
Chapter 6 Overall Summary of the Thesis and Future Plan	103
6.1 The Summary of the Research.....	103
6.2 Future Works	106
Appendix A The Matlab Program for the Theoretical Model in Chapter 3	109
Appendix B The Matlab Program for the Theoretical Model in Chapter 4.....	112
Appendix C The Publications During the PhD Period	116
Reference.....	117

List of Figures

Fig. 1.1 The logical framework of the thesis	6
Fig. 2.1 Schematic of the sound energy conversion in materials.....	8
Fig. 2.2 (a) Typical micro perforated plate structure and (b) its equivalent circuit [62]. (Here p is the air pressure, ρ is the density of the air, c is the velocity of the air, R is the acoustic impedance of the micro perforated plate, M is the acoustic mass of micro perforated plate and Z_D is the specific impedance of the cavity.	15
Fig. 2.3 Active AMs sound absorption system: (a) electrically driven laminated active acoustic metamaterials with PVC plasticization[89], (b) helical acoustic meta surface capable of providing a modulated sound-reflected wavefront and a continuously tunable broadband feature [92], (c) acoustic metamaterials by active control of the dynamic density [97], (d) Tunable broadband multi-function acoustic meta surface by nested resonant rings [95].....	17
Fig. 2.4 Typical acoustics metamaterials: (a) membrane acoustics metamaterials [83], (b) meta-porous materials [107], (c) space-coiling fractal acoustic metamaterials [112], (d) classical space-coiling acoustic metamaterials [110], (e) Helmholtz resonators AMs with various depth cavities [116].....	19
Fig. 2.5 The improvement of micro perforated plate structure: (a) multi-layer helmholtz resonators with extended necks [140], (b) Adjustable sound absorption frequency honeycomb-MPP structure [150], (c) Compact multifunctional meta-structure and geometric topology of the single sound-absorbing component [151], (d) An absorptive barrier comprised of a micro-perforated membrane facing and a corrugated Miura-ori sheet [152].....	24
Fig. 2.6 Common metal foams: (a) A opened-cell aluminum foam cylindrical specimen [172], (b) A closed-cell aluminum foam cylindrical specimen [173].	26
Fig. 3.1 3d models of: (a) the honeycomb panel with hierarchical pore structure, and (b) the details for a single cell within this structure.....	30
Fig. 3.2 Dimensions of the structure: (a) top face sheet (b) honeycomb.	31
Fig. 3.3 The preparation of carbonized cotton: (a) tube furnace (b) carbonized cotton.	31
Fig. 3.4 Preparation of specimens with a hierarchical pore structure.	32
Fig. 3.5 Impedance tube testing system.....	33
Fig. 3.6 The principle of impedance tube test.	34
Fig. 3.7 Sound absorption performance test results of all samples. The shadow around the curves shows the standard deviation from the mean of three samples.	35
Fig. 3.8 Comparison of average sound absorption coefficients across existing literature.	36
Fig. 3.9. 2D model of the sound absorbing honeycomb.....	39
Fig. 3.10 Process of sound wave propagation through the sound absorbing structure.	39
Fig. 3.11 Honeycomb structure decomposition for 2D modeling.	39
Fig. 3.12 The results of analytical modeling compared with experimental data for the carbon cotton and hierarchical pore structures.	45
Fig. 3.13 The structure of a single cell within an impedance tube.	47

Fig. 3.14 Load application and meshing method of the FEA model	48
Fig. 3.15 Average carbonized cotton diameter measured using SEM.	49
Fig. 3.16 The pressure (Pa) distribution of micro perforated sandwich panel with honeycomb-hierarchical pore structure (6000 Hz).	51
Fig. 3.17 Comparison of FEA and experimental sound absorption results for the two different structures.	51
Fig. 3.18 Comparison of FEA, analytical model, and experimental results for: (a) carbonized cotton, and (b) hierarchical pore structure.	52
Fig. 3.19 The influence of the parameters of the structure: (a) The height of the structure, (b) the Diameter of the hierarchical pore structure, (c) the Diameter of pores on the micro perforated plate, (d) the Perforation rate of the micro perforated plate, (e) Thickness of the micro perforated plate and (f) the type of the porous materials (Porosity).	52
Fig. 4.1: Woven ramie prepreg:(a) Vertical view;(b) Front view;(c) Microscopic view.	58
Fig. 4.2 Hot-press machine.....	59
Fig. 4.3: Composite materials:(a) Vertical view and microscopic view (b) Front view and microscopic view.	59
Fig. 4.4: 3D-models of: (a) the folded structure and; (b) the geometric parameters of the folded structure unit cell.	61
Fig. 4.5: Folded structure samples for sound absorption tests: (a) at low frequency, (b) at high frequency, (c) 3D model of low frequency sample, (d) 3D model of high frequency sample.....	62
Fig. 4.6: Sound absorption test system.	63
Fig. 4.7: The influence of different materials and structures on sound absorption ability: (a) sound absorption coefficient curves, and (b) experimental setup.	64
Fig. 4.8: Extracting the minimum unit cell of the structure.....	66
Fig. 4.9 The sketch of different structures: (a) Helmholtz resonance (b) Micro perforated plate structure with a flat plate (c) Micro perforated plate structure with an inclined plate.....	66
Fig. 4.10: The simplified model of the folded structure: (a) Minimum cell of the folded structure, (b) The equivalent model of the folded structure.....	67
Fig. 4.11: Analytical diagram of the equivalent model for the folded structure.	70
Fig. 4.12: The theoretical model and experimental results of the folded structure.....	72
Fig. 4.13: The theoretical model and experimental results of the composite materials.	72
Fig. 4.14: The influence of the thickness of composite materials in folded structure on: (a) Sound absorption coefficient, and (b) The specific acoustic impedance (resistance, R_e , and reactance, I_m).	74
Fig. 4.15: The influence of the height of the whole structure on: (a) Sound absorption coefficient, and (b) The specific acoustic impedance (resistance, R_e , and reactance, I_m).	75
Fig. 4.16: The influence of the inner cavity height in folded structure on: (a) Sound absorption coefficient, and (b) The specific acoustic impedance (resistance, R_e ,	

and reactance, lm).....	76
Fig. 5.1 The drying box	82
Fig. 5.2 Schematics of the foldable structure: (a) CAD model with dimensions and (b) the sample fabrication process.....	83
Fig. 5.3 FE model of the (a) impedance tube, (b) sound absorption structure, and (c) foldable frame structure.....	86
Fig. 5.4 The sound absorption coefficient of the foldable structure with different mass block diameters. The shadow around the curves shows the standard deviation from the mean of three samples.	89
Fig. 5.5 The sound absorption coefficient curve of the foldable structure with 6mm mass block diameters. The red arrows show the positions of the sound absorption peak frequencies predicted by the finite element model.....	90
Fig. 5.6 The sound absorption coefficient curve of the foldable structure with 8mm mass block diameters. The red arrows show the positions of the sound absorption peak frequencies predicted by the finite element model.....	90
Fig. 5.7 The sound absorption coefficient curve of the foldable structure with 10mm mass block diameters. The red arrows show the positions of the sound absorption peak frequencies predicted by the finite element model.....	91
Fig. 5.8 The strain of the membrane in foldable structure with 8mm mass block (a)All membranes (b) One membrane.....	91
Fig. 5.9 Vibration isolation test: The testing sample of the (a) PLA foldable metamaterials and (b) honeycomb structure, along with the (c) transmissibility of both structures.	93
Fig. 5.10 Samples for mechanical testing: (a) Foldable structure (b) Honeycomb structure.	94
Fig. 5.11 The Compression testing of the foldable structures with several cells.....	95
Fig. 5.12 Compression testing of the honeycomb and foldable structures: Images from the beginning (a) and end (b) of testing, along with the load-displacement curves of honeycomb and foldable structures (One group).	96
Fig. 5.13 Mechanical testing sample of Al sample: (a) Frame structure before assembly (b) Foldable structure	97
Fig. 5.14 Mechanical testing sample of CFRP sample: (a) Frame structure before assembly (b) Foldable structure.....	98
Fig. 5.15 Compressing testing results (One sample).	99
Fig. 5.16 Ashby charts displaying the properties of compression strength and density in this work and some latest references[233-244], reprinted from [232].....	100
Fig. 6.1 The characteristics of three works.....	104

List of Tables

Table 3.1: Parameters of theoretical models to predict the sound absorption coefficient of the different structures.....	45
Table 4.1: Geometric parameters of the folded structure unit cell.....	61
Table 4.2: Relevant parameters of the theoretical model.....	71
Table 5.1 Compression properties of honeycomb structure and foldable structure....	99

Acknowledgment

Over the course of my PhD study and writing of this thesis, I would like to express my thanks to all those people who have helped me.

First, I would like to thank my principal supervisor Prof. Xiaosu Yi. Prof. Yi is a person with profound knowledge and the desire for discovery. Although working on a very busy schedule, he still answers my questions promptly and gives me generous support and guidance. It is my honor to follow him and complete this research, I believe his personality and calm attitude towards difficulties will be treasured throughout my whole life.

I also want to thank my supervisors Prof. Xiaoling Liu, Prof. Jian Yang, Dr. Robert Pierce, and internal reviewer Prof. Halim. They have provided me with kind and rigorous mentoring and proposed important comments about this research.

And my warm gratitude also goes to my friends and colleagues. Thanks to Zhao Liu and Jiafei Gu for their help with my experiments and papers. Thanks to Sicong Yu, Dongyuan Hu, Minqiang Jiang, Lu Tong, Xiaoye Cong, Saihua Li, and Xin Wang for their care for me. I also thank Zhiyuan Chen, Liyue Zhang, and Minghui Wu for their companionship on the path of the PhD. I would like to thank all the people who help me, care about me, and support me. I really wish them all the best in the future.

Lastly, I want to express my appreciation to my wife Yujie Yao, and my parents. Thanks for their patience in listening to my complaints and helping me manage the pressure. They have given me much encouragement at every moment I feel lost and confused. They give me a haven that I can forever return.

Abbreviations

AMs: Acoustic Metamaterials

CFRP: Carbon Fiber Reinforced Plastics

FEA: Finite Element Analysis

FSI: Fluid-Structure Interaction

JCA: Johnson-Chamoux-Allard

MWCNTs: Multi-Walled Carbon Nanotubes

MAM: Membrane Acoustics Metamaterials

MRS: Magnetic Resonance Imaging

MPP: Micro Perforated Plate

PEO: Plasma Electrolytic Oxidation

PLA: Poly Lactic Acid

UTM: Universal Testing Machine

Chapter 1 Introduction

1.1 Background

With the rapid development of society and technology, noise pollution has become one of the leading environmental risk factors for health in the world. A study based on disease data in Europe by the World Health Organization showed that traffic noise is associated with 600-1200 disability-adjusted life years per one million people, which is the second highest environmental risk [1]. For China, the Ministry of Ecology and Environment of the People's Republic of China issued the annual report on the prevention and control of noise pollution in China in 2022. The report counted the 45,000 environmental complaints in 2021, the noise issues accounted for 45% of all complaints [2].

In physics, noise is defined as the sound wave generated by random vibrations of any matter. However, because noise is more a subjective assessment than an objective fact, we usually define any unwanted sound including unpleasant, loud, or disruptive to hearing as noise [3]. Noise not only hurts quality of life and working efficiency but also will truly harm human health. Extensive research has proved that transportation noise can lead to negative health effects in adults and children including blood pressure changes, ischemic heart disease risk, sleep disturbance, hearing loss, and so on [4-9]. At present, unaddressed hearing loss is the third largest cause of disability globally. It is mentioned in the World Report on Hearing that nearly 1 in 4 people are expected

to have hearing problems in 2050 [10], where noise pollution is one of the main causes of hearing loss. In view of this, noise suppression has attracted wide attention to satisfy the demand for health and high quality of life.

Normally, there are three main methods to control the noise: controlling the noise source, noise reduction at the transmission path, and protection at the receiver end. Controlling the noise needs to give a specific design for each noise source, for instance, changing the process method, adjusting the working hours, etc. The protection at the receiver usually refers to the use of earmuffs or earplugs to reduce the noise. It can be found that these two methods are not general enough, thus this research concentrates on the second method which is mainly achieved by sound absorption materials.

1.2 Motivations of the Research

With the development of society, on the one hand, industrial and traffic noise pollution is becoming a serious problem, and on the other hand, people's requirements for the high quality of their living environment are also increasing. Therefore, the issue of noise pollution, which is closely related to the quality of life, is receiving increasing attention from researchers around the world. Meanwhile, the sound absorption ability and mechanical strength of materials are often a pair of contradictory physical quantities. At present, sound-absorbing materials generally lack the mechanical characteristics of lightweight and high-strength. However, in addition to the demand for the sound absorption performance of sound absorbing materials, their mechanical properties and

weight are also factors that cannot be ignored in practical applications. For example, a lightweight, high-strength sound-absorbing material can achieve energy conservation and emission reduction more easily in the design process of cars, airplanes, or walls. The motivation of this research is based on the desire for energy-saving and emission reduction, the study hopes to solve this problem and prepare a novel structure that can achieve sound absorption, high strength, and lightweight at the same time.

At present, there are three main methods in sound absorption: micro perforated plate, porous materials, and acoustic metamaterials. Although each method can achieve the aim of this study, different methods have their advantages and disadvantages (as shown in Table 1.1), therefore, to show the potential of different kinds of methods in multifunctional sound absorption materials, this thesis uses different kinds of methods to achieve lightweight and load-bearing sound absorption materials.

In this study, the combination design strategy is the core idea and the core issue lies in how to make trade-offs and how to combine them more harmoniously together. Chapter 3 selects a micro perforated plate, and porous materials as the acoustic part and chooses a honeycomb structure as the structural part, the results show an excellent sound absorption ability but the diverse elements also make the structure appear overly complex. Chapter 4 only combined micro perforated plate and porous materials, trying to use micro perforated plate acts as a structural component. At last, the simple structure can

absorb sound effectively but the overly thin micro perforated plate cannot bear the load-bearing responsibility. Chapter 5 abandons the idea of using a micro perforated plate for load-bearing, opting instead to directly use a solid frame for support. At the same time, it utilizes membrane acoustic metamaterials in the gaps of the frame for sound absorption. Although the structure is slightly more complex compared to the previous chapters, it effectively achieves the initial goals set for this research.

Table 1.1 Advantages and disadvantages of different design strategies

Design strategy	Advantages	Disadvantages
Micro perforated plate	Simple manufacturing; strong design ability; good sound absorption performance at resonance frequency	Narrow sound absorption frequency
Porous materials	Simple manufacturing; broadband sound absorption; good sound absorption performance at high frequency	Limited designability; bad sound absorption in low frequency
Acoustic metamaterials	Low frequency sound absorption with thin thickness	Complex manufacturing
Combination method	Combination of advantages of different design strategies	Complex manufacturing

This research provides the theoretical basis and design ideas for lightweight and high strength sound absorption composite materials. At the same time, the structure also has the characteristics of simple structure and easy processing, which shows good engineering application value and scientific significance.

1.3 Aims and Objectives

It can be found that there are three core issues in different sound absorption methods: broadband sound absorption, low-frequency sound absorption, and

simple manufacturing. Therefore, this research focuses on these three parts, using porous materials to enhance the broadband sound absorption ability of MPP, and hierarchical pore structure to improve the low frequency sound absorption of porous materials. Although each of these design strategies has been studied before, it is still not clear the mechanism between them and how to use them to manufacture a sound absorption structure effectively. Meanwhile, a honeycomb structure is a common method to achieve load-bearing in sound absorption structure because of its high strength and lightweight. However, the honeycomb structure also caused complex manufacturing when researchers hoped to improve it to achieve better acoustic performance as it occupied the most volume with a limited contribution to sound absorption. Therefore, this research designed a folded structure with membrane acoustic metamaterials to achieve load-bearing, lightweight, and simple manufacturing.

Because the MPP-honeycomb structure is one of the most common sound absorption structures, the primary aim of this research is to use the MPP-honeycomb structure as a comparison, develop a structure or a material that can achieve sound absorption, high-strength and lightweight at the same time. Based on this, this thesis also seeks the mechanism of the sound absorption materials to optimize the sound absorption materials. In addition, this study also intends to demonstrate the application potential of the structures.

To achieve these aims, the following objectives have been set:

- (1) Optimize the typical MPP-honeycomb sound absorption materials to

obtain a better sound absorption ability.

(2) Design the novel folded sound absorption structures to achieve simple manufacturing, lightweight, and load-bearing.

(3) Establish the theoretical model of the structures.

(4) Establish the Finite element analysis (FEA) model of the structures.

(5) Characterize the sound absorption structures.

1.4 Thesis Outline

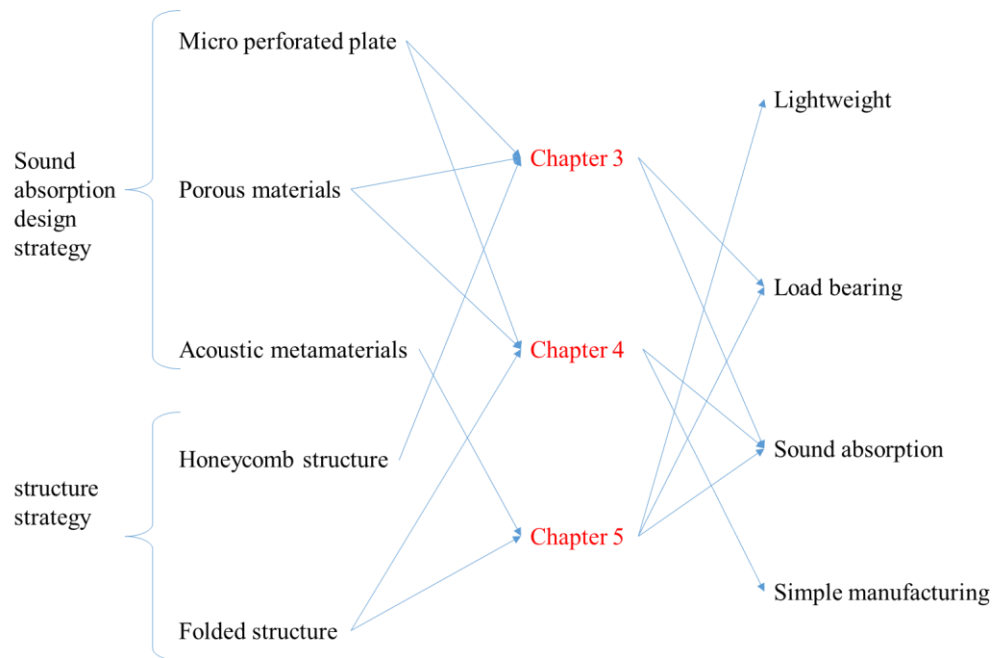


Fig. 1.1 The logical framework of the thesis

Chapter 2 showed the recent studies' development and the current status of research in sound absorption materials and integration of sound absorption and structural bearing.

Chapter 3 proposed a new micro perforated sandwich panel with a honeycomb-hierarchical pore structure core in this study. Carbonized cotton with a hierarchical pore structure is combined with a micro perforated honeycomb

core sandwich panel, which enhances the sound-absorbing performance of the structure without significantly increasing its weight.

Chapter 4 designed and fabricated a composite material composed of a woven prepreg and ventilated felt designed and prepared in the form of a folded structure to obtain excellent sound absorption performance. Absorption experiments of the woven prepreg, composite materials, and folded structure are carried out respectively.

Chapter 5 redesigned the structure in Chapter 3, and presented a membrane-coupled foldable structure that incorporates mass blocks for resonant damping. The sound absorption, compressive strength, and vibration control properties have been studied.

Chapter 6 summarizes the research findings and considers possible future research based on this thesis.

Chapter 2 Literature Review

2.1 The Research about Sound Absorption Materials

Once the sound wave comes into a material, the energy of the incident sound wave will convert into three types of energy: reflection sound energy, absorption sound energy, and transmission sound energy (As shown in Fig. 2.1). The sound absorption is defined as the loss of sound energy in the process of the sound wave contact with a material. The method of sound absorption is increasing the absorbed energy in the process of propagation.

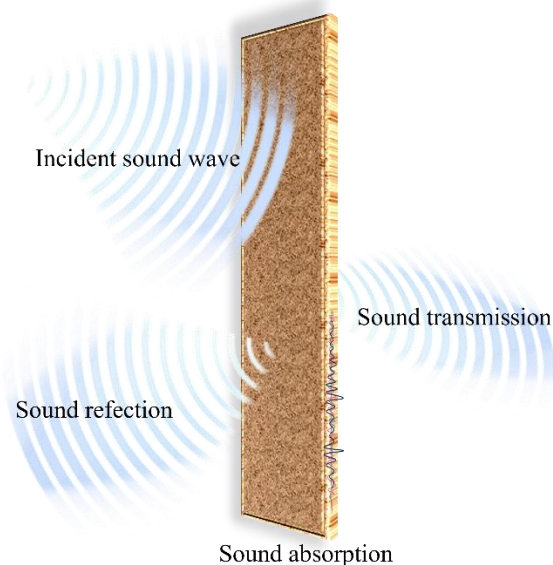


Fig. 2.1 Schematic of the sound energy conversion in materials

The sound absorption coefficient is the ratio of the absorption sound energy and incident sound wave energy. Impedance tube and reverberant room are two main ways of testing the sound absorption coefficient for sound absorption materials. In general, an impedance tube is used for small and regular samples, and a reverberant room is used for large and irregular samples. Besides, the

impedance tube can only measure normal incidence sound absorption coefficient while the reverberant room can test with a diffuse sound field [11-13]. Although reverberant room measurement is closer to many practical applications, impedance tube measurement is more common in the laboratory as it is convenient and lower costs.

In general, the average sound absorption coefficient in 125 Hz, 250 Hz, 500 Hz, 1000 Hz, 2000 Hz, and 4000 Hz can represent the average sound absorption coefficient for a material [3]. The sound absorption materials means the average sound absorption coefficient of the materials can exceed 0.2. However, this definition isn't available for the materials that is designed for specific frequency sound absorption. The method of sound absorption is increasing the absorbed energy in the process of propagation. The sound absorption mechanism can be mainly divided into two parts. One is the friction between the sound wave and the materials can transform the sound power into internal energy, the other is the resonance between materials and the sound wave consumes the sound power. At present, there are four main design strategies for sound absorption materials: porous materials, micro perforated plate structure, acoustics metamaterials, and the combination sound absorption structure.

2.2.1 Porous materials

Using porous materials (such as glass wool [14], mineral wool [15], and rock wool [16]) is a common way to achieve sound absorption by using friction between materials and sound waves. Porous materials have a large number of

tiny, interconnected pores inside the materials, which means sound can penetrate into the materials along these pores. This process will transform sound energy into heat energy by friction. Therefore, friction is the main sound absorption mechanism for porous materials. Previous research on porous materials can be roughly divided into two directions: the first direction is foam porous materials [17-19] and fiber porous materials [20-22].

Foam is the most common porous materials because it can adjust internal pore structure by changing the chemical composition or optimizing formulation. Generally, changing the type and ratio of matrix materials, foaming agents, surfactants, and catalyzers is the main method to obtain excellent sound absorption performance. Hosseinpour et al. [23] filled multi-walled carbon nanotubes (MWCNTs) into ethylene-propylene-diene-monomer rubber to fabricate a novel elastomeric nanocomposite foam. The sound absorption ability of the foam with different MWCNTs content is compared to investigate the influence of the MWCNTs filler. The results showed that the sample with 0.1phr (parts per hundred rubber) MWCNTs has the best sound absorption coefficient. At present, the common sound absorption foam includes metallic foams [24-27], polyurethane foams [28-30], ceramic foams[31-33], Inorganic polymeric foam [34], et al. Besides, the combination of different fillers (e.g., kenaf fiber [35], wool fiber [16], inorganic filler [28], et al.) and matrix is also a common method to improve the sound absorption performance of foams. In this process, fillers can improve the flow resistance and tortuosity of the foams which means more

sound energy will be converted into internal energy during the sound wave transmission process.

Fiber porous materials refers to the sound absorption materials made by inorganic or organic fibers. Inorganic fibers (including metal fiber [36-38], glass wool [14], rock wool [39], et al.) are mainly applied to high temperature environments as they usually have high heat resistance. Organic fibers (including flax fiber [40], cotton [41], Wooden fiber [42], et al.) are widely used in building and decoration filed owing to the characteristics of low cost, renewable, and environmental protection [43]. Reprocessing these fibers to achieve better sound absorption performance is the main research method. Bhingare et al. [44] prepared porous materials with coconut shell fiber with different thicknesses and densities. The experiment results found the best sample and proved the porous materials has a good sound absorption ability.

Based on these research about porous materials, there are also some researchers who focus on the relationship between sound absorption performance and the parameter of porous materials to better understand and predict the sound absorption of porous materials [45-47]. Hirosawa et al. [48] considered the influence of fiber cross-section on the sound absorption performance of fiber porous materials by finite element analysis. Circular, elliptical, three arrows, and six arrows were studied in this research, and the sound absorption performance of materials with different cross-sections was evaluated by the Johnson-Chamoux-Allard (JCA) model. The results showed

that the sound absorption performance was related to fiber cross-sections, therefore changing the cross-section shape was a method to improve the sound absorption performance of materials.

However, porous materials can only absorb sound effectively when the thickness of porous materials exceeds $1/4$ of the wavelength, which means the porous materials often have poor sound absorption performance at low frequencies [3]. Compared with other noise, low frequency noise is notoriously difficult to reduce in many applications, such as dwellings, walls, and hearing protection [49-51]. While the commonly stated range of human hearing is 20 to 20,000 Hz, it cannot be ignored the low frequency noise. Evidently, this low frequency performance can be compensated by increasing the thickness of the porous materials [52], but such increases in thickness are not always feasible from a structure design perspective. To solve this problem, researchers have found that increasing the pore size of porous materials can have a beneficial effect on their sound absorption properties [53]. However, a uniform change in regular pore size has only limited benefits, instead, researchers have attempted to make the materials with apertures of different sizes to provide a more tortuous propagation path and larger influence range. Hence, the concept of a hierarchical pore structure was proposed [54-61]. Shen et al. [55] combined cellulose nanofiber and melamine foam in order to form a hierarchical porous fiber materials. Experimental testing showed the noise absorption performance of the new composite materials at 500 Hz to increase by 104%, and the noise reduction

coefficient to improve by 80%. Cai et al. [56] presented a type of carbonized cotton that has controllable hierarchical porosity to improve sound absorption performance over selective frequency ranges. According to their experimental results, the low-frequency sound absorption performance of the materials was improved significantly by this method.

2.2.2 Micro perforated plate structure

Micro perforated plate structure is composed of a micro perforated plate and an air cavity behind the plate (As shown in Fig. 2.2). Compared with porous materials, it uses the resonance between air in the cavity and sound wave to achieve sound absorption. The micro perforated is a perforated panel with perforations reduced to the submillimeter level so that the flow resistance itself will be enough to match the characteristic impedance of surrounding air to obtain a good sound absorption performance. Maa [62] first presented the theory of the micro perforated plate structure. Then, some research found that the sound absorption performance of variable cross-section perforated plates often had a better performance than that of straight holes. Wang et al. [63] proposed a multi-layer composite structure that could achieve effective sound absorption at medium and low frequencies by combining variable cross-section ethylene-propylene-diene monomer foams and perforated plates. The results showed that the structure could get the best sound absorption effect in 300-1300 Hz. Artificial fish swarm algorithm and improved particle swarm optimization were presented to optimize the structure parameters of the structure. Liu et al. [64] proposed a

sound absorption structure of perforated porous materials with variable cross-section backed with Helmholtz resonant cavity. Established the corresponding theoretical and finite element model and verified the model by experiment. The results showed that variable cross-section could improve the impedance match between the structure and air to enhance broadband sound.

Nowadays, micro perforated plate structure is a common structure in sound absorption structures design [65-70]. Meng et al. [71] experimentally and numerically studied the sound absorption ability of a corrugated sandwich panel with small perforations. The results showed that the structure with non-uniform perforations could achieve a lower resonance frequency and wider absorption frequency compared with uniform perforations. Furthermore, as the properties of the structure itself (i.e. strength, stiffness, and weight) are also important for acoustic structural design, honeycomb structures have always been of great research interest due to their lightweight and high strength [72-76]. In addition, Boccaccio et al. [77] combined a micro perforated plate and Archimedean-inspired spiral to obtain broadband sound absorption at low frequencies. Three optimized structures were designed to get sound absorption in different frequency ranges. The results showed that such structures can achieve 60% sound absorption from 400 Hz to 2800 Hz.

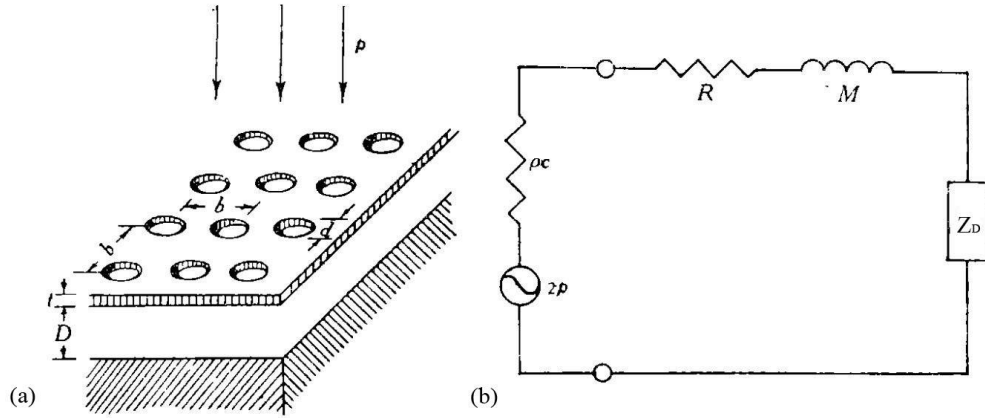


Fig. 2.2 (a) Typical micro perforated plate structure and (b) its equivalent circuit [62]. (Here p is the air pressure, ρ is the density of the air, c is the velocity of the air, R is the acoustic impedance of the micro perforated plate, M is the acoustic mass of micro perforated plate and Z_D is the specific impedance of the cavity.

2.2.3 Acoustics metamaterials

Acoustics metamaterials (AMs) is a kind of artificial material that contains sub-wavelength meta-atoms or microstructure units with periodic arrangement to achieve excellent acoustic performance that cannot be found in natural materials [78-82]. It has been proven to be an effective strategy in low-frequency noise absorption [83-87]. In general, the acoustic metamaterials can be divided into active AMs and passive AMs.

Active AMs generally refers to the AMs system consisting of components that can exchange energy with acoustic waves (e.g., extracting electrical energy or providing energy input). The effective frequency range can be adjusted by several methods, including external voltages [88, 89], temperature-control method [90], piezoelectric elements [91], mechanical deformation [92-95], and pressure [96], for multi-functional applications.

In general, active AMs can be divided into measure effective density and bulk modulus two types according to their implementation method. The adjustable effective density active AMs usually achieved through specific materials (most commonly, piezoelectric elements). The element can control sound absorption components by shunting with external electronic components. Akl et al. [97] developed a metamaterial cell with truly programmable dynamic density, the effective dynamic density of the cell is controlled by tuning the stiffness of the boundary piezoelectric elements (as shown in Fig. 2.3(d)). The experimental results showed that the dynamic density of incompressible fluid was controlled from 0.35 times to 13 times in different conditions. Meanwhile, the adjustable bulk modulus active AMs usually achieved in the same way as adjustable effective density active AMs. The specific materials (piezoelectric elements or temperature-sensitive materials) are connected to external control components with suitable control strategies to tune their effective bulk modulus. Xia et al. [90] controlled the negative effective bulk modulus of the AMs through the temperature of the water. The results indicated that the negative effective bulk modulus can be tuned about 11% while the temperature of the water is varied from 0 °C to 75 °C.

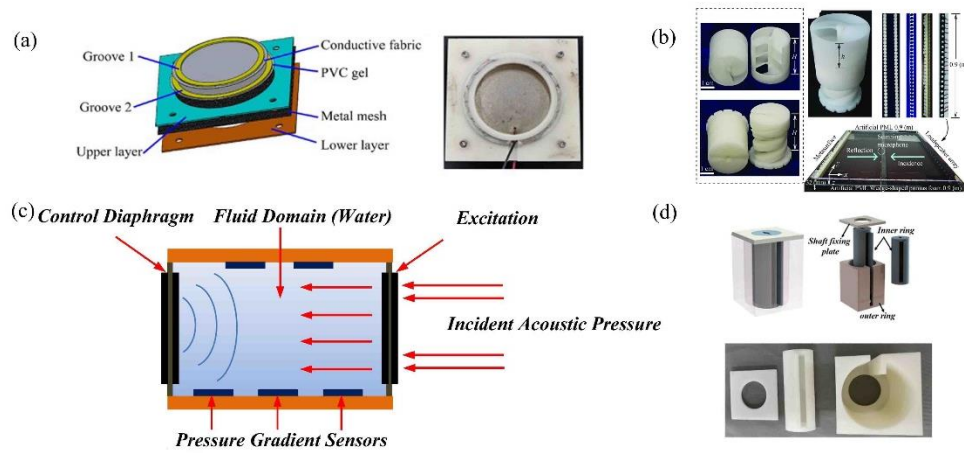


Fig. 2.3 Active AMs sound absorption system: (a) electrically driven laminated active acoustic metamaterials with PVC plasticization[89], (b) helical acoustic meta surface capable of providing a modulated sound-reflected wavefront and a continuously tunable broadband feature [92], (c) acoustic metamaterials by active control of the dynamic density [97], (d) Tunable broadband multi-function acoustic meta surface by nested resonant rings [95].

Passive AMs is the AMs that do not provide extra energy to the AMs sound absorption system. Normally, the passive AMs can only absorb sound in a specific designed frequency range by structural design. Currently, the passive AMs can be divided into membrane AMs, porous AMs, space coiling structures AMs, and Helmholtz resonators AMs according to the characteristics of artificial structures in the structure design method.

Membrane acoustics metamaterials (MAMs) (As shown in Fig. 2.4(a)) combine membrane and tiny rigid mass block to achieve excellent sound absorption ability at low frequencies by negative dynamic effective density[98-102]. Because of the ultra-lightweight structure and perfect sound absorption at low frequencies of MAMs, many studies have been conducted to expand the application. Tuo et al. [103] composed MAMs with a negative pressure cavity.

The experiment results showed that the structure with a negative pressure cavity can obtain a higher absorption peak at low frequency compared with the structure without negative pressure. Besides, the structure could adjust the sound absorption frequency by changing the negative pre-pressure. Lucas et al. [104] assembled membrane-type metamaterials of different shapes and sizes into a panel. The whole panel can express great sound insulation and aesthetic performance at the same time. The finite element model and experiment were used to validate the design scheme.

Normally, porous AMs achieve the improvement of acoustic properties by embedding intricate rigid geometries inside porous materials so that the porous materials can have extra excellent sound absorption and sound transmission loss properties, such as porous layers backed by rigid periodic rectangular irregularities [105], embedded partitions [106-108], and with rigid resonant [109].

Space coiling structures AMs is the AMs based on space coiling cells. The space coiling cells are used to expand working space and control sound speed, which helps the AMs achieve quasi-perfect sound absorption on deep sub-wavelength scales. As one of the first research about space coiling structures AMs, Cai et al. [110] presented bent and coiled up quarter-wavelength sound damping tubes into a panel to form sound absorption AMs (as shown in Fig. 2.4(d)). The experimental results showed that the space coiling structure AMs can absorb sound with the $\lambda/50$ thickness (λ is the wavelength corresponding to

the sound absorption peak frequency). Recently, the space coiling structure AMs has been further developed into several different kinds geometries to obtain specific functions, such as rotatable space coiling-up structure [111], quasi-fractal geometries space coiling structure [112], multi-cavity of coiled-up spaces [113], horn-like space coiling structure [114], sandwich-like space coiling structure [115] and so on.

Helmholtz resonators AMs is the structure consisting of several Helmholtz resonators [116]. The structure can obtain phase shift according to the requirements so that the AMs can have meta-acoustics properties [117], including broadband sound absorption frequency [118], high transmission coefficient, and cloak [119].

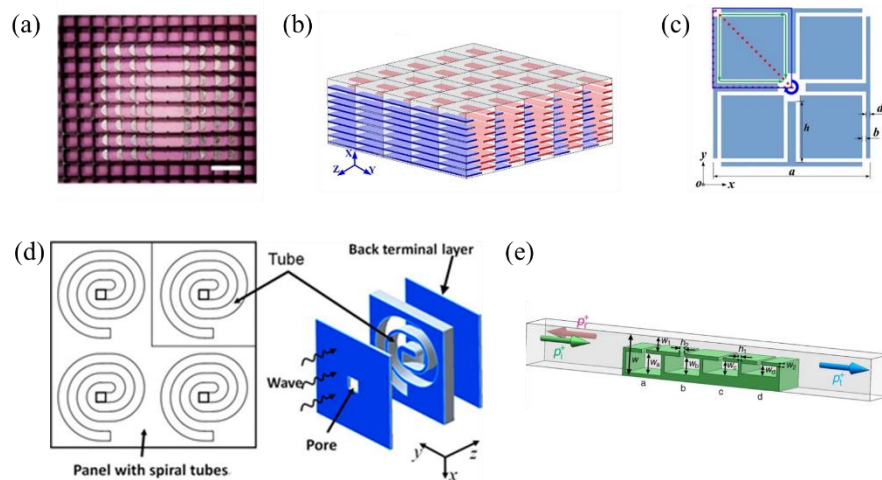


Fig. 2.4 Typical acoustics metamaterials: (a) membrane acoustics metamaterials [83], (b) metaporous materials [107], (c) space-coiling fractal acoustic metamaterials [112], (d) classical space-coiling acoustic metamaterials [110], (e) Helmholtz resonators AMs with various depth cavities [116].

2.2.4 The combination sound absorption structure

From the previous studies, it can be found that both porous materials and

structural considerations have advantages and disadvantages. For example, porous materials have good sound absorption performance at high frequencies while acoustics metamaterials have good sound absorption characteristics at low frequencies. Therefore, the combination of structural absorption and porous materials absorption is an inevitable trend in sound absorption research, and significant research has been carried out in this direction [106, 120-126]. Zhao et al. [127] designed a porous material with two kinds of pores, which they investigated by experimental, finite element, and analytical methods. The results showed that the dual porosity structure could obtain better sound absorption at low frequencies than a conventional porous material of the same thickness. Pereira et al. [128] designed a meta-porous concrete by embedding acoustic resonators into porous concrete to improve sound absorption performance. Additionally, a numerical model was established to predict the sound absorption coefficient of the porous concrete. The results showed that compared with traditional porous concrete, the meta-porous concrete showed an additional absorption peak at 200 Hz which shows great potential for noise control in civil engineering exterior applications.

In addition, it should be noted that the structural design should be carried out under the premise of ensuring thinness as much as possible. From the previous research, we can find that porous materials can easily achieve excellent sound absorption ability with a large thickness, especially for high frequency. Therefore, the issue for sound absorption structure design is how to achieve an

excellent sound absorption performance, especially in low frequency, with a thin thickness.

2.2 The Research about the Integration of Sound Absorption and Structural Bearing

From the previous section, it can be found that many studies have focused on sound absorption performance while less attention was paid to the load-carrying properties which is also important in sound absorption design. In general, porous materials usually have a weak mechanical property due to their own materials characteristics [129]. The micro perforated plate does not have bearing capacity itself, currently, a solution is to combine it with a honeycomb structure [130-132]. In addition, a micro perforated plate can only absorb sound through resonance so it only has a narrow sound absorption range. Although acoustic metamaterials can achieve a significant sound absorption ability in the low frequency range, it has a similar issue that can only absorb sound in resonance frequency [133]. Additionally, structural performance is often neglected in acoustic metamaterials design. The combination sound absorption structure is an effective method to achieve integration of sound absorption and structural bearing, but in most cases, the structure is complex which increases the weight and cost of the application. In conclusion, there is still a general lack of comprehensive performance on high sound absorption and high mechanical properties (Including lightweight and high strength). The sound absorption materials are generally not equipped with overall performance in sound

absorption and mechanical properties: high strength, lightweight, and excellent sound absorption ability in a wide frequency range. However, sound absorption materials with lightweight and high strength have a wide application prospect in transportation, architecture, aeronautics, and astronautics areas. For instance, the noise inside the room can be reduced effectively by using such sound absorption materials replacing traditional sound absorption materials (sound insulation cotton, micro perforated plate). It can also reduce the weight of the structure to realize energy conservation and emission reduction if used in a vehicle or airplane. Even though acoustic and mechanics performance contradict each other in most cases, the improvement of acoustic performance usually means the weakening of the mechanical performance. Therefore, developing a sound-absorbing material with lightweight and high-strength is gradually becoming an important topic and attracting more attention from researchers around the world. Until now, the research on the integration of sound absorption and structural bearing is mainly focused on the improvement of traditional micro perforated plate structures and metal foam.

2.2.1 The improvement of micro perforated plate structure

At present, the micro perforated plate-honeycomb structure has been widely used in engineering because of its simple structure and easy instalment, such as ventilating windows [134], automobile engines [135], interior decorative walls [136], MRI scanners [137], and so on. Therefore, the improvement of the micro perforated plate is a popular method to achieve the integration of sound

absorption and structural bearing. The common method includes adjusting the location and size of holes [138], adding porous materials [139], and multilayer micro perforated plates [140] (As shown in Fig. 2.5 (a)), et al.

On the basis of these simple modifications of micro perforated plate structure, some researchers have conducted further research [141-149]. Zhang et al. [150] designed a kind of micro perforated honeycomb plate that could adjust sound absorption frequency. The structure could change the sound absorption performance by installing a mechanical rotating mechanism into the honeycomb cell (As shown in Fig.2.5 (b)). Ren et al. [151] presented a novel compact multifunctional meta-structure that can achieve low-frequency sound absorption and excellent crash energy dissipation at the same time. The structure uses an internally extended tube to improve the sound absorption ability of the micro perforated plate at the low frequency range and the meta hexagonal realizes excellent mechanical properties (As shown in Fig. 2.5 (c)). Finally, the average sound absorption coefficient of the structure was measured to exceed 0.9 in the range of 600-1000 Hz. Yu et al. [152] combined a micro-perforated membrane with an origami sheet in order to form backing cavities and act as a resonant sound absorber. In this structure, the foldable origami sheet can adjust the shape and depth of the backing cavities during folding to achieve different sound absorption effects which shows the acoustic potential of the foldable structure (As shown in Fig. 2.5 (d)).

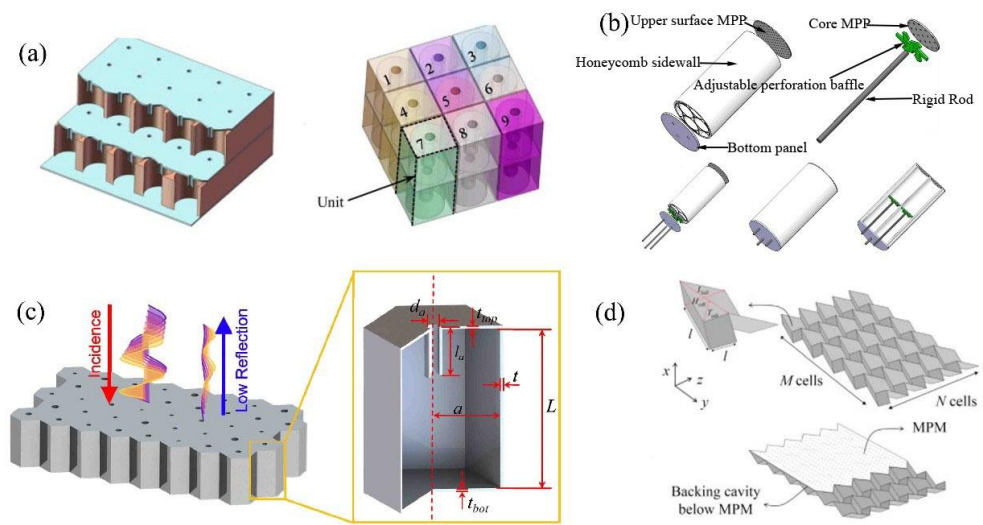


Fig. 2.5 The improvement of micro perforated plate structure: (a) multi-layer helmholtz resonators with extended necks [140], (b) Adjustable sound absorption frequency honeycomb-MPP structure [150], (c) Compact multifunctional meta-structure and geometric topology of the single sound-absorbing component [151], (d) An absorptive barrier comprised of a micro-perforated membrane facing and a corrugated Miura-ori sheet [152].

Besides, in order to reduce weight and simplify the fabrication process, some researchers have tried to use woven and non-woven fabrics as a structural replacement for the heavier and thicker micro perforated plates [153-158]. Li et al. [159] tested the sound absorption properties of plain weave, twill weave, and honeycomb weave, exploring the relationship between sound absorption properties and thickness, surface density, porosity, and pore size of the woven fabric. Prasetyo et al. [160] studied the influence of flow resistance on the sound absorption performance of a double-layer braided structure, establishing a theoretical JCA model of the structure. The results showed that when the two layers had the same flow resistance, the higher flow resistance would produce a

lower absorption amplitude, but a broader frequency band. When the flow resistance of the two layers is different, the flow resistance of the structure surface should be lower than the inner layer to obtain a better sound absorption effect.

It can be found that although these schemes can enhance the sound absorption performance of the micro perforated plate structure and basically ensure the mechanical properties of the structure, they increase the weight of the structure and the complexity of the structure at the same time, which loses the characteristic of simple structure and easy installation of the traditional micro perforated plate structure. Therefore, it is still a challenging task to optimize the structure of the micro perforated plate while maintaining the weight and keeping the simplicity of the structure.

2.2.2 Metal foam

Metal foam is a cellular structure consisting of a solid metal with gas-filled pores containing a large volume fraction [161]. The pores are generated within the base metal (in an uncontrolled way), following different process routes (including using blowing agents or granules [162]), to create a highly stochastic porous metallic structure. The volume fraction of the pores thus developed is very high as compared to the base metal, which makes the materials lightweight [163-165]. There are many kinds of foam metals, including Aluminum metal foam [166], iron metal foam [167], copper metal foam [168], nickel metal foam [169], magnesium metal foam [170], et al. Normally, metal foam can be divided

into two types: closed-cell and open-cell foam depending on whether the pores are sealed or interconnected [171-180] (As shown in Fig. 2.6). Although the closed-cell foams normally have better mechanical properties than opened-cell foams, it usually cannot absorb sound effectively as the sound wave couldn't penetrate into the surface of it. Meanwhile, the open-cell foam is a good sound absorption material, the energy of the sound wave can be consumed through the friction between the sound wave and the metal frame.

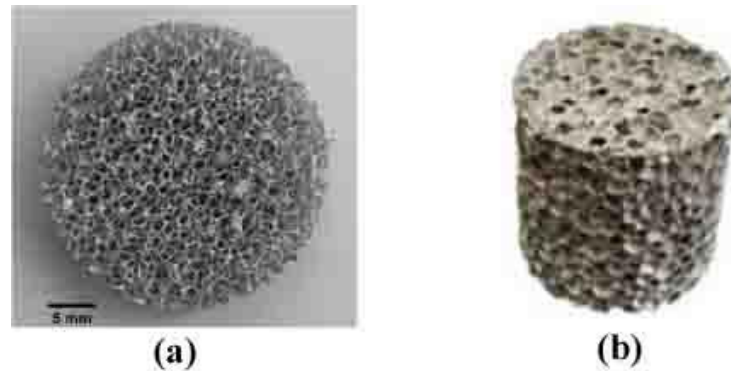


Fig. 2.6 Common metal foams: (a) A opened-cell aluminum foam cylindrical specimen [172], (b) A closed-cell aluminum foam cylindrical specimen [173].

At present, open-cell foam has been proven to be an effective method for sound absorption [181-189]. Liu et al. [190] deposited a ceramic coating on the open-cell Mg foams through plasma electrolytic oxidation (PEO) technology. The experimental results showed that the PEO-coated Mg foams have a better sound absorption ability than the uncoated foam, which can be attributed to the increasing viscous friction caused by PEO coating. Ren et al. [191] used a cell modification method to synthesize needle-like Co_3O_4 on an open-cell Al foam to improve the flow resistance. After the modification, the airflow resistance of the

Al foams increased from 30 Pa·s/m to 93 Pa·s/m, and the sound absorption peak increased from 0.65 to 0.95. Which showed an effective way to improve the sound absorption ability of metal foams.

Meanwhile, opened-cell metal foam also shows a great mechanical performance. In general, the mechanical properties of foam metal are closely related to its matrix materials, relative density, inside pore structure, and so on [192-196]. Zhao et al. [197] investigated the effect of grain structure on the compressive mechanical response of open-cell metallic foams. The relationship between grain size and compressive stress was studied through a crystal-plasticity finite element model. Results showed that there is a threshold for grain size, and the plateau stress and energy absorption ability of the foams exhibit Hall-Petch-like behavior when the grain size is lower than the threshold. Once the grain size exceeds the threshold the mechanical response would not change significantly. Jung et al. [198] investigated the compression and low-velocity impact properties of Ni/Al hybrid foam composites. The strain-rate effects and size effects were evaluated, and the results showed that Ni/Al foams showed a better energy absorption ability as Ni/Al foams provided strain-rate sensitivity for all investigated benchmarks while pure Al foams only showed strain-rate sensitivity for plastic collapse stress.

From the above research, it can be found that open-cell foam metal can basically achieve sound absorption while maintaining good mechanical properties. However, because of the sound absorption mechanism of open cell

foam metal belongs to porous materials which means its sound absorption performance greatly depends on the thickness of the materials. It is difficult for metal foams to achieve lightweight and sound absorption at the same time. Therefore, metal foam is not an effective solution to realize lightweight and high-strength sound absorption materials.

Chapter 3 Sound Absorption Performance of a Micro Perforated Sandwich Panel with Honeycomb-hierarchical Pore Structure Core

From Chapter 1 we can find that both materials and structural considerations each have advantages and disadvantages. Porous materials have good sound absorption performance at high frequencies while resonant structures have good sound absorption characteristics at low frequencies [144-149]. Therefore, the combination of structural absorption and porous materials absorption is an inevitable trend in sound absorption research, and significant research has been carried out in this direction [122-126]. Besides, hierarchical pore structures have proven to be an effective way to address the issue of low frequency sound absorption in porous materials [55]. However, there is still little research investigating the integration of a porous material with hierarchical pore structures into a more complex sound absorbing structure. Hence, this study aims to integrate a hierarchical porous material into a micro perforated sandwich panel to produce a light, low frequency, and broadband sound absorbing structure.

3.1 Experiment

3.1.1 Preparation

The new sound absorbing structure was composed of a top face sheet, a bottom face sheet, an internal honeycomb structure, and a porous filling material (as shown in Fig. 3.1). The top face sheet was made of acrylic with 1mm

thickness, and included 1.3mm diameter perforation holes that were hexagonally arranged 4.7 mm apart (as shown in Fig. 3.2(a)), the diameter and distribution of the perforation holes are determined by the needles in hierarchical pore structure and honeycomb structure to ensure the needles can across the micro perforated plate. The honeycomb was made from an aramid paper honeycomb (produced by CMAG Composite Co., Lt, Jiaxing, China) with 50mm thickness and 5.5mm side length (as shown in Fig. 3.2 (b)). In order to reduce the weight and improve the heat resistance of the structure, carbonized cotton was selected as the porous filling material. The carbonized cotton was prepared by a tube furnace (OTF-1200X, Hefei Kejing Materials Technology Co., Ltd) (As shown in Fig. 3.3(a)), and the temperature was set as 600 °C to pyrolysis the cotton and nitrogen was always present during the heating process to avoid the burning, Fig. 3.3(b) showed the carbonized cotton. Additionally, large pores of 1.0mm diameter were also created through the thickness of the porous materials to form the hierarchical pore structure.

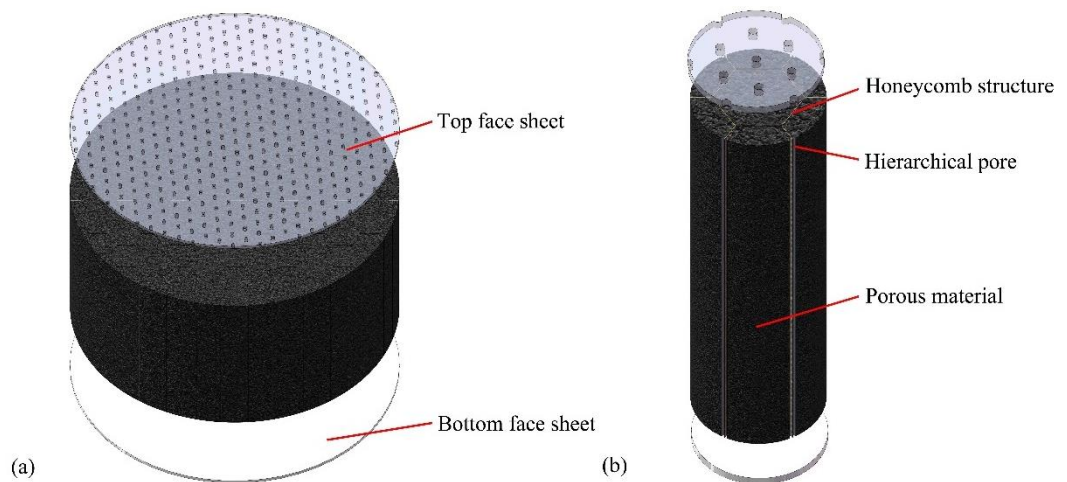


Fig. 3.1 3d models of: (a) the honeycomb panel with hierarchical pore structure, and (b) the details for a single cell within this structure.

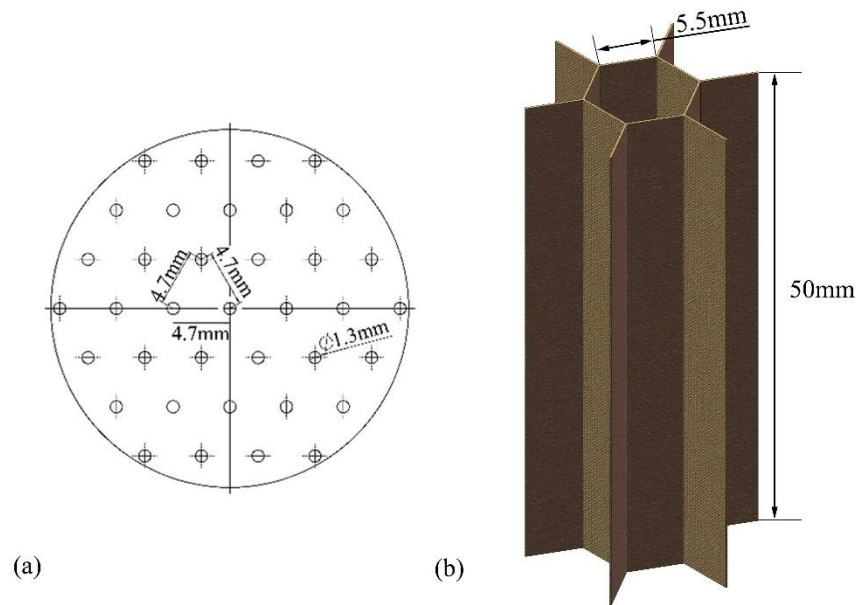


Fig. 3.2 Dimensions of the structure: (a) top face sheet (b) honeycomb.

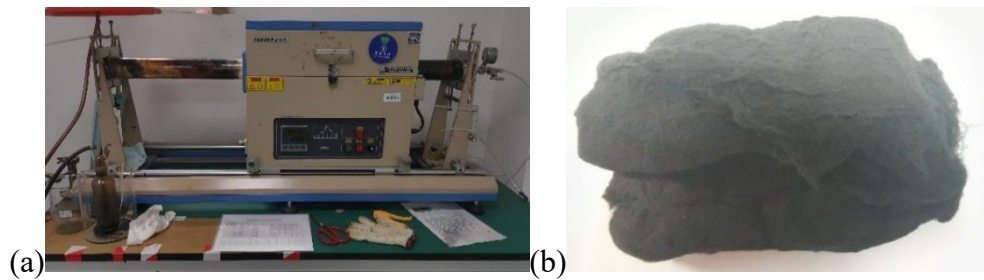


Fig. 3.3 The preparation of carbonized cotton: (a) tube furnace (b) carbonized cotton.

The preparation process of the structure is shown in Fig. 3.4. Firstly, the micro perforation plate was bonded with the honeycomb to form the specimen without filler. At this stage, a circle of thin plastic plate was adhered to the outside of the honeycomb to form a continuous perimeter barrier. Then the carbonized cotton was put into the honeycomb cell. In order to ensure a uniform density of carbonized cotton, each honeycomb cell was filled with 200 mg of carbonized cotton. Lastly, needles with 1.0 mm diameter were used to penetrate into the carbonized cotton through the micro perforations in the top face sheet and were pulled out after 24 hours to form the large pore structures in the

carbonized cotton. Besides, it should be noted that the needles should be kept vertical to form the hierarchical pore structures. Thus, a same micro perforated plate was fixed on another side to keep the needle vertical and a plastic foam was placed in the bottom of the structure to lock the needles.

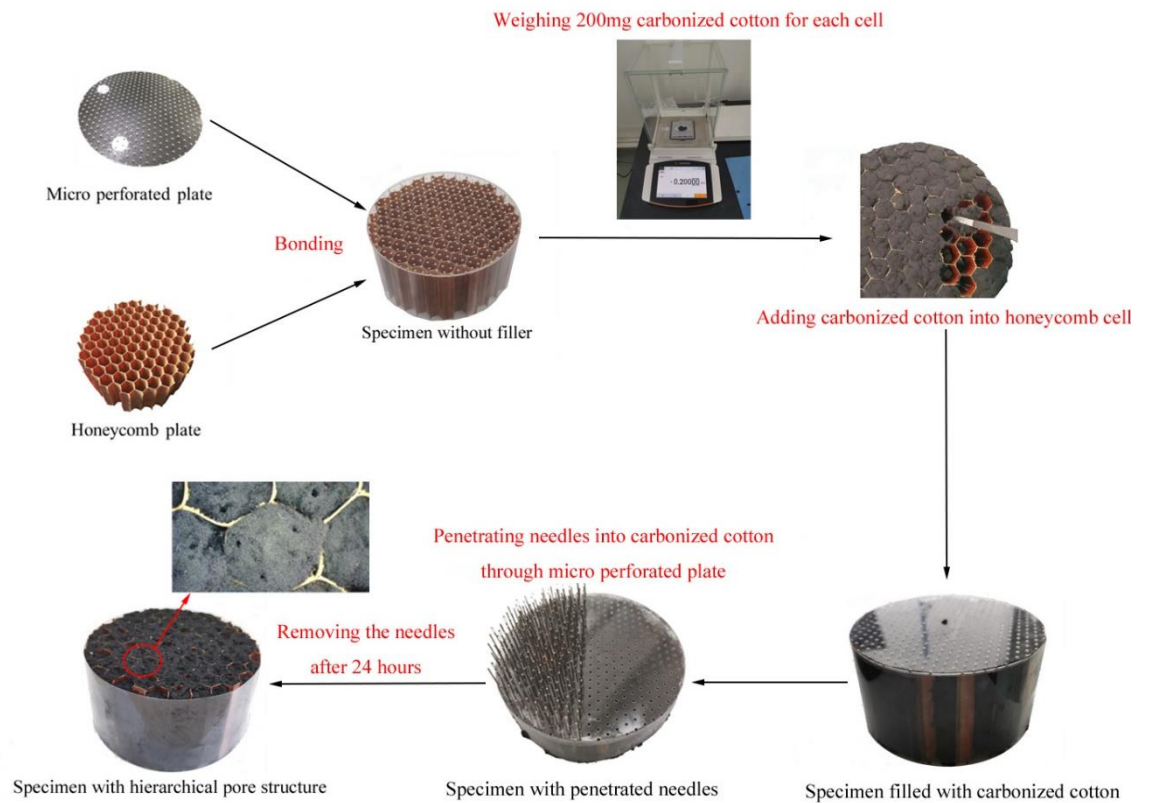


Fig. 3.4 Preparation of specimens with a hierarchical pore structure.

3.1.2 Sound absorption performance test

The sound absorption performance test was carried out according to the ISO 10534-2 standard [12], using an impedance tube test system (as shown in

Fig. 3.5). An SW 466 impedance tube testing system from Beijing Shengwang Acoustic-electric Technology Co., Ltd was used in this work.



Fig. 3.5 Impedance tube testing system.

Normally we determine the sound pressure of the incident sound wave and reflect the sound wave as:

$$p_i = P_I e^{jk_0 x} \quad (3.1)$$

$$p_r = P_R e^{-jk_0 x} \quad (3.2)$$

Where P_I and P_R are the amplitude of p_i and p_r at the reference plane, x is the position of the wave.

Therefore, the sound pressure at microphone A and microphone B (as shown in Fig. 3.6) can be written as:

$$p_1 = P_I e^{jk_0 x_1} + P_R e^{-jk_0 x_1} \quad (3.3)$$

$$p_2 = P_I e^{jk_0(x_1-s)} + P_R e^{-jk_0(x_1-s)} \quad (3.4)$$

The transfer function of the incidence wave and reflection wave are:

$$H_i = \frac{p_{2i}}{p_{1i}} = e^{-jk_0 s} \quad (3.5)$$

$$H_r = \frac{p_{2r}}{p_{1r}} = e^{jk_0 s} \quad (3.6)$$

Then, the transfer function of the whole sound field (impedance tube) can be determined by the formula (3.3) and (3.4):

$$H_{12} = \frac{p_2}{p_1} = \frac{e^{jk_0(x_1-s)} + re^{-jk_0(x_1-s)}}{e^{jk_0x_1} + re^{-jk_0x_1}} \quad (3.7)$$

Therefore, the reflection coefficient r can be written as:

$$r = \frac{H_{12} - H_i}{H_r - H_{12}} e^{j2k_0x_1} \quad (3.8)$$

At last, the sound absorption coefficient α can be calculated by:

$$\alpha = 1 - r^2 \quad (3.9)$$

At this time, all the parameters can be obtained in the experiment so that the sound absorption coefficient can be tested from the impedance tube test system. In addition, the sound pressure sensors will switch position tests twice and take the average results to eliminate errors of the sound pressure sensors.

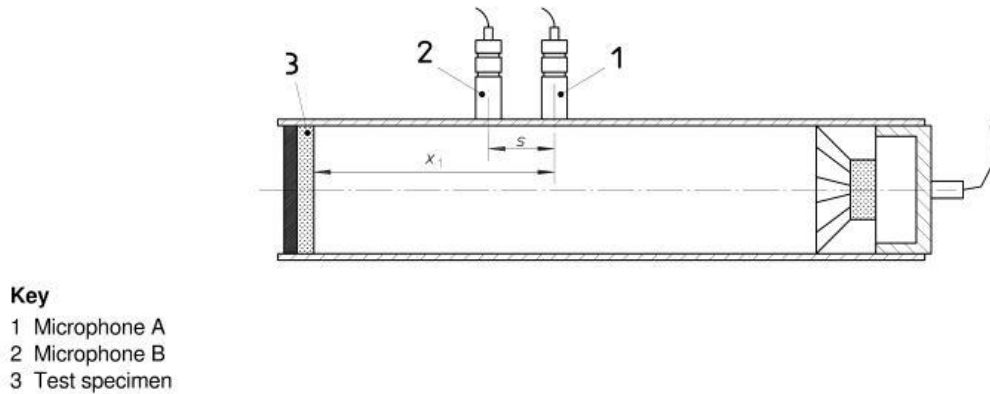


Fig. 3.6 The principle of impedance tube test.

A large impedance tube and a small impedance tube were used to test the sound absorption coefficient in the 63-1600 Hz and 1000-6300 Hz frequency ranges respectively. The diameter of the large tube was 100 mm and the small one was 30 mm (as shown in Fig. 3.5), which required the separate preparation of 30 mm and 100 mm specimens. Three specimens were prepared for each type to ensure accuracy and to quantify the variability of the experimental results. In

order to compare and analyze the role of carbonized cotton and hierarchical pore structure in the sound absorption process, the sound absorption coefficients of the structure under three different statuses were tested: no filling, filled with carbonized cotton, and filled with hierarchical pore structure. The test results are shown in Fig. 3.7.

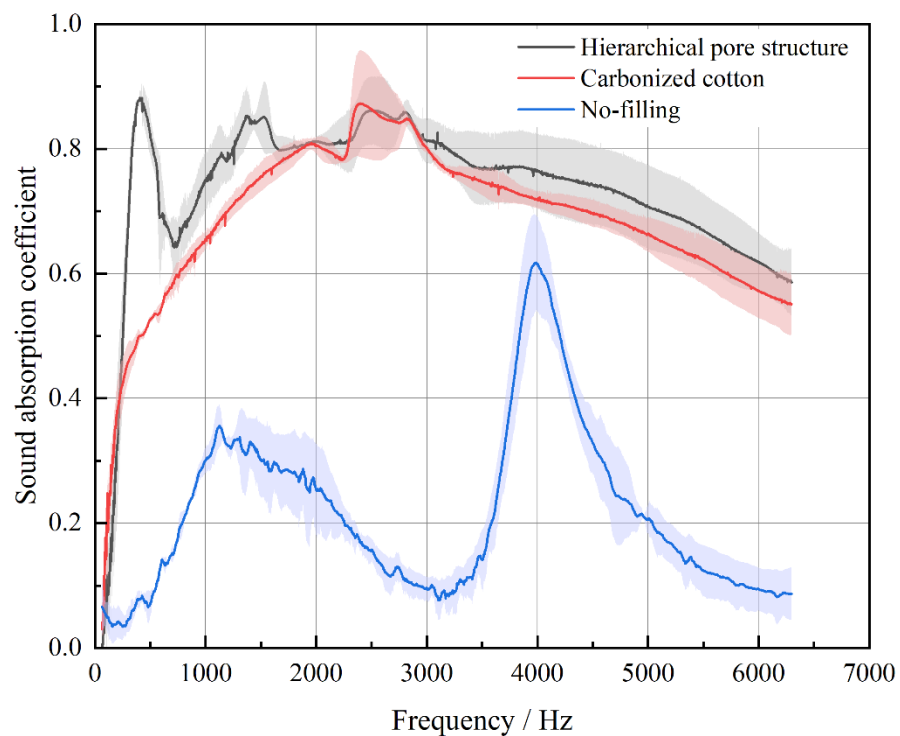


Fig. 3.7 Sound absorption performance test results of all samples. The shadow around the curves shows the standard deviation from the mean of three samples.

In order to directly compare the different results, the average sound absorption coefficient is usually considered, representing the average of the sound absorption coefficient of 125, 250, 500, 1000, 2000, and 4000 Hz [3]. Comparing the ‘no-filling’ specimens against the filled with ‘carbonized cotton’ specimens, it can be found that adding carbonized cotton can significantly enhance the sound absorption ability of the structure, the average sound

absorption coefficient increased from 0.220 ± 0.031 to 0.558 ± 0.006 . The hierarchical pore structure was also seen to further enhance the sound absorption performance of the structure, with the average sound absorption coefficient increasing from 0.558 ± 0.006 to 0.626 ± 0.028 . According to ISO 11654, the weighted sound absorption coefficient α_w is 0.8, classified as the Class B level sound absorption [199].

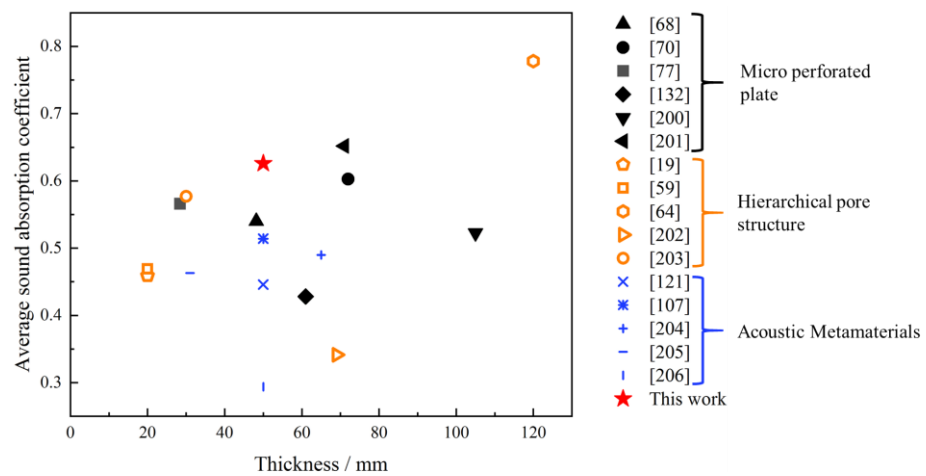


Fig. 3.8 Comparison of average sound absorption coefficients across existing literature [19, 59, 64, 68, 70, 77, 107, 121, 132, 200-206].

The comparison of the average sound absorption coefficient between this work and other studies in different thicknesses [19, 59, 64, 68, 70, 77, 107, 121, 132, 200-206] is shown in

Fig. 3.8. It can be found that the average sound absorption coefficient is increased with the thickness of the structure, and our work obtain the best result in 50mm. Even when it is compared with the thicker structure also show the excellent sound absorption results. However, it should be noted that this comparison is not entirely fair as they have different weights and design

objectives.

Due to the resonance of the micro perforated plate, the specimens with no-filling showed two sound absorption peaks at 1500 Hz and 4000 Hz. However, without the effect of porous material, the structure cannot absorb sound in other frequencies. The specimens without carbonized cotton only showed an indistinct peak at 2500 Hz, but because of the carbonized cotton, it can absorb sound effectively except in the low frequency range. Finally, the hierarchical pore structure exhibited a new distinct sound absorption peak at 400 Hz by resonant sound absorption (of the entrapped air in the structure) which significantly enhances the sound absorption ability of the structure at such low frequencies. However, because of the characteristic of the resonant sound absorption, this effect soon degrades as the frequency shifts away from the resonance frequency (400 Hz), leading to a local dip at 750 Hz. In general, hierarchical pore structure was found to be an effective way to improve sound absorption ability in low frequency, and the sound-absorbing honeycomb structure with it can be an effective sound absorber over the 200-6000 Hz frequency range.

3.2 Analytical Model

The sound absorption performance of a structure is often judged by the sound absorption coefficient, which is defined as the ratio of the unreflected sound power entering the surface of the object to the incident sound power of a plane wave at normal incidence [207]. which is usually calculated according to Eq. (3.10) [208]:

$$\alpha = 1 - \left| \frac{Z_s - \rho_0 c_0}{Z_s + \rho_0 c_0} \right| \quad (3.10)$$

Where Z_s means the specific acoustic impedance, ρ_0 and c_0 mean the air density and the sound velocity in air respectively. However, the specific acoustic impedance of such a complex structure is difficult to calculate, so the structure must be simplified first.

The 3D model of the honeycomb with a hierarchical pore structure is shown in Fig. 3.1(a). The structure is transformed from a 3D model to a 2D model for acoustic analysis as shown in Fig. 3.9 (since the wallboard of the honeycomb has the same direction as the sound wave, its influence on the sound wave is ignored [130]). The propagation process of the sound wave is shown in Fig. 3.10, where the sound wave firstly passes through the top face sheet to the porous materials, and then through the porous materials to the bottom face sheet that reflects it. The bottom face sheet, without perforations, is regarded as a rigid panel. The sound absorbing components of the structure can be divided into two parts: the top face sheet and the porous materials. In addition, as large holes are drilled into the porous materials, the porous materials can be further divided into pure porous materials and multiple parallel through holes. In this way, the whole structure is divided into three parts as shown in Fig. 3.11.

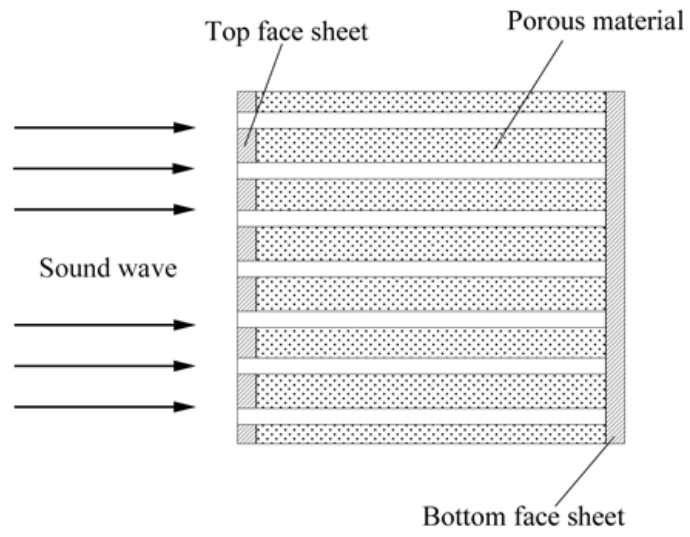


Fig. 3.9. 2D model of the sound absorbing honeycomb.

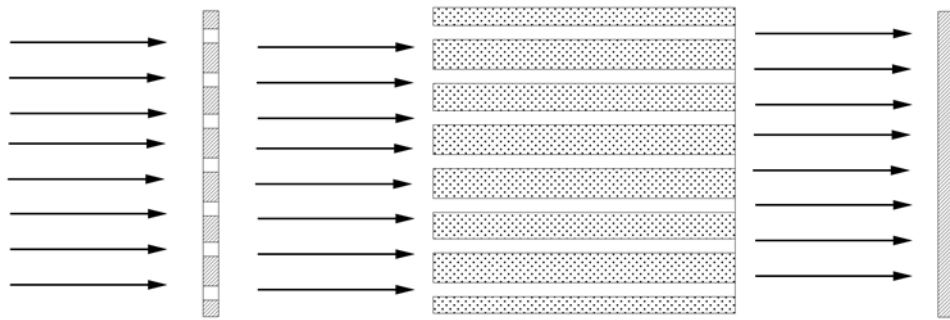


Fig. 3.10 Process of sound wave propagation through the sound absorbing structure.

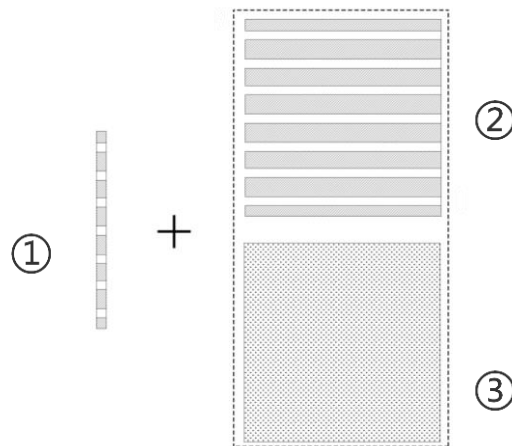


Fig. 3.11 Honeycomb structure decomposition for 2D modeling.

Now, the micro perforated plate (part 1) and the porous materials (parts 2 and 3) act in series, so they can be analyzed separately and later recombined. In addition, the collection of multiple parallel through holes (part 2) and the pure porous materials (part 3) can be considered as a parallel system or double porosity materials. Therefore, the specific acoustic impedance of the whole structure can be calculated by calculating the specific acoustic impedance (Z_{s1} , Z_{s2} , Z_{s3}) of each structural feature.

3.2.1 Analytical model of micro perforated panel

For the micro perforated panel, the specific acoustic impedance can be regarded as the acoustic impedance of a single hole divided by the perforation ratio [62]. In the case of a single circular tube, Crandall [209] deduced its motion equation according to Eq. (3.11):

$$\rho_0 \dot{u} - \frac{\eta}{r_1} \frac{\partial}{\partial r_1} \left(r_1 \frac{\partial}{\partial r_1} u \right) = \frac{\Delta P}{t} \quad (3.11)$$

where η is the dynamic viscosity constant of air, u is the axial particle velocity of the air in the tube (a function of radius vector r_1), t is the length of the tube, and ΔP is the pressure difference between the two ends of the tube.

From the Eq.(3.11), the specific acoustic impedance of the small single circular tube can be calculated according to the definition:

$$Z_1 = \frac{\Delta p}{\bar{u}} = j\omega\rho t \left(1 - \frac{2}{x\sqrt{-j}} \frac{J_1(x\sqrt{-j})}{J_0(x\sqrt{-j})} \right)^{-1} \quad (3.12)$$

Where $x = \sqrt{\frac{\rho\omega}{\eta}}$, J_0 and J_1 are Bessel's function of the first kind in zeroth and first order.

Then Maa [62] rewrite Eq.(3.12) to Eq.(3.13) a wider application range :

$$Z_1 = \frac{\Delta P}{\bar{u}} = j\omega\rho_0 t_1 \left[1 - \frac{2}{x\sqrt{-j}} \frac{J_1(x_1\sqrt{-j})}{J_0(x_1\sqrt{-j})} \right]^{-1} \quad (3.13)$$

$$\approx \frac{32\rho_0\mu t_1}{d_1^2} \sqrt{1 + \frac{x_1^2}{32}} + j\omega\rho_0 t_1 \left(1 + \frac{1}{\sqrt{3^2 + \frac{x_1^2}{2}}} \right)$$

$$x_1 = \sqrt{\frac{\omega d_1}{\mu} \frac{d_1}{2}} \quad (3.14)$$

where j is the imaginary number, ω is the angular frequency, d_1 is the diameter of the micro perforated holes, $\mu = \eta/\rho_0$ is the kinematic viscosity of the air, and t_1 is the thickness of the micro perforated panel.

Then, the specific acoustic impedance of the micro perforated panel can be calculated from Eq. (3.15) [62]:

$$Z_{s1} = \frac{Z_1}{p_1} \quad (3.15)$$

where p_1 is the perforation ratio (the total area of perforation holes divided by the area of the plate) of the micro perforated panel.

3.2.2 Analytical model of the double porosity materials

The specific acoustic impedance of porous materials can be divided into two conditions:

(1) The back is a hard surface

$$Z_s = -jZ_0 \cot kl \quad (3.16)$$

$$k = \omega\sqrt{K/\rho} \quad (3.17)$$

$$Z_0 = \rho c = \sqrt{K\rho} \quad (3.18)$$

where K means the elastic modulus of porous materials, ρ is the complex density, and Z_0 is the characteristic impedance of the materials.

(2) The back isn't a hard surface

The back is a cavity with a depth of D

$$Z_s = -j\rho_0 c_0 \cot kD \quad (3.19)$$

The back is a backing with the specific acoustic impedance Z_t

$$Z_s = jZ_0 \frac{jZ_0 + Z_t \cot kl}{jZ_0 \cot kl - Z_t} \quad (3.20)$$

In this structure, the back of the porous materials is the bottom face sheet which fits the first case. Therefore, Eq. (2.16-2.18) is used to calculate the specific impedance of the porous materials. In this condition, the complex density and elastic modulus of the porous materials need to be calculated respectively. It should be noted that since there are two kinds of pores in this porous material, it is necessary to calculate the complex density ρ_2, ρ_3 and elastic modulus K_2, K_3 for part 2 and part 3 respectively, and then combine them according to Eq. (3.21) and (3.22) [210]:

$$\rho_{23} = \left[\frac{1}{\rho_2} + (1 - \phi) \frac{1}{\rho_3} \right]^{-1} \quad (3.21)$$

$$K_{23} = \left[\frac{1}{K_2} + (1 - \phi) \frac{W_i}{K_3} \right] \quad (3.22)$$

Where ϕ is the perforation ratio of the through pores, and W_i is the ratio of the average pressure in the larger and smaller pores. In this structure, where the diameter of the larger pores is only around 5.3 times larger than that of the small pores, the W_i can be given a value of 1 (since this ratio is much less than 100) [210].

For porous materials, the complex density ρ of part 2 (ρ_2) and part 3 (ρ_3) can be calculated as shown in Eq. (3.23) and (3.24)[3, 62]:

$$\rho_2 = \frac{s_2 \rho_0}{\varphi} \left[1 + \left(3^2 + \frac{x_2^2}{2} \right)^{-\frac{1}{2}} + \frac{32}{j\omega \rho_0 d_2^2} \left(1 + \frac{x_2^2}{2} \right)^{\frac{1}{2}} \right] \quad (3.23)$$

$$\rho_3 = \frac{s_3 \rho_0}{\varphi} \left[1 + \left(3^2 + \frac{x_3^2}{2} \right)^{-\frac{1}{2}} + \frac{32}{j\omega \rho_0 d_3^2} \left(1 + \frac{x_3^2}{2} \right)^{\frac{1}{2}} \right] \quad (3.24)$$

Where $x = \sqrt{\frac{\omega d}{\mu^2}}$, d_2 is the diameter of the multiple parallel through holes (part 2), d_3 is the diameter of the pure porous materials (part 3), φ is the porosity of the porous materials, and s is the structure factor. Generally, the structure factor of a porous material like part 3 (s_3) is taken as 3 [3], however, because the parallel through holes in part 2 do not have a tortuous path, the structural factor for this part (s_2) is taken as 1 instead.

The compression modulus of the tube per unit thickness can be calculated according to Eq. (3.25) [3]:

$$K = P_0 \left[1 + \frac{1}{8} (\gamma - 1) \frac{j\omega d^2}{4\nu} \right] \quad (3.25)$$

Where γ is the specific heat ratio of the air, d is the diameter of the tube.

Then the compression modulus of two types of porous materials (part 2 and part 3) can be written as:

$$K_2 = P_0 \left[1 + \frac{1}{8} (\gamma - 1) \frac{j\omega d_2^2}{4\nu} \right] \quad (3.26)$$

$$K_3 = P_0 \left[1 + \frac{1}{8} (\gamma - 1) \frac{j\omega d_3^2}{4\nu} \right] \quad (3.27)$$

By substituting Eq. (3.21) and (3.22) into Eq. (2.20), the characteristic impedance of porous materials can be calculated as:

$$Z_{23} = \sqrt{K_{23}\rho_{23}} \quad (3.28)$$

Then the specific acoustic impedance of porous materials can be given by:

$$Z_{s23} = -jZ_{23}\cot k_{23}l \quad (3.29)$$

Where,

$$k_{23} = \omega\sqrt{K_{23}/\rho_{23}} \quad (3.30)$$

At this point, the specific acoustic impedance of each part, Z_{s1} , and Z_{s23} , has been defined, and the specific acoustic impedance of the whole structure can be determined from its equivalent circuit relation in Eq. ((3.31):

$$Z_s = Z_{s1} + Z_{s23} \quad (3.31)$$

Finally, the sound absorption coefficient α can be calculated using Eq. (1).

3.2.3 Results of analytical modelling

The formulas for the analytical model were implemented in MATLAB (As shown in Appendix A), using the parameters shown in Table 3.1, to calculate the sound absorption performance of the structure. The constant value of the air is under room temperature (20 °C) and 1 standard atmosphere pressure, the parameters of the sample are tested from the real sample. The analytical predictions for the carbonized cotton and hierarchical pore structures are shown in Fig. 3.12 against the experimental results. The analytical results well reflect the sound absorption characteristics of the structures, predicting average sound absorption coefficients of 0.556 (0.4% error) and 0.731 (16.8% error) for the carbonized cotton and hierarchical pore structures respectively. The greater error for the hierarchical pore structure, particularly at lower frequencies, is attributed

to the over-estimation of the perforation ratio ϕ and diameter d_2 of the through holes since the elasticity of the porous materials allows for some recovery (and reduction in diameter) after the needles are removed in the production of the holes. Additionally, since the theoretical model ignores the influence of the structure's natural resonance (the structures are regarded as rigid boundaries), the peak at 2500Hz of the experimental sound absorption curve is not reflected by the theoretical calculation. This error is assumed to be caused by the resonance of the whole structure.

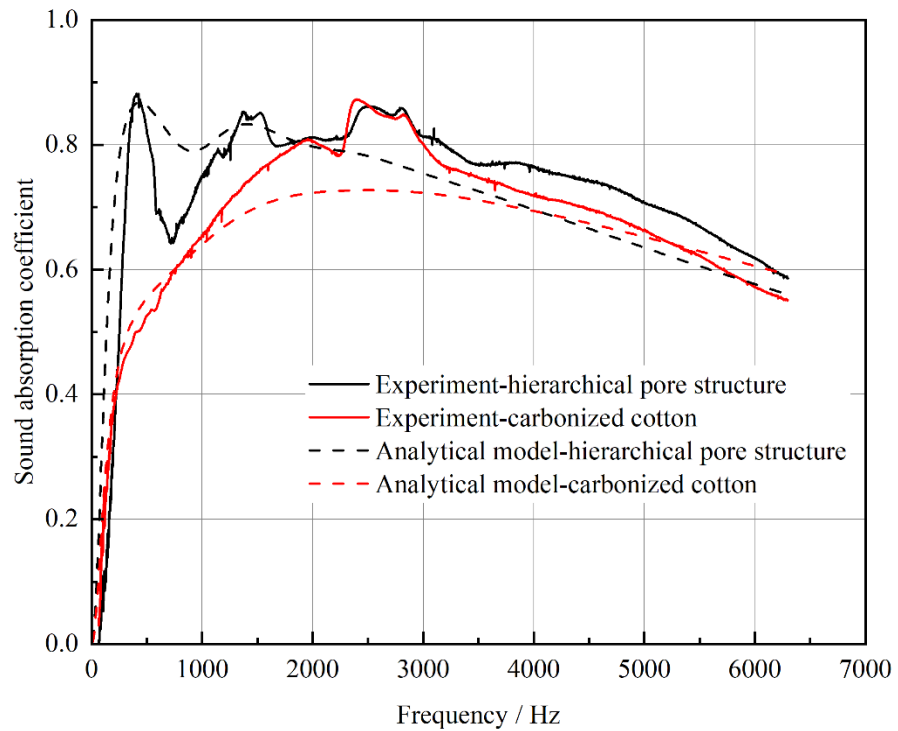


Fig. 3.12 The results of analytical modeling compared with experimental data for the carbon cotton and hierarchical pore structures.

Table 3.1: Parameters of theoretical models to predict the sound absorption coefficient of the different structures.

Property	Value
Air density, ρ_0 (Kg/m ³)	1.295
Atmosphere pressure, P_0 (Pa)	1.01×10^5
Dynamic viscosity of air, η	1.85×10^{-5}
specific heat rate of air, γ	1.4
Perforation rate of perforated plate, p_1	0.07
Perforation rate of the through pores, φ	0.0538
Porosity of carbonized cotton, φ	0.97
Thickness of micro perforated plate, t_1 (mm)	1
Thickness of porous materials, l (m)	0.05
Diameter of perforation, d_1 (mm)	1.3
Diameter of through pores, d_2 (m)	0.001
Diameter of aperture in porous materials, d_3 (m)	0.00015

3.3 Finite Element Analysis (FEA)

3.3.1 Finite element model

The acoustic finite element model can be divided into the acoustic field model and structure model, the acoustic field model simulates the status of sound pressure in the air and the structure model is used to simulate the influence of the structures on the sound pressure. At last, the sound absorption coefficient can be calculated by the sound pressure in the acoustic field at different frequencies.

The 3D model of the honeycomb with a hierarchical pore structure is shown in Fig. 3.1(a). As each honeycomb cell has the same effect on the sound wave, a single honeycomb cell was considered for simplified calculation (as shown in Fig. 3.13). Besides, to ensure the influence of honeycomb cell number, the finite element model of one honeycomb cell and five honeycomb cells are established

respectively. The sound pressure simulation results showed that they had the same results. This model also included an impedance tube; representative of the experimental conditions for measuring the sound absorption coefficient of the structure.

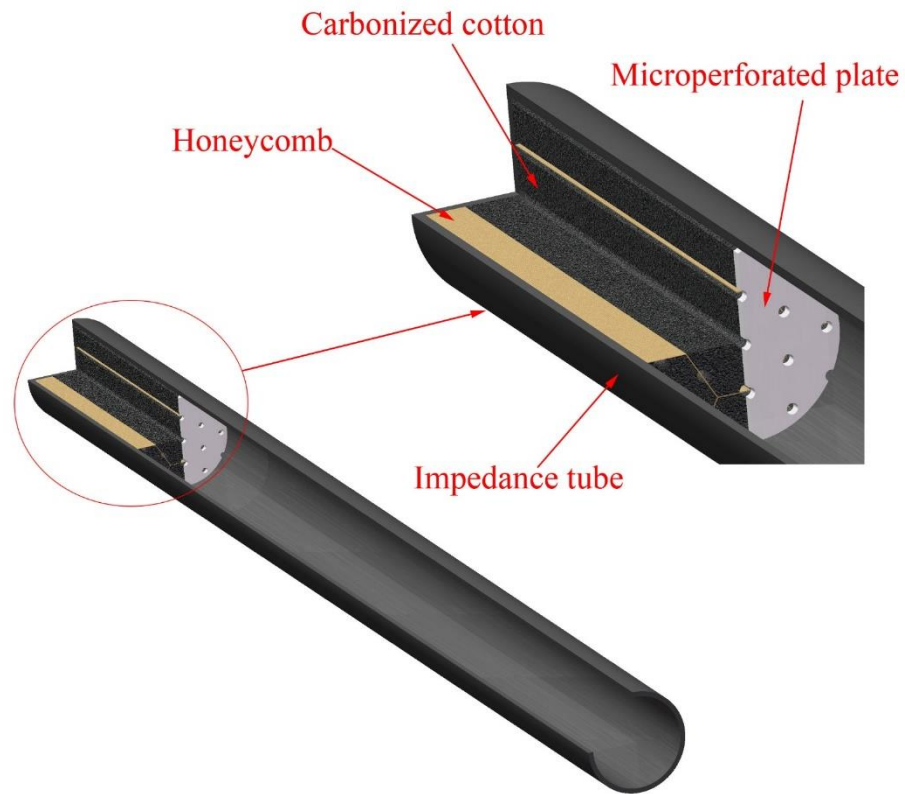


Fig. 3.13 The structure of a single cell within an impedance tube.

The sound absorption behavior of the model relied on fluid-solid interactions between the structure and sound waves. Hence, fluid element 30 was used to simulate the air and porous materials (depicted in purple and red in Fig. 3.14 respectively), while solid element 185 was used to model the honeycomb structure, micro perforated plate, and impedance tube (cyan and teal). A mesh consisting of around 33000 solid and 37000 fluid finite elements were used for the simulation, with the sound wave source originating from one end of the

impedance tube and the sound absorbing structure existing at the other (fixed) end as shown in Fig. 3.14.

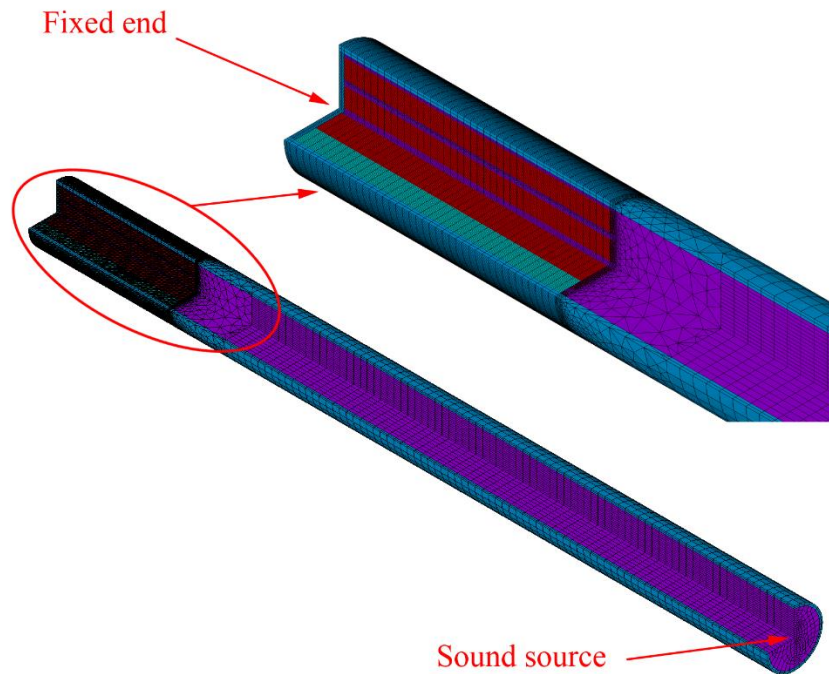


Fig. 3.14 Load application and meshing method of the FEA model

The porous materials was simulated using a Delany-Bazley model, relying on flow resistance as the input parameter. To get the flow resistance of the carbonized cotton, pictures of carbonized cotton fiber were taken with a Scanning Electron Microscope (SEM), while the average fiber diameter was 6 μm (an SEM picture example from ten pictures was shown in Fig. 3.15. In the experiments, the bulk density of the 200 mg carbonized cotton in each honeycomb cell was 52.8 kg/m^3 . Therefore, the flow resistance of carbonized cotton R_1 was calculated according to Eq. (25) [211]:

$$R_1 = K_1 \rho_m^{1.53} / d^2 \quad (25)$$

where the constant K_1 has the value 3.18×10^{-9} , d is the diameter of the fiber, and

ρ_m is the bulk density of the porous materials. This results in a flow resistance value of 38173 Pa·s/m. Additionally, the density and acoustic velocity of the air in the porous materials can be calculated from Eq. (26) and (27) [3]:

$$\rho = \frac{s}{\varphi} \rho_0 + \frac{R_1}{j\omega} \quad (26)$$

$$c = \sqrt{\frac{K}{\rho}} \quad (27)$$

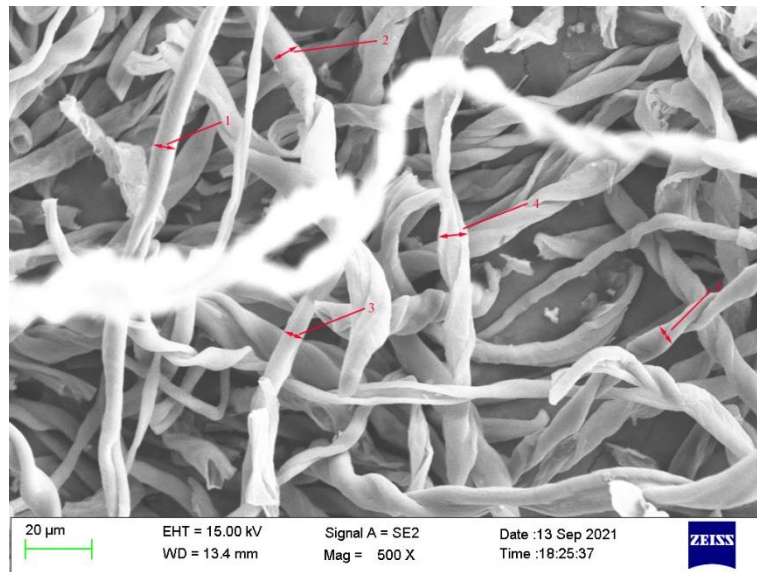


Fig. 3.15 Average carbonized cotton diameter measured using SEM.

3.3.2 Results of FEA

Fig. 3.16 illustrates the pressure distribution of the micro perforated sandwich panel with a honeycomb-hierarchical pore structure at 6000 Hz. It can be found that the pressure was affected by the structure extremely, especially at the surface of the MPP., The sound absorption coefficient of the structure of this frequency can be obtained by extracting pressure at appropriate positions (according to ISO 10534-2) in the impedance tube.

The results of the fluid-structure interaction FEA model, compared with

experimental data, can be seen in Fig. 3.17. In general, the FEA results fit the experiment data well as the average sound absorption coefficient of the carbonized cotton filled and hierarchical pore structures were 0.499 and 0.572, showing 10.6% and 8.6% error respectively. Like the theoretical model, the natural resonance was not considered in the FEA model and the experimental absorption peak at 2500Hz could not be predicted.

The analytical and FEA results for carbonized cotton and hierarchical pore structure are both directly compared against the experimental results in Fig. 3.18. Qualitatively, the results for both models appear to be quite effective in predicting the sound absorption coefficient curves. In terms of the average sound absorption coefficient, the FEA model appears to be much less accurate (10.1% error) compared to the analytical model (0.4% error) when the structure is filled with carbonized cotton. For the hierarchical pore structure, the FEA model appears to be more accurate (8.6% error) than the analytical model (16.8% error). For both models, the characteristic of a new peak in the sound absorption curve which is established by hierarchical pore structure can be reflected in low frequency. However, it can be found that both model models can now show the peak exactly which we attribute to the resonance of the whole structure.

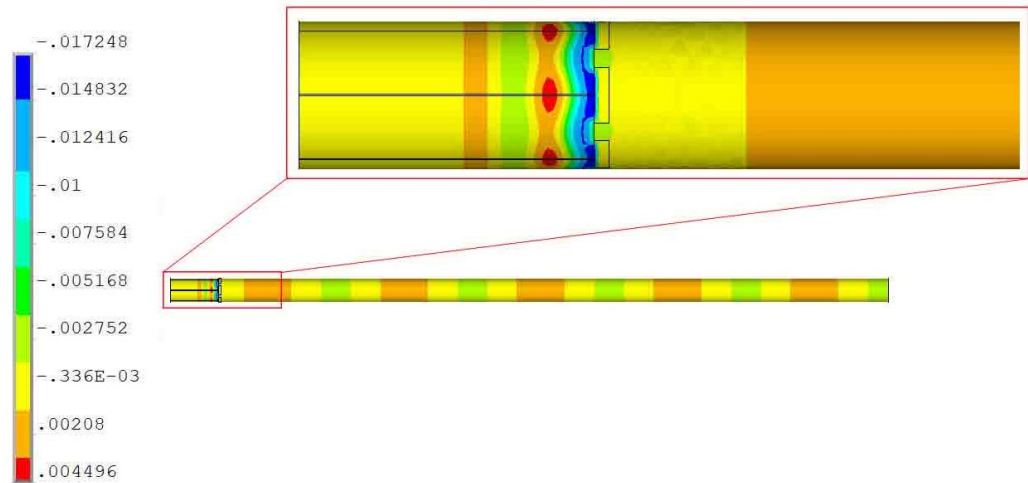


Fig. 3.16 The pressure (Pa) distribution of micro perforated sandwich panel with honeycomb-hierarchical pore structure (6000 Hz).

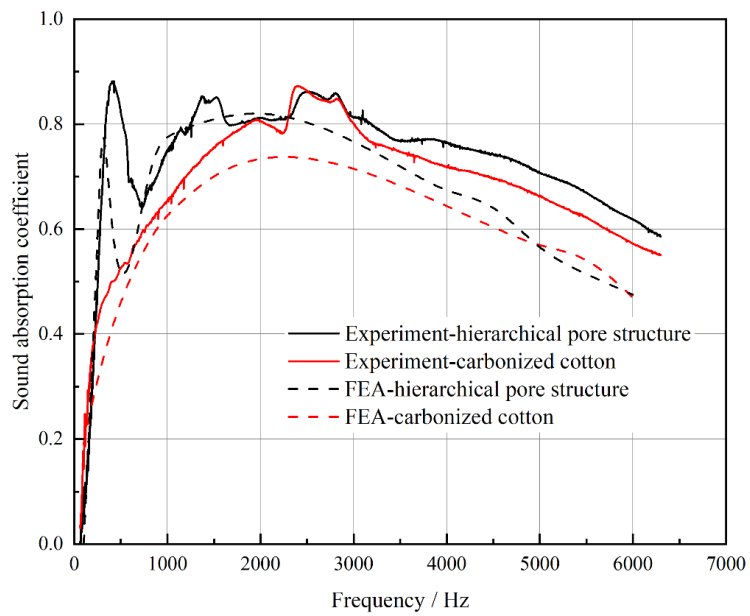


Fig. 3.17 Comparison of FEA and experimental sound absorption results for the two different structures.

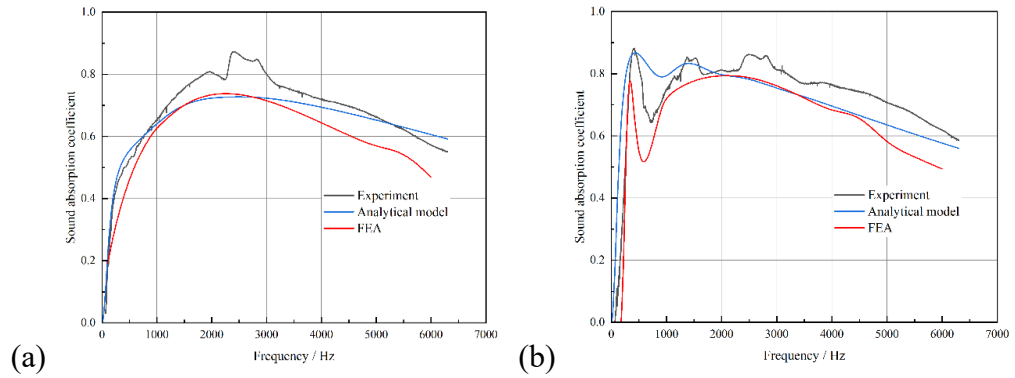


Fig. 3.18 Comparison of FEA, analytical model, and experimental results for: (a) carbonized cotton, and (b) hierarchical pore structure.

3.4 The Influence of the Parameters

In order to better understand the influence of the different parameters and optimize the structures. The height of the structure, diameter of the hierarchical pore structure, the diameter of pores on the micro perforated plate, the perforation rate of micro perforated plate, the thickness of the micro perforated plate, the type of the porous materials (Porosity) are analyzed through the theoretical model.

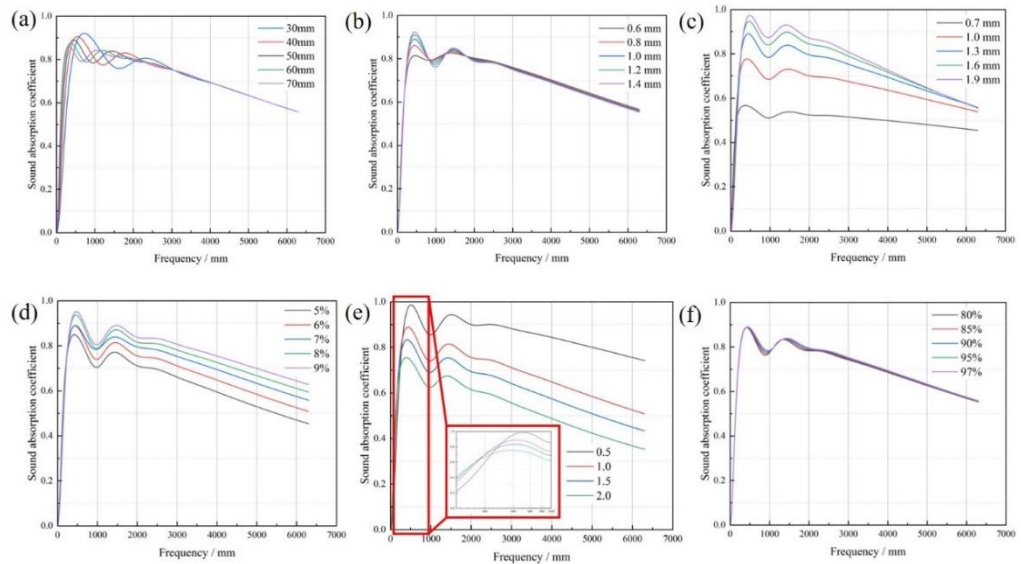


Fig. 3.19 The influence of the parameters of the structure: (a) The height of the structure, (b) the Diameter of the hierarchical pore structure, (c) the Diameter of pores on the micro perforated plate, (d) the Perforation rate of the micro perforated plate, (e) Thickness of the micro perforated

plate and (f) the type of the porous materials (Porosity).

The influence of the thickness of porous materials is considered at first, the thickness of porous materials is increased from 30mm to 70mm in the theoretical model, and then the sound absorption coefficient is calculated again. As shown in Fig.3.19 (a), it can be found that with the increase of the thickness, the maximum sound absorption coefficient of the structure decreases slightly, but the peak frequency gradually moves to the lower frequency. Therefore, increasing the thickness of porous materials can improve the sound absorption performance of the structure at low frequencies effectively.

Experiments have proved that hierarchical pore structure in porous materials can enhance the sound absorption performance effectively, because of that how to design the hierarchical pore structure reasonably is extremely important. Fig.3.19 (b) shows the sound absorption coefficient curve with different perforated diameters of multiple parallel through holes. The results show that the maximum sound absorption coefficient increases with the increase of perforation diameter. At the same time, the overall sound absorption coefficient also increases slightly while the characteristic of the curve does not change a lot.

Fig.3.19 (c) and Fig.3.19 (d) show the influence of micro perforated plate (diameter of the pores and perforation rate), it is clear that increasing the diameter of the pore and perforation rate can increase the sound absorption ability in entire frequency.

Then, the influence of the thickness of the micro perforated plate is studied (As shown in Fig.3.19 (e)). The results show that the sound absorption ability decreases significantly with the increase of the thickness of the micro perforated plate. In addition, the sound absorption performance of the structure increases slightly at low frequency with the increase of the thickness, but the performance is not obvious.

At last, the porosity of the porous materials is investigated to show the influence of the porous materials type (as shown in Fig.3.19 (f)). The sound absorption curve does not change a lot with different porosity. However, it should be noted that this does not mean the porous materials aren't important in the structure as porous materials have many other parameters (e.g. diameter of the pores inside the porous materials, tortuosity), this phenomenon just gives a refer that we can choose the porous with high porosity to obtain a lower weight.

3.5 Conclusion

In this chapter, a micro perforated sandwich panel with a honeycomb-hierarchical pore structure core has been developed. This structure combines a porous material with a hierarchical pore structure and a micro perforated sandwich panel with a honeycomb core together to achieve a lightweight broadband sound absorbing structure. Experimental results show that the structure can absorb sound in the range 200-6000Hz effectively, with an average sound absorption coefficient of 0.626 ± 0.028 . Theoretical and FEA models have been established to predictively calculate the sound absorption performance of

such structures, showing agreement with experiment results (16.8% and 8.6% error respectively). The related parameters are investigated by the theoretical model, and the results showed that the parameters of the micro perforated plate (diameter of the pores, perforation rate, thickness) will significantly affect the sound absorption ability of the structure. In conclusion, although the method that adding porous materials into a honeycomb would inevitably increase the weight of the structure, this structure is useful for situations that are not highly sensitive to the weight (e.g. expressway, factory, elevator). Meanwhile, the hierarchical pore structure can increase the sound absorption ability without increasing the weight is based on the structure that already added. We foresee this work can be a better replacement structure for traditional micro perforated plate structures.

Chapter 4 Sound Absorption Performance of Folded Structures Prepared from Woven Prepreg and Porous Materials Composites

Previous work has shown that the combination of a micro perforated plate and porous materials is an effective way to realize broadband sound absorption. However, the improvement of the traditional micro perforated plate-honeycomb structure has a limited weight that the weight cannot be less than traditional MPP-honeycomb structure, and the manufacturing is a little complex especially when adding porous materials into honeycomb cells. Therefore, there should be a new design method to achieve high sound absorption ability, lightweight, and easy production. Meanwhile, the ancient art of paper folding has been recently employed for sound-absorbing structures because of its excellent design flexibility and fabricability [212-220]. Compared with conventional honeycomb structures, folded structures can provide an open channel to absorb sound rather than a closed cell. However, only a few studies applied the method in structure design despite showing great potential in the acoustic field. In most conditions, the origami structure just be used as a sound absorption component rather than a load-bearing structure[221-223]. Yu et al. [152] combined a folded structure and a micro perforated plate to construct a resonant sound absorber, analyzing the effect of the depth and shape of the folded structure on the sound absorption performance of the whole structure. The results showed that the change of

folding angle can move the insert loss curve peak frequency, which means the sound absorption performance of the structure can be adjusted by the required condition.

Meanwhile, the replacement of a micro perforated plate with a woven fabric can reduce weight with little effect on the sound absorption characteristics of the structure[155, 156, 159, 160, 224]. Hence, this chapter hopes to combine porous materials with woven preregs to make structural and functional composite materials. Furthermore, this study also forms the composite materials into a folded structure for further improvements to its sound absorption performance. A theoretical model for the sound absorption performance is also established and experimentally verified for the novel structures.

4.1 Experiment

In order to determine the influence of the composite materials and folded structure on sound absorption performance, three test samples of woven prepreg, composite materials, and folded structure were prepared. The sound absorption coefficients of different structures with the same thickness were tested through impedance tubes.

4.1.1 Materials and fabrication

Ventilated felt made from jute fiber (315 g/m²) and a woven ramie prepreg (shown in Fig. 4.1) were chosen for the composite due to their high porosity, air permeability, and sustainability. Ventilated felt is made in the laboratory [225], and the woven prepreg is AGMP/ramie fabric. Epoxy resin AGMP 3600 applied

by AVIC Composite Co., Ltd (Beijing, China) and ramie fabric bought from Hunan Huasheng Dongting Ramie Co., Ltd. The woven prepreg was made by the wet method in the laboratory. A hot press (as shown in Fig. 4.2) was used to fuse the two materials together with 2 mm thickness to form the woven ramie-porous composite materials shown in Fig. 4.3. To manufacture the composite materials, two woven prepreg are put on the top and bottom surface of the ventilated felt at first, and then put the iron bar with 2mm thickness around the composite materials to control the thickness. At last, use the hot press machine to press them together. The thickness is determined according to the initial thickness of the ventilated felt to ensure the composite can be made in an accurate thickness and easy fold. Although increasing the thickness of the composite will increase the sound absorption ability. The excessive thickness will lead to an increase in the weight and difficulty in manufacturing. Therefore, the thickness was chosen to be 2mm after comparing with 1mm, 3mm, and 4mm samples.

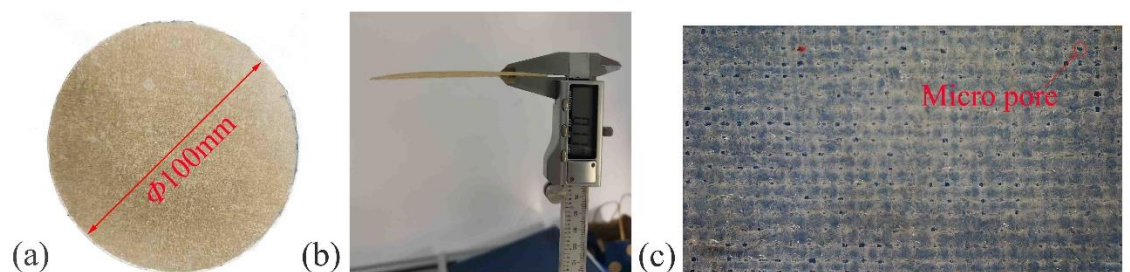


Fig. 4.1: Woven ramie prepreg:(a) Vertical view;(b) Front view;(c) Microscopic view.



Fig. 4.2 Hot-press machine.

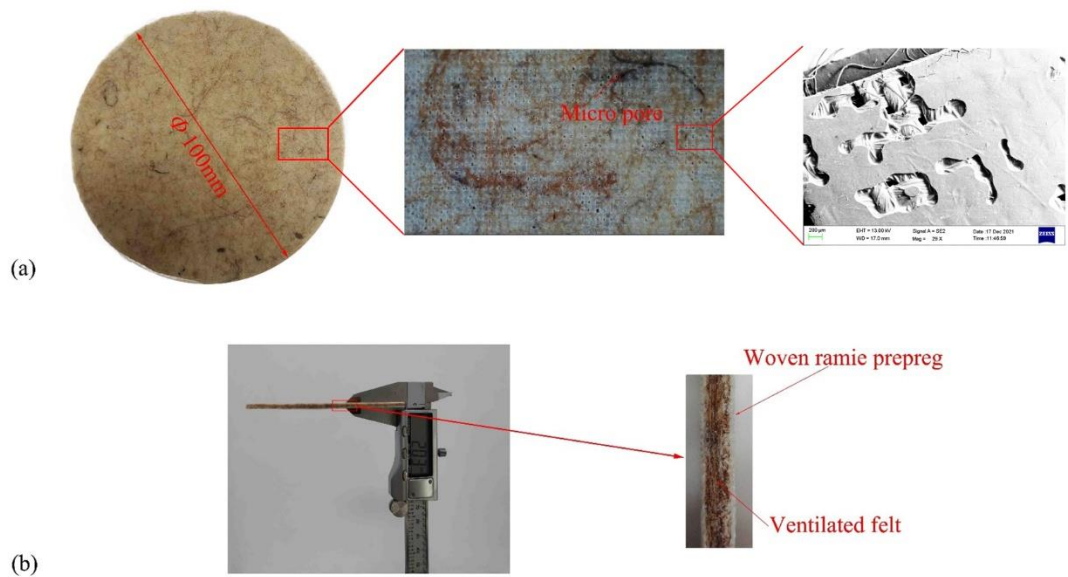


Fig. 4.3: Composite materials:(a) Vertical view and microscopic view (b) Front view and microscopic view.

The composite materials were then folded into their final form structure as shown in Fig. 4.4(a). The parameter values are decided according to better sound

absorption performance and simple manufacturing. The reason why we want to use the folded structure is because the incline wall can utilize the sound absorption ability of the composite materials. The height of the folded structure will determine the thickness of the porous materials in the inclined wall. Therefore, the height of the structure (H) is determined to be 50 mm at first because 50 mm is a common height for sound absorption structure (as shown in Fig.3.8) so that we can have an intuitive impression to judge whether this structure achieves a good sound absorption performance. Then the folded angle and length of the edge are determined according to the diameter of the impedance tube. If we want to test the sound absorption coefficient of the structure we need to put at least one minimum cell into the impedance tube, which means the edge of the folded structure should not make the cell larger than 100 mm. At the same time, the thickness of the composite (2mm) limits the minimum size of the edge, otherwise, the folded process will damage the composites or make the structure cannot be kept in an accurate condition because of the elasticity of the porous materials. According to the 3D model in Solidworks, the geometric parameters are determined as Fig. 4.4(b) and Table 4.1 show.

Both the top face sheet and the folded core structure were made of composite materials. The bottom face sheet would be a rigid panel, which was replaced by the bottom of the impedance tube in the actual testing process. It should be noted that as the prepreg cannot be folded after solidification, the prepreg and ventilated felt needed to be pressed at 90°C and folded before final

curing in an oven at 150°C for 3 hours. The final structure is shown in Fig. 4.5. Since the 30 mm diameter impedance tube was used for high frequency (1000-6000 Hz) testing, the folded structure would not fit in the impedance tube completely. Therefore, according to the sound absorption characteristics of the structure, a 60° inclined composite materials plate (determined by the theoretical model in Section 3.2), was used to represent the 60° folded structure for the high-frequency sound absorption test. Ultimately, sound absorption tests were carried out for the flat woven prepreg, and the flat composite materials, in addition to the folded structure.

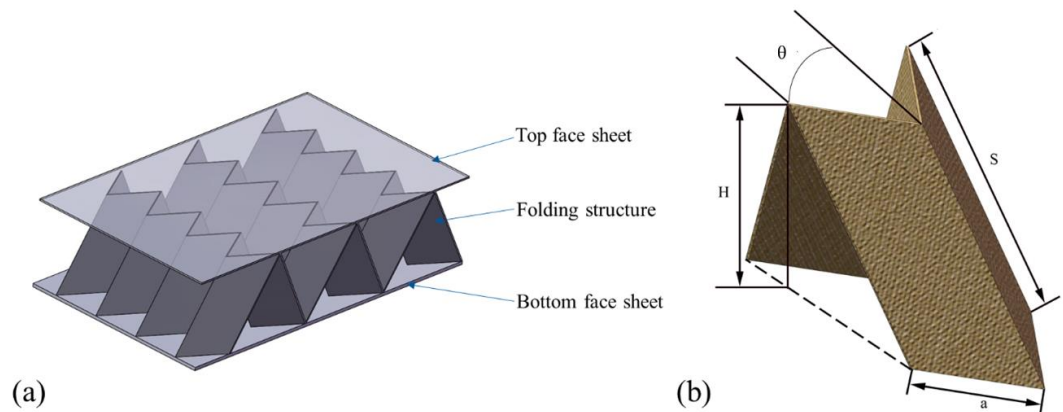


Fig. 4.4 3D-models of: (a) the folded structure and; (b) the geometric parameters of the folded structure unit cell.

Table 4.1: Geometric parameters of the folded structure unit cell.

Geometric parameter	Value
Height of the structure, H (mm)	50
Length of the edge, S (mm)	60
Length of the edge, a (mm)	30
The folding angle, θ	55°

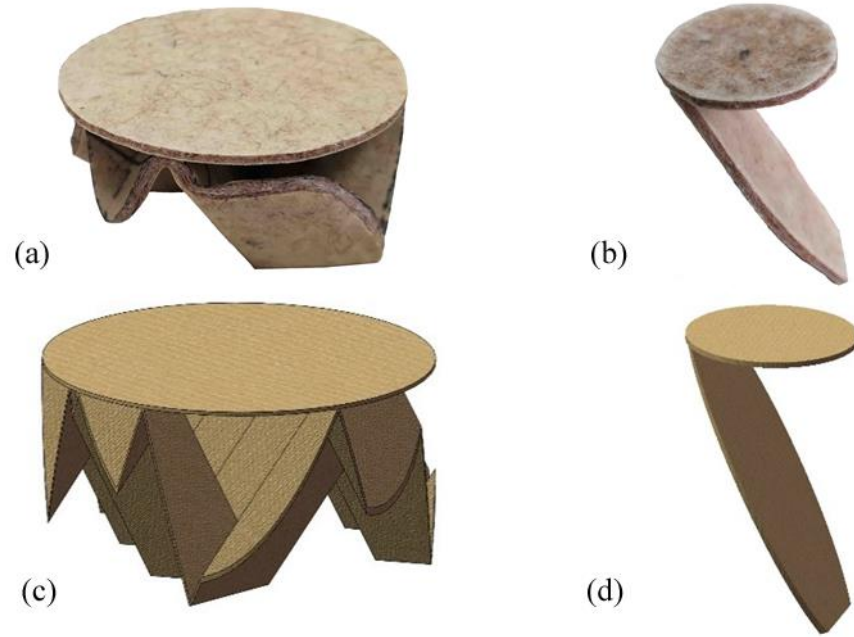


Fig. 4.5: Folded structure samples for sound absorption tests: (a) at low frequency, (b) at high frequency, (c) 3D model of low frequency sample, (d) 3D model of high frequency sample.

4.1.2 Sound absorption test system

The sound absorption performance test was carried out according to the ISO 10534-2 standard [207] through an impedance tube test system shown in Fig. 4.6. A large (100 mm diameter) and a small (30 mm) impedance tube were used to test the sound absorption coefficient of the different structures in the 63-1600 Hz and 1000-6300 Hz frequency ranges respectively. Therefore, two different sample types with diameters of 30 mm and 100 mm were prepared for characterization over the full 63-6300 Hz range.

In setting up the experiment, each of the woven prepreg and composite materials samples was placed in the impedance tube such that there was a 50 mm long cavity behind them, to be consistent with the height of the folded structure (as shown in Fig. 4.7(b)).

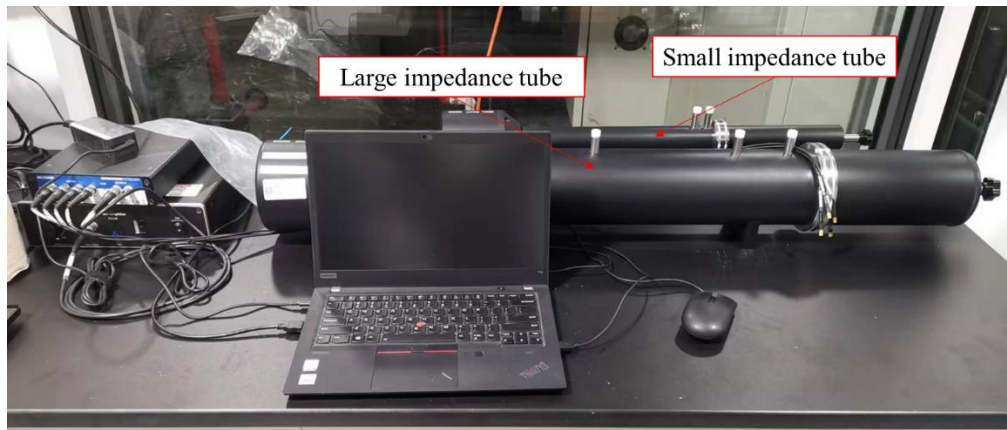


Fig. 4.6: Sound absorption test system.

4.1.3 Experimental results

The test results are shown in Fig. 4.7. An 'average sound absorption coefficient' is often used to evaluate and compare the sound absorption ability of different materials, based on absorption coefficient values taken at six discrete points across the acoustic spectrum (125, 250, 500, 1000, 2000, and 4000 Hz) [3]. In this study, the average sound absorption coefficients of the woven prepreg, composite materials, and folded structure are 0.360, 0.562, and 0.491 respectively. Suggesting the composite materials to be the best sound absorbing structure. However, across the continuous sound absorption spectrum it is obvious that folded structure has a better sound absorption performance than composite materials from Fig. 4.7.

Hence, for this study, the magnitudes of peaks and troughs are used as a more reliable comparison of the different materials and structures instead. The maximum sound absorption coefficient of the woven prepreg is 0.78 and the minimum sound absorption coefficient is 0.02. The composite materials show a

maximum sound absorption coefficient of 0.99, while the minimum sound absorption coefficient has only slightly increased to 0.07. Alternatively, the sound absorption characteristics of the folded structure have shown a slight decrease in the second absorption peak (to 0.83), but the absolute minimum sound absorption coefficient has greatly improved to 0.43. Hence the structural sound absorption coefficient remains above 0.4 in the complete range of 400-6300 Hz, realizing broadband sound absorption.

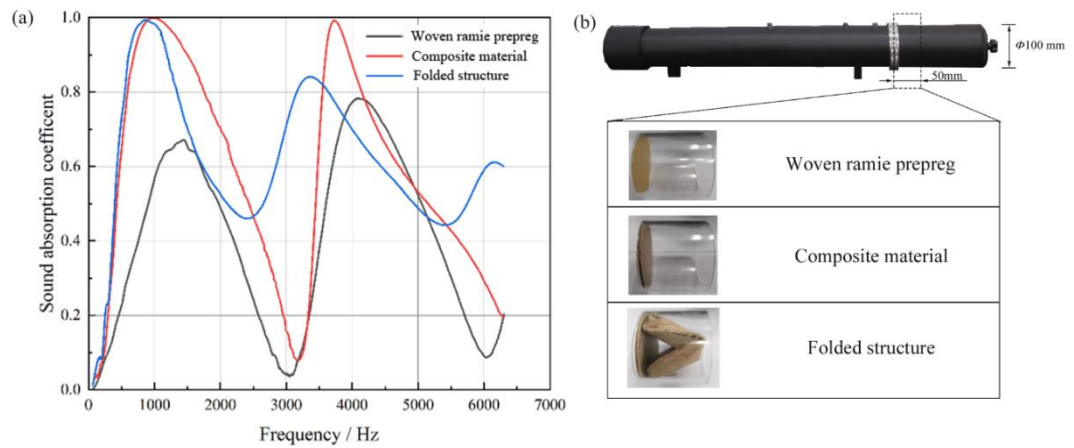


Fig. 4.7: The influence of different materials and structures on sound absorption ability: (a) sound absorption coefficient curves, and (b) experimental setup.

It can be found that although Chapter 3 and Chapter 4 both use micro perforated plates and porous materials to achieve sound absorption, they represent significant differences in sound absorption characteristics. This is mainly caused by the thickness and pore size of the micro perforated plate, the extremely thin thickness and small pore size make the micro perforated plate in Chapter 4 have higher and more compact peaks. In addition, the thickness of porous materials in Chapter 4 also makes it not obvious which makes the curve have obvious troughs. The folded structure using an inclined plate makes up so

that the blue curve in Fig 4.7 can have much higher troughs.

4.2 Theoretical Model

In order to establish a theoretical model of the 3D folded structure, it was first simplified to a 2D minimum unit cell and equivalent model as shown in Fig. 4.8. This simplified model is composed of a top face sheet, a middle-inclined plate, and a bottom face sheet. The top face sheet and middle inclined plate are made from composite materials, and the bottom face sheet is a rigid plate. Since the composite materials are formed by sandwiching the ventilated felt between the surface layers of the woven prepreg, the composite materials can be further approximated by upper and lower micro perforated plates and a porous material in the middle. The perforation ratio of the micro perforated plate can be determined from images taken with an SEM (as shown in Fig. 4.3).

Since the thickness of the bottom air cavity is less than the wavelength, the sound wave mainly propagates along the axis. At this time, the specific acoustics impedance of the micro perforated plate can be regarded as the combination of many Helmholtz resonances (as shown in Fig. 4.9(b) and (c)). It can be found that whether the plate is inclined or not will not affect the formula of Z_1 . Therefore, the formula of the specific acoustics impedance of the micro perforated plate will not change when the plate is inclined. Meanwhile, the cavity forms a resonance system with a micro perforated plate. It also can be regarded as a Helmholtz resonance and the volume of the cavity rather than the shape will determine the acoustic compliance which affects the sound absorption ability of

the system. Therefore, this research regarded the inclined plate as a flat plate in this study.

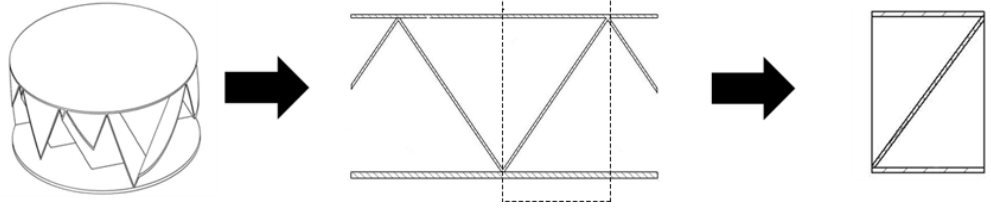


Fig. 4.8: Extracting the minimum unit cell of the structure.

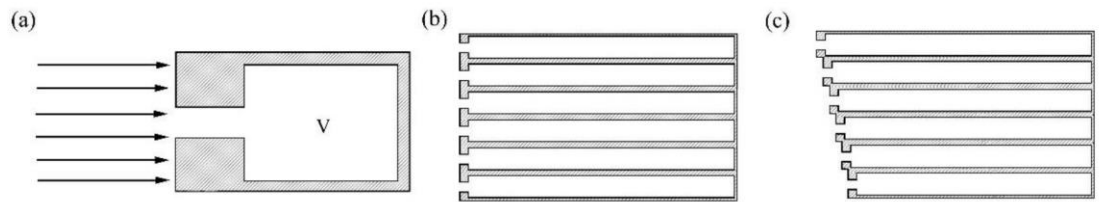


Fig. 4.9 The sketch of different structures: (a) Helmholtz resonance (b) Micro perforated plate structure with a flat plate (c) Micro perforated plate structure with an inclined plate

In this condition, the inclined plate that divides the cell into two cavities can be considered equivalent to a flat plate, and its position can be related to the cavity volume and incident surface area. The specific formulas are:

$$D_2 = \frac{V_2}{S_2} \quad (4.1)$$

$$D_1 = D - D_2 - 2t_2 \quad (4.2)$$

where D is the height of the whole structure, D_2 and D_1 are the height of the upper and lower cavities in the equivalent model respectively, S_2 is the area of the inclined plate, V_2 is the volume of the lower cavity and t_2 is the thickness of the composite materials. It should be noted that since the internal flat plate is transferred from an inclined condition, the thickness needs to be adjusted according to the inclination angle in the calculations.

In this way, a sound absorption model of the folded structure can be generated as shown in Fig. 4.10, and the theoretical sound absorption coefficient of the structure can be obtained by measuring the acoustic impedance of the equivalent model. It should be noted that the equivalent model ignores local experimental differences between the edge of the experimental sample and the minimum unit cell, as the effects are expected to be negligible.

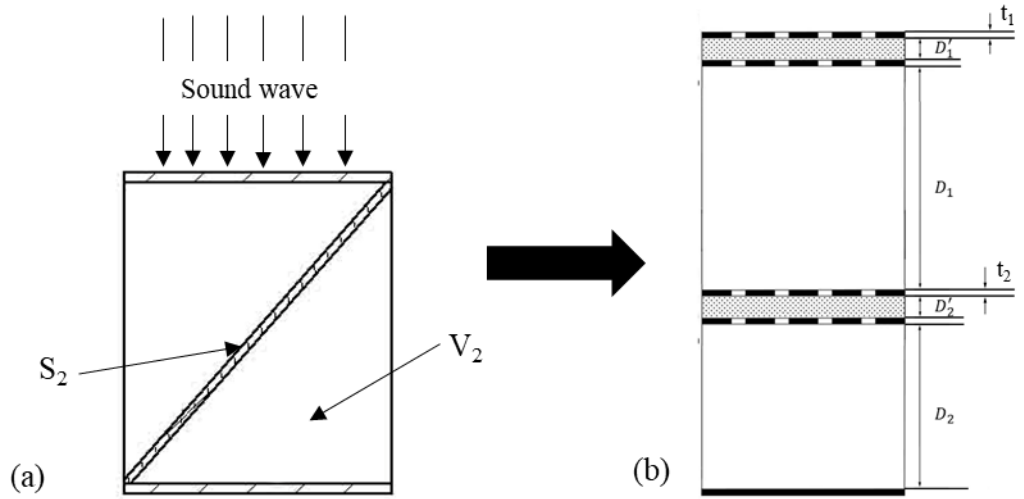


Fig. 4.10: The simplified model of the folded structure: (a) Minimum cell of the folded structure, (b) The equivalent model of the folded structure.

The equivalent model shown in Fig. 4.10 (b) is clearly similar to a multi-layer micro perforated plate. As such, the transfer functions for the acoustic impedance of such models are well established [226]:

$$Z_{CN} = -jZ_0 \cot(kD_2) \quad (4.3)$$

$$Z_{Cn} = Z_0 \frac{Z_{n+1} \cos(kD_n) + jZ_0 \sin(kD_n)}{Z_0 \cos(kD_n) + jZ_{n+1} \sin(kD_n)} \quad (4.4)$$

$$Z_n = Z_{mn} + Z_{Cn} \quad (4.5)$$

where Z_{CN} is the specific acoustic impedance of the bottom cavity of the

structure, $Z_0 = \rho_0 c_0$ is the specific acoustic impedance of the air, and Z_n and Z_{cn} are the specific acoustic impedance of the location of the cavity and the micro perforated plate respectively.

Lastly, Z_{mn} is the specific acoustic impedance of the micro perforated plate itself with the following formula [62]:

$$Z_{mn} = \frac{32\rho_0\mu t}{pd_1^2} \sqrt{1 + \frac{x_1^2}{32}} + j\omega\rho_0 t \left(1 + \frac{1}{\sqrt{32 + \frac{x_1^2}{2}}} \right) \quad (4.6)$$

$$x_1 = \sqrt{\frac{\omega d_1}{\mu} \frac{d_1}{2}} \quad (4.7)$$

where d_1 is the diameter of perforation in woven prepreg, t is the thickness of the woven prepreg, $\mu = \eta/\rho_0$ is the kinematic viscosity of the air, η is the dynamic viscosity constant of air.

However, in this research, the structure is represented by two porous materials parts between the micro perforated plates, which is a significant deviation from the standard theory for a multi-layer micro perforated plate system. Therefore, an additional transfer function is required. The specific acoustic impedance for the porous materials can be calculated by the following formulas [3]:

$$Z_s = jZ_0 \frac{jZ_p + Z_t \cot k l}{jZ_p \cot k l - Z_t} \quad (4.8)$$

$$Z_p = \sqrt{K\rho} \quad (4.9)$$

$$k = \omega\sqrt{K/\rho} \quad (4.10)$$

where Z_t is the specific acoustic impedance of the structures between the

porous materials and the rigid back wall, ρ is the complex density of the porous materials, and K is the complex compression modulus of the porous materials.

The complex density ρ can be written as:

$$\rho = \frac{s\rho_0}{\phi} \left[1 + \left(3^2 + \frac{x_2^2}{2} \right)^{-\frac{1}{2}} + \frac{32}{j\omega\rho_0 d_2^2} \left(1 + \frac{x_2^2}{2} \right)^{\frac{1}{2}} \right] \quad (4.11)$$

where $x_2 = \sqrt{\frac{\omega}{\mu}} \frac{d_2}{2}$, d_2 is the pore diameter of porous materials, ϕ is the porosity of porous materials, and s is the structural factor. For ordinary porous materials, the structural factor is generally taken as 3 [3].

K is the compression modulus of the tube per unit thickness which can be calculated by:

$$K = P_0 \left[1 + \frac{1}{8} (\gamma - 1) \frac{j\omega d^2}{4\nu} \right] \quad (4.12)$$

where γ is the specific heat ratio of the air, d is the diameter of the pores in porous materials, and ν is the kinetic viscosity of the air.

The full composition of the equivalent model for the folded structure is shown in Fig. 4.11. According to Equations (3.3-3.12), the specific acoustic impedance of the different components can be calculated from Z_{C4} to Z_1 step by step, and finally the specific acoustic impedance of the whole structure Z_1 can be calculated. Then substitute the specific impedance of the structure Z_1 into the formula:

$$\alpha = 1 - \left| \frac{Z_1 - \rho_0 c_0}{Z_1 + \rho_0 c_0} \right| \quad (4.13)$$

The sound absorption coefficient (α) of the structure at different frequencies can be obtained.

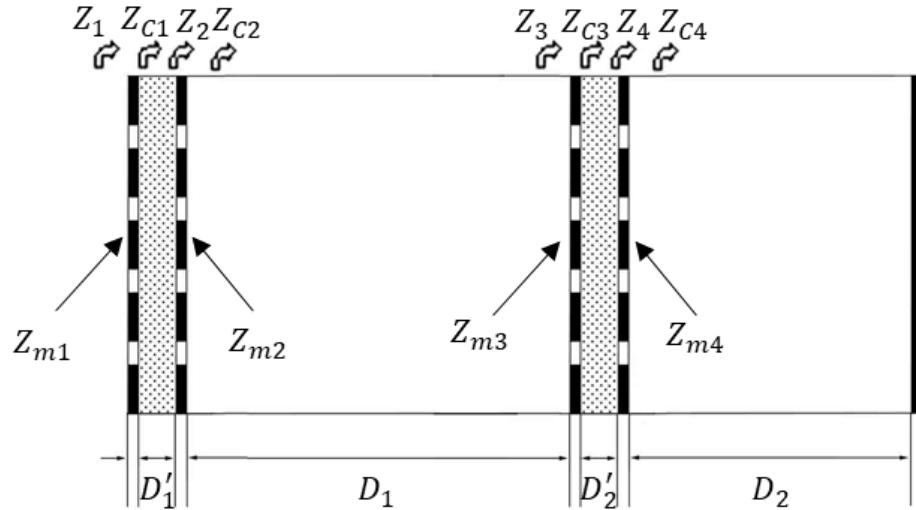


Fig. 4.11: Analytical diagram of the equivalent model for the folded structure.

Substitute the transfer functions into MATLAB for calculation, the relevant data are shown in table 4.2. The experimental results of the sound absorption coefficient of the folded structure are shown in Fig. 4.12 (compared against the theoretical results). Three absorption peaks appear at 874 Hz (1040 Hz theoretical), 3390 Hz (3440 Hz), and 6156 Hz (6050 Hz) for the folded structure with 19%, 1.5%, and 1.7% error respectively. Meanwhile, the magnitude of the first 2 sound absorption peaks differed by less than 1% between the experimental and theoretical results, however, greater error (27%) was observed for the third peak above 4500 Hz. Additionally, by removing the internal layer of the equivalent structure, the theoretical model can be used to calculate the sound absorption ability of unfolded composite materials alone, with results shown in Fig. 4.13. In both cases, the theoretical model results are in strong qualitative and quantitative agreement with the experimental results. Hence, the analytical model can accurately reflect the sound absorption characteristics of the structure.

However, there still some discrepancies exist, especially at the third absorption peak in Fig. 4.12 and the second trough in Fig. 4.13. We attribute the mismatch to the assumption of considering the woven prepreg as a micro perforated plate in the theoretical model. For a normal micro perforated plate, the sound wave can only pass through the plate via the perforation holes, but the woven prepreg can also let the sound wave pass through the fabric. This phenomenon, as observed in both Fig. 4.12 and Fig. 4.13) will be more obvious at high frequencies where the wavelength becomes shorter.

Table 4.2: Relevant parameters of the theoretical model.

Property	Value
Air density, ρ_0 (Kg/m ³)	1.293
Atmosphere pressure, P_0 (Pa)	1.01×10^5
Dynamic viscosity of air, η	1.85×10^{-5}
The specific heat ratio of air, γ	1.4
Thickness of the cavity, D_1 (m)	0.0117
Thickness of the cavity, D_2 (m)	0.0363
Porosity of porous materials, ϕ	0.8
Thickness of woven prepreg, t_1 (mm)	0.1
Thickness of woven prepreg, t_2 (mm)	0.1
Thickness of porous materials, D'_1 (m)	0.002
Thickness of porous materials, D'_2 (m)	0.002
Diameter of perforation, d_1 (mm)	0.1
Perforation ratio of the woven prepreg, p (%)	8.6
Pore diameter of porous materials d_2 (m)	0.00015

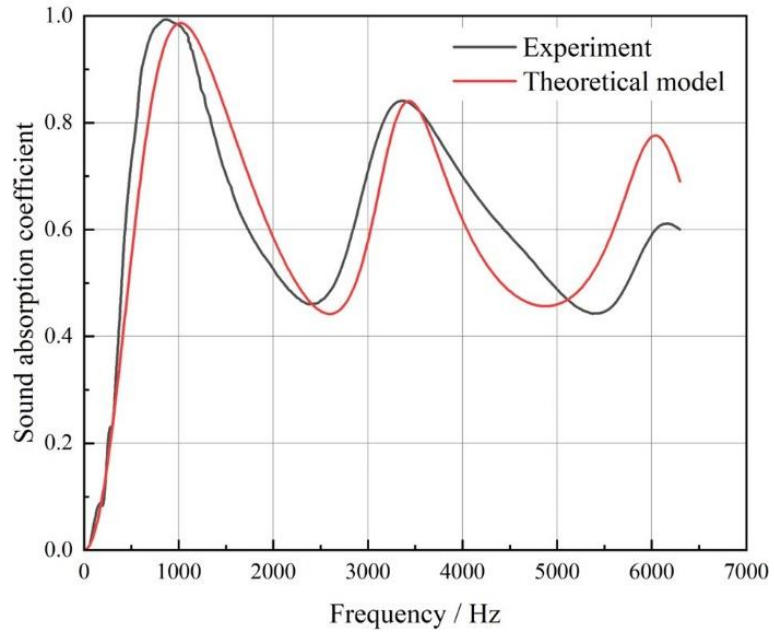


Fig. 4.12: The theoretical model and experimental results of the folded structure.

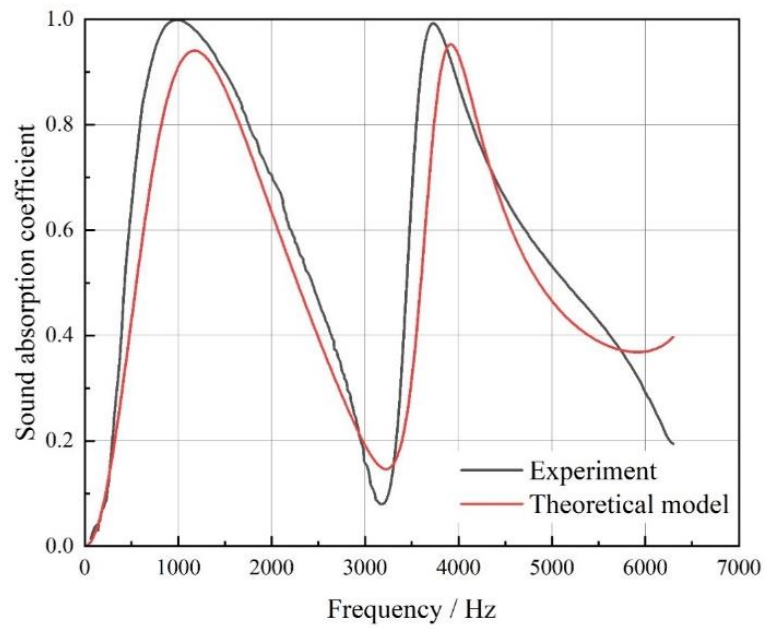
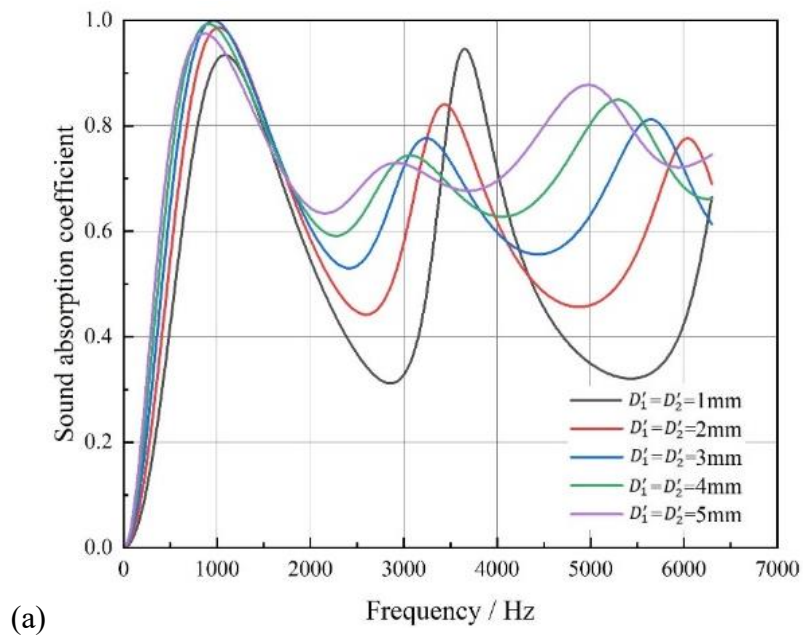


Fig. 4.13: The theoretical model and experimental results of the composite materials.

4.3 Parametric Investigation of Sound Absorption Performance

With the valid theoretical model, the influence of different structural design parameters on the sound absorption characteristics could be investigated. Firstly, the influence of composite materials thickness in the folded structure was

considered (as shown in Fig. 4.14). It should be noted that the thickness of the composite panel ‘t’ was not changed at this time, but only the thickness of the porous materials ‘ D_1 ’ and ‘ D_2 ’ inside the composite. From the Fig. 4.14(a), it can be seen that with increasing thickness, the sound absorption coefficient curve moves to a lower frequency, and the second absorption peak is declining while the third absorption peak is rising. Meanwhile, the minimum sound absorption coefficient of the curve is increasing from 0.32 to 0.62 with the thickness increasing from 1 mm to 5 mm. Additionally, Fig. 4.14(b) shows where the resistance (Re) is around 1 and the reactance (Im) is zero. Increasing the thickness of the composite will also increase resistance and make reactance closer to zero in most frequencies. Therefore, it can be concluded that increasing the thickness of composite materials can improve the sound absorption ability of the whole structure.



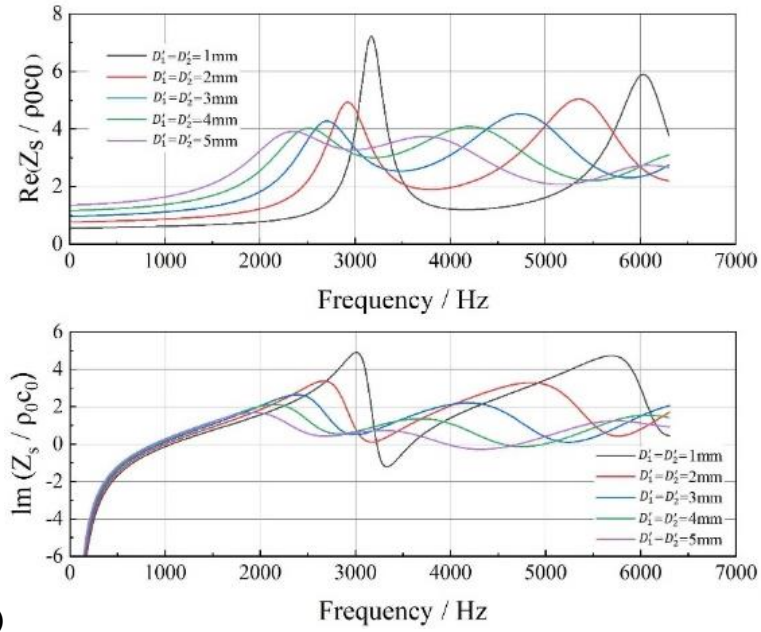


Fig. 4.14: The influence of the thickness of composite materials in folded structure on: (a) Sound absorption coefficient, and (b) The specific acoustic impedance (resistance, Re, and reactance, Im).

The influence of the height of the whole structure ‘H’ has also been studied parametrically (as shown in Fig. 4.15). It shows an interesting phenomenon that the height of the whole structure does not significantly affect the absolute maximum and minimum values, only changing the peak frequencies. With increasing height, the peak frequency moves to a lower frequency and the period of the curve decreases. This means the height of the whole structure will not affect the sound absorption ability but only the sound absorption characteristics of the structure.

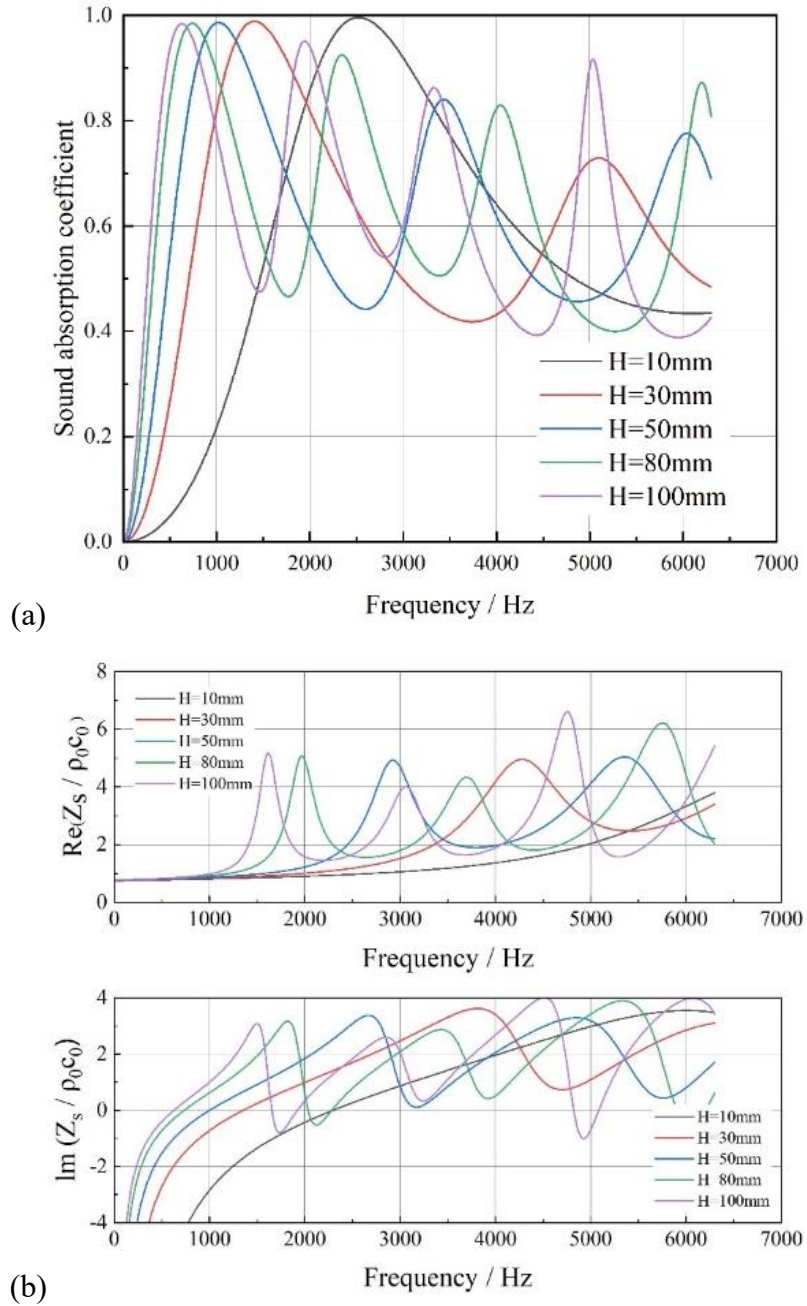


Fig. 4.15: The influence of the height of the whole structure on: (a) Sound absorption coefficient, and (b) The specific acoustic impedance (resistance, Re, and reactance, Im).

The height of the two cavities in the theoretical model can be effectively changed by changing the folding angle of the structure. Hence, the influence of the inner cavity height ‘ D_2 ’ on the sound absorption ability is considered at last in Fig. 4.16. It should be noted that the total height of the structure is not changed

in this process. The results show that there is no obvious difference in the sound absorption coefficient curve while the height increases. Thus, the folding angle should be considered for mechanical properties rather than sound absorption properties.

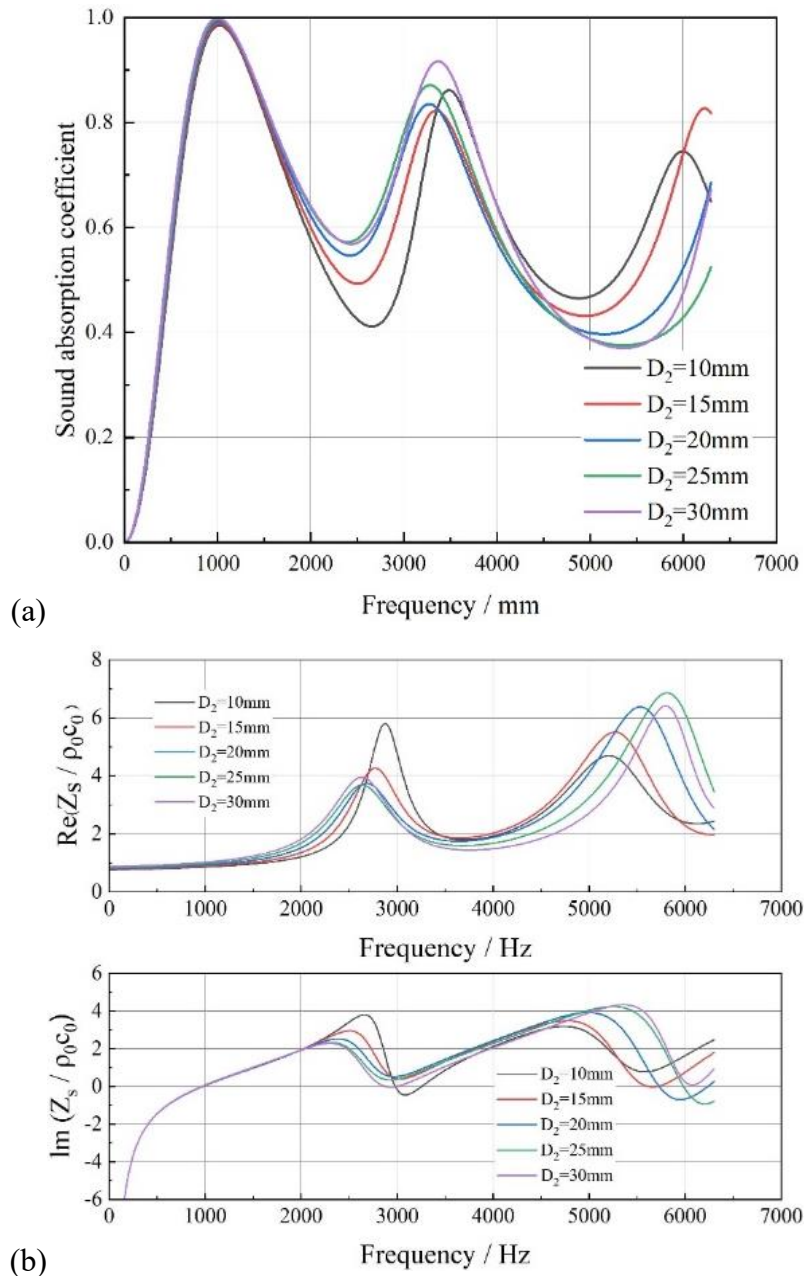


Fig. 4.16: The influence of the inner cavity height in folded structure on: (a) Sound absorption coefficient, and (b) The specific acoustic impedance (resistance, Re, and reactance, Im).

4.4 Conclusion

In this study, a composite material composed of woven prepreg and ventilated felt has been designed and prepared. The composite materials have also been processed to form a folded structure and the sound absorption performance of the structure and materials were experimentally tested. The results showed that compared with the woven prepreg the composite materials could significantly improve the sound absorption coefficient of the wave troughs in the sound absorption coefficient curve. Folding the composite into a structure can further improve the wave troughs in the sound absorption curve. The experimental results showed that the folded structure could maintain the sound absorption coefficient over 0.4 in the range of 400-6300 Hz, realizing broadband sound absorption. In addition, the corresponding theoretical model has been established according to the characteristics of the structure, and the calculation results showed good agreement with the experimental results. Lastly, according to the theoretical model, several key parameters in folded structure design have been analyzed with the following results:

(1) Increasing the thickness of the composite materials will shift the sound absorption curve to lower frequencies, increase the trough values, and reduce the peak values.

(2) The height of the whole structure will not affect the sound absorption ability but only the sound absorption characteristic of the structure.

(3) The folding angle of the folded structure does not significantly affect the sound absorption ability of the structure.

Because the composite is light and easy to produce, the materials can be widely used in interior decoration (e.g. rooms, cars, trains). At present, different porous materials are widely used in commercial areas to absorb sound. The composite proposed in this part can be a better replacement as it mixed micro perforated plate and porous materials in a simple method which makes it not only better absorb sound in resonance frequency but also keep a smooth surface (better appearance).

Chapter 5 A Novel Membrane-coupled Foldable Structure with Low Frequency Sound Absorption and Vibration Isolation Performance

From Chapter 4 it can be found that although folded structure can achieve sound absorption ability, it cannot bear load without a structure component. Therefore, Chapter 5 wants to use a rigid material as the structure frame component and the sound absorption can be achieved by the surface inside the frame component. In this situation, the membrane acoustic metamaterials is the best choice as it can achieve excellent sound absorption ability with a thin thickness.

Acoustic metamaterials are a kind of artificial material that contain sub-wavelength meta-atoms or microstructural units with a periodic arrangement, such as membrane resonators [98], space-coiling fractals [112], or porous metamaterials [36], to achieve excellent acoustic performance that cannot be found in natural materials [78]. These have proven effective for low frequency noise absorption as well [83-87]. Among such designs, Membrane Acoustics Metamaterials (MAMs) combine membranes and tiny rigid mass blocks to achieve improved sound absorption ability in low frequency ranges by negative mass density. Because of this, and their ultra-lightweight structure, many studies have been conducted to expand the application of MAMs. Xing et al. [103] developed a MAM with a negative pressure cavity. The experiment results

showed that the structure with a negative pressure cavity, showing that it can obtain a higher absorption peak at low frequencies than a similar structure without negative pressure. Furthermore, the initial negative pressure could be tailored to target particular sound absorption frequencies. Lucas et al. [104] assembled membrane-type metamaterials of different shapes and sizes into larger panels for effective sound insulation, Using Finite Element models and experiments to validate the designs. It can be found that previous studies of MAM often pay much attention to sound absorption performance and ignore the load-carrying properties which is an important index in the application of sound absorption structure [79].

However, it is difficult to balance both the acoustic and mechanical performance of MAMs as they have some conflicting characteristics. For example, if the panel of micro perforated plate (MPP) honeycomb structure is replaced with a membrane, the structure will lose its ability to withstand bending [227]. Therefore, it is necessary to find a new strategy that can better combine MAMs and structural components to expand the application of these materials for noise absorbing structures. Origami-based foldable structures are widely used in sound absorption applications because of their excellent design flexibility and fabricability [152, 212-214]. Compared with traditional honeycomb structures, origami-based foldable structures have interconnected cavities rather than enclosed cavities which means the sound waves can be better absorbed. For example, Yu et al. [152] combined a micro-perforated membrane

with an origami sheet in order to form backing cavities and act as a resonant sound absorber. In their structure, the foldable origami sheet can adjust the shape and depth of the backing cavities during folding, enabling different sound absorption effects. This demonstrates the acoustic potential of the origami-based foldable structure.

In this study, the novel combination of a foldable frame structure with membrane-type acoustic metamaterials panels is proposed to achieve the unification of acoustic and mechanical performance.

5.1 Materials and Methods

5.1.1 Materials

In order to prepare the complex foldable structures suitable for the size of impedance tubes, relatively versatile and easy to manufacture materials with good properties were required. Hence, a modified polylactic acid (PLA+, Shenzhen Esun Industrial Co., Ltd.) was used in this research as the frame material for the foldable structure. Because the membrane resonator is highly sensitive to the membrane tension, the Polyolefin Film (POF) was used to cover the frame and act as the sound-absorbing membrane material. After the POF membrane is bonded on the frames, all the frames will be put into the drying box for about 30s under 150°C to make the membranes have the same tension condition (as shown in Fig.5.1). Cylindrical steel blocks 1mm thick and 6mm, 8mm, or 10mm in diameter were bonded to the POF as mass blocks to improve the sound absorption performance. An aramid paper honeycomb with 50mm

thickness and 5.5mm side length was used as a conventional control structure for the mechanical and vibration isolation tests.



Fig. 5.1 The drying box

5.1.2 CAD models and 3D printing

CAD models of the whole folded structure were prepared according to the geometric parameters outlined in Fig. 5.2 (a). The 3D printed frame components were designed as a periodic foldable structure, consisting of several parallelograms. However, in order to fit within the diameter of the impedance tube (100mm), a suitable cylindrical slice of the repeating design from Fig. 5.2 (a) had to be modified and prepared for printing of the PLA frame components. Then, the frame, membrane, and mass block components were bonded together using cyanoacrylate glue and folded into the testing sample configuration shown in Fig. 5.2(b). Fig. 5.2(c) shows the folding process of the foldable structure connected by hinges. Besides, a POF membrane is also covered on the top of the structure to make the surface smooth and improve the sound absorption ability. Because at least one minimum cell should to put into the impedance tube, the

parameters of the height and edge length are kept as the Chapter 4 sets. The thickness of the frame is set to 2 mm to achieve a balance between weight and compression strength. At last, The height of the structure is 50mm, the minimum cell of the foldable frame is a parallelogram with 60mm length and 30mm width, the acute angle of the parallelogram is 60° and the folded angle is 55° . The frames were printed in 10 layers (20um in height), with 100% fill density at a speed of 30mm/s.

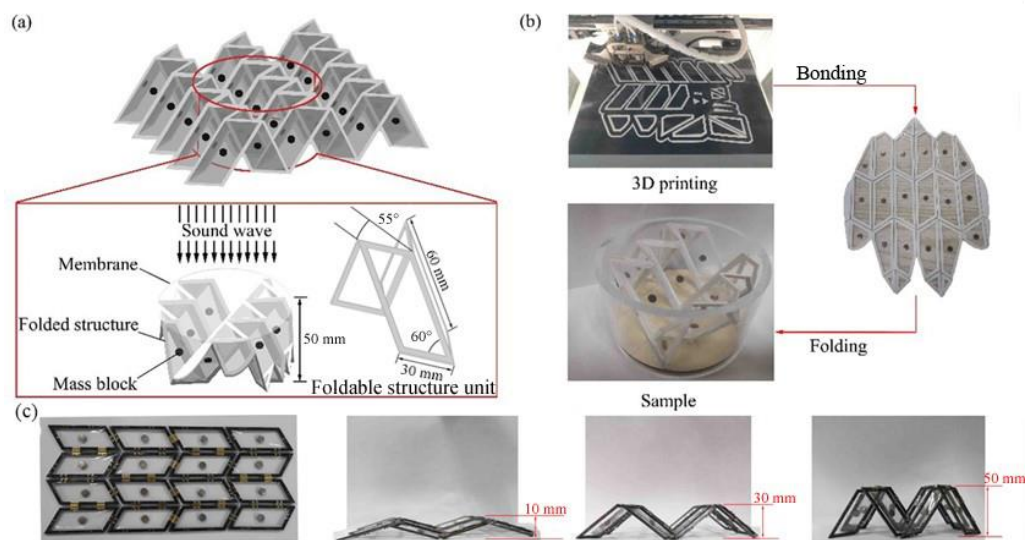


Fig. 5.2 Schematics of the foldable structure: (a) CAD model with dimensions and (b) the sample fabrication process.

5.1.3 Mechanical testing

Due to the foldable structure is a noise reduction structure, which is commonly used for parts such as fan inlets and outlets, and building surfaces that do not need to bear the main load. The foldable structure mainly bears the compressive load caused by its weight and the connection structure in the application. In addition, the foldable structure is bonded to the upper and the

bottom panel through resin or glue. When the structure receives tensile or shear forces, the strength of the structure mainly depends on the adhesive materials rather than the structure components. Therefore, only compression tests are conducted in mechanical testing. In order to compare the load-bearing capacity of the foldable and honeycomb structures, compressive mechanical testing was performed on an MTS E45 universal testing machine, with a -0.2mm/s constant rate of extension. The compressive stiffness and strength of the different structures were assessed according to the ASTM C 365/C 365M-05.

5.1.4 Sound absorption testing

The sound absorption test was carried out according to the ISO 10534-2 standard, using an SW 466 impedance tube testing system (Beijing Shengwang Acoustic-electric Technology Co., Ltd) with an internal diameter of 100mm, the details of it can be found in [228]. During the test, the sound wave with a range of 63-1600Hz was made by the speaker to test the sound absorption ability of the foldable structure in low frequency, and the data was collected by the microphone to calculate the sound absorption performance of the structure. In order to analyze the influence of the mass block, three different structures with 6mm, 8mm, and 10mm diameter mass blocks were tested.

5.1.5 Vibration isolation testing

The vibration isolation test system consisted of a vibration generator (m120-CE, IMV corporation, Japan), acceleration sensors (VP-32, IMV corporation, Japan), a data acquisition system (K2 sprint, IMV corporation,

Japan), and a power amplifier. Two acceleration sensors were fixed on the top and bottom surfaces of the structure respectively. The upper sensor was used to measure the acceleration of the structure and the bottom sensor was used to control the acceleration of the vibration generator. The bottom of the test sample was mechanically fastened to the vibration generator. Ultimately, the vibration isolation behaviour of the structure was obtained from the ratio of the upper and the bottom acceleration sensors.

5.1.6 Finite element modeling

The sound absorption characteristics of the foldable structure were analyzed in ANSYS using a Finite Element (FE) model consisting of Fluid30 (shown in purple in Fig. 5.3) and Shell181 (cyan) elements to simulate the air and membrane regions respectively. Solid181 (red) elements were used for the frame, mass block, and impedance tube components of the model, while the frame and impedance tube were considered as fixed boundaries. Fluid-structure interaction (FSI) was added between the Fluid30 elements and other elements. A sound source with 0.2Pa pressure was set in the impedance tube, and the model was meshed with 72156 elements. Hexahedral elements were used for the impedance tube while all other regions consisted of tetrahedral or triangular elements.

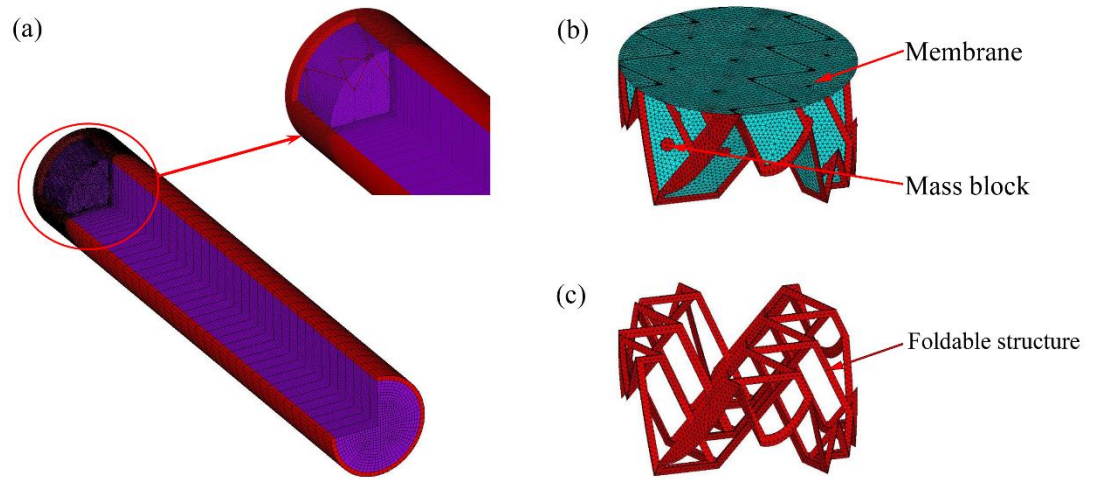


Fig. 5.3 FE model of the (a) impedance tube, (b) sound absorption structure, and (c) foldable frame structure.

5.2 Results and Discussion

5.2.1 Sound absorption performance

The results from sound absorption testing are shown in Fig. 5.4. It can be found that the sound absorption curve has a lower first absorption peak with the increase of the mass block diameters, which draws a similar result to the previous research [229]. The different mass block size has a similar sound absorption characteristic from an overall perspective (the average sound absorption coefficients of structure with 6 mm, 8 mm, and 10 mm diameter mass blocks are 0.227, 0.419, and 0.303). The different mass block sizes clearly produce different sound absorption peaks. There are four main sound absorption peaks for 6 mm and 8 mm type samples and three sound absorption peaks for 10 mm type sample (298 Hz, 688 Hz, 1160 Hz and 1362 Hz for 6mm type sample; 352 Hz, 764 Hz, 1228 Hz and 1568 Hz for 8mm type sample; 348 Hz, 764 Hz and 1230 Hz for 10mm type sample) and the peak is moved to a higher frequency with the

increase of the diameter of the mass block. The green curve is the testing results of the typical MPP-honeycomb structure as a comparison, it is clear that all the foldable metamaterials samples have a better sound absorption performance than it. At this time the average sound absorption coefficient of MPP-honeycomb structure is 0.201.

It can be found that although the mass block with a 6 mm diameter has the lowest sound absorption peak, it does not show a good sound absorption ability in a wide range. The sample with an 8 mm diameter mass block has the best sound absorption performance. When the diameter increased from 8 mm to 10 mm, the sound absorption coefficient decreased again. We assume this phenomenon is caused by the influence between frame size and diameter of the mass block. The increase in the diameter of the mass block will also lead to a decrease in the area of the membrane. Therefore, although the increase in the diameter of the mass block can promote sound absorption, when the diameter of the mass block exceeds a certain range, the smaller membrane area will lead to a weakening of the sound absorption effect.

Compared with the folded structure presented in Chapter 4, it can be found that although they use a similar structure, the sound absorption characteristics are totally different. Chapter 4 folded structure achieves sound absorption by the combination of MPP and porous materials. Compared with the membrane-mass block sound absorption structure, MPP also uses resonance to achieve sound absorption but both MPP and porous materials highly depend on the height to

obtain good sound absorption performance. The membrane-mass block structure is mainly determined by the membrane tension and the weight of the mass block. Therefore, the foldable does not rely on the height to keep a good sound absorption ability and we can see the different sound absorption characteristics in Chapter 4 and Chapter 5 structures as they have different sound absorption strategies.

At last, a finite element model was established to analyze the sound absorption performance of the foldable metamaterials. Fig. 5.5-5.7 show the test results between different test samples. The red arrows in Fig. 5.5-5.7 represent the positions of the peak frequency calculated by the finite element model (300 Hz, 660 Hz, 1140 Hz, 1400 Hz for 6mm type sample; 340 Hz, 800 Hz, 1200 Hz, 1550 Hz for 88mm type sample; 410 Hz, 830 Hz, 1320 Hz for 10mm type sample). The finite element results show a good agreement with the experiment results. Besides, it also shows that the foldable metamaterials have a higher sound absorption peak frequency with a larger mass block diameter. This feature is consistent with the experimental results.

Fig. 5.8(a) and Fig. 5.8(b) show the strain intensity of all membranes, and a single membrane, at a resonance frequency of 350 Hz. It is clear that in resonance frequency the strain at the mass block area is much less than in other places which proves the assumption that the area of the mass block will limit the strain of the membrane, and the resonance of the membrane was the main sound absorption method in the foldable metamaterials.

It can be concluded that resonance is the main sound absorption method in membrane-mass structures, where the sound energy is consumed by the vibration of the membranes and mass blocks [230, 231]. This is, therefore, most effective at the resonant frequencies, where the absorption peaks are observed and are well modeled by the FE simulations. Subsequently, the foldable metamaterials can achieve sound absorption in different frequencies by changing the diameter of the mass blocks, and the finite element model can help to choose suitable mass blocks to target absorption at specific frequencies.

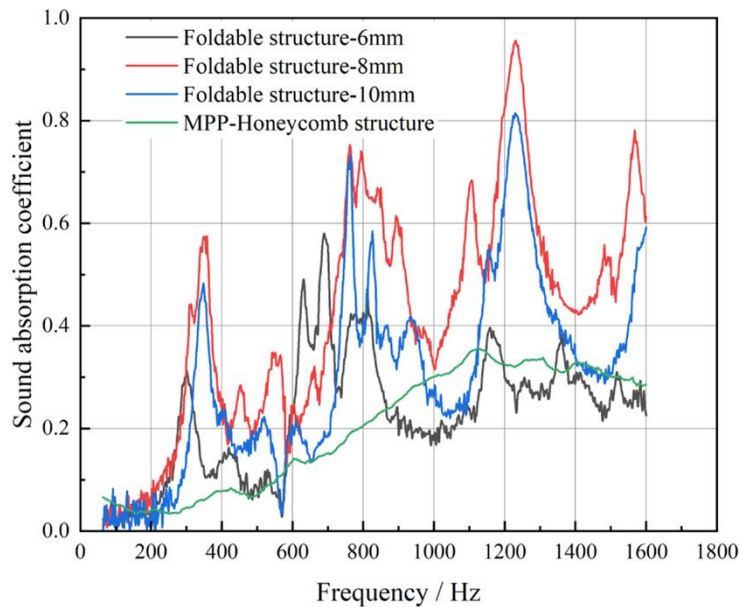


Fig. 5.4 The sound absorption coefficient of the foldable structure with different mass block diameters. The shadow around the curves shows the standard deviation from the mean of three samples.

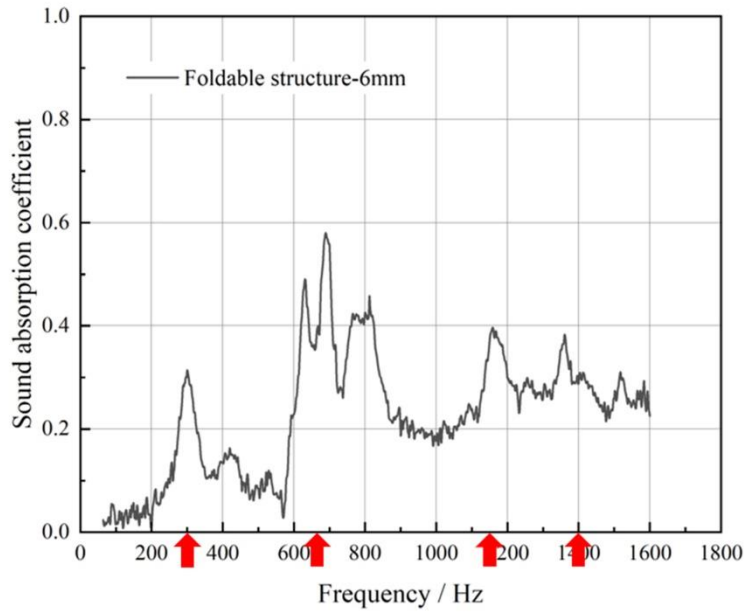


Fig. 5.5 The sound absorption coefficient curve of the foldable structure with 6mm mass block diameters. The red arrows show the positions of the sound absorption peak frequencies predicted by the finite element model.

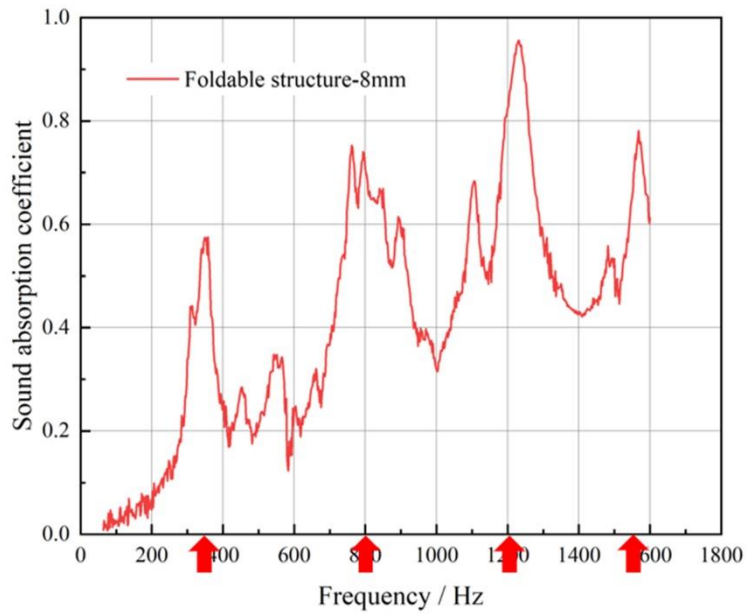


Fig. 5.6 The sound absorption coefficient curve of the foldable structure with 8mm mass block diameters. The red arrows show the positions of the sound absorption peak frequencies predicted by the finite element model.

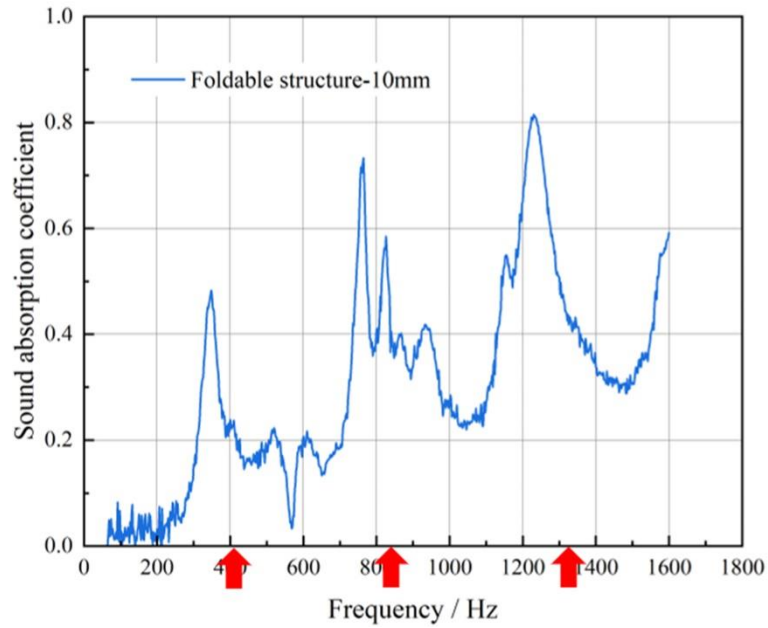


Fig. 5.7 The sound absorption coefficient curve of the foldable structure with 10mm mass block diameters. The red arrows show the positions of the sound absorption peak frequencies predicted by the finite element model.

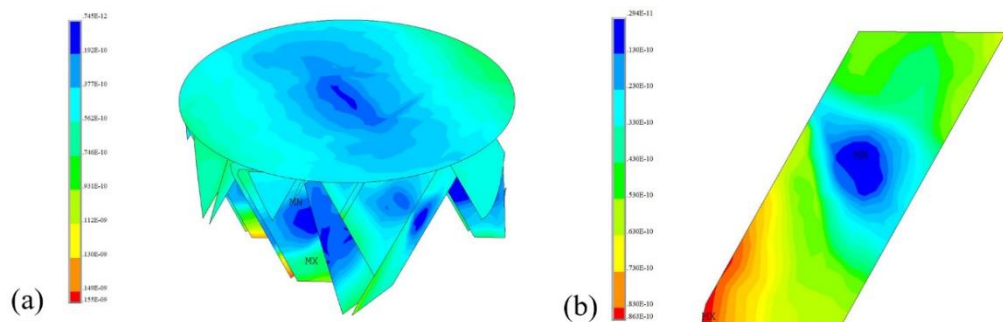


Fig. 5.8 The strain of the membrane in foldable structure with 8mm mass block (a) All membranes (b) One membrane.

5.2.2 *Vibration isolation test results*

The main noise transmission methods can be divided into air transmission and solid transmission. Hence, this study has also investigated the vibration isolation ability of the PLA foldable metamaterials since noise can also transmit through the structure itself. The honeycomb structure was used again as the

control structure to analyze the vibration isolation efficiency. Samples of both structures had the same cross-section area and height, while the 6mm diameter mass blocks were chosen for the foldable metamaterials. Aluminum plates were bonded to the top and bottom surfaces of the structures to better monitor the vibration of the structures.

The resonance frequency and vibration transmission coefficient were the main factors resulting from the vibration isolation tests. In order to compare with sound absorption performance, a vibration generator was used to apply a simple harmonic vibration from 10 Hz to 1600 Hz. The output acceleration was recorded by the upper acceleration sensor (as shown in Fig. 5.9(a)), and the input acceleration was kept at 3m/s^2 , controlled by the bottom acceleration sensor (Fig. 5.9(b)). Lastly, the vibration transmission coefficient was determined by the ratio of the output and the input accelerations in Equation 5.1:

$$T = \lg \frac{a_{out}}{a_{in}} \quad (5.1)$$

The vibration isolation test results can be seen in Fig. 5.9(c). This research mainly compared the first resonant peak of honeycomb structure and foldable structure which can directly indicate the vibration isolation performance. Here the resonance frequency of the honeycomb structure was much higher (750 Hz) than that of the foldable structure (350 Hz), indicating better vibration isolation in the foldable structure. This is attributed to the compliance of the foldable frame structure that allows for some bending and thus greater damping. Additionally, the resonance frequency of the foldable metamaterials (350 Hz) is

also the frequency of the first sound absorption peak in Fig. 5.4, which can also substantiate that the sound absorption ability of the foldable structure comes from its resonance.

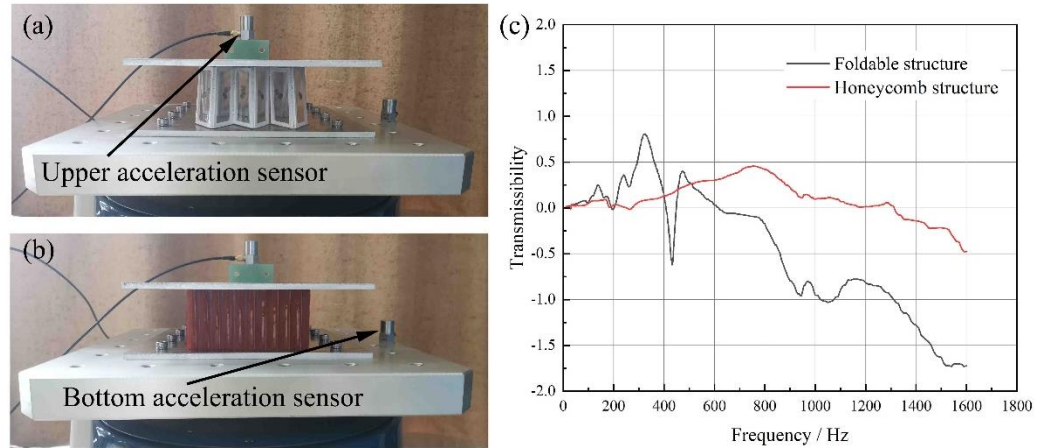


Fig. 5.9 Vibration isolation test: The testing sample of the (a) PLA foldable metamaterials and (b) honeycomb structure, along with the (c) transmissibility of both structures.

5.2.3 Mechanical performance

The combination of a honeycomb structure and a micro perforated plate is the most common design for dealing with transportation noise. Therefore, this configuration has been used as a control case, to evaluate the relative mechanical performance of the foldable metamaterials. Since the micro perforated plates do not affect the mechanical properties during compression and the compress strength is much larger than aramid honeycomb structure, only the honeycomb structure was tested. A minimum unit of the foldable metamaterials frame was extracted for testing convenience (shown in Fig. 5.10(a)), the honeycomb structure had the same area (18 cm^2) and height (50 mm) as the foldable structure sample (Fig. 5.10(b)). Three repeats were conducted for each sample type. Additionally, grooves were added to the bottom plate of the folded structure to

avoid sliding and to replicate a strong adhesive connection to a rigid surface, as would be the case in a real application.

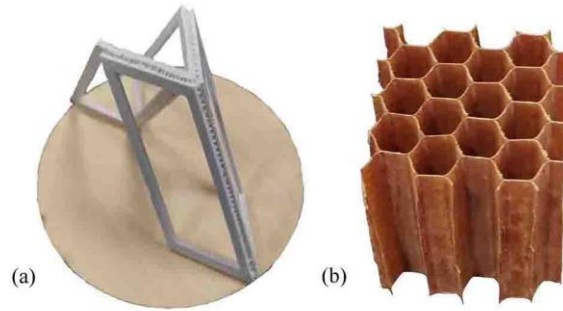


Fig. 5.10 Samples for mechanical testing: (a) Foldable structure (b) Honeycomb structure.

The formula (5.2) and (5.3) show the calculation method for compression strength and modulus:

$$\sigma = P_{max}/A \quad (5.2)$$

$$E = ((P_{50\%} - P_{25\%})/A)/((\delta_{50\%} - \delta_{25\%})/t) \quad (5.3)$$

where P_{max} is the max load before failure, A is the area of the sample, $\delta_{50\%}$ and $\delta_{25\%}$ are 50% and 25% max deflection value, $P_{50\%}$ and $P_{25\%}$ are loads corresponding to the deflection, and t is the thickness of the sample.

To ensure the compression testing of foldable metamaterials with one cell and several cells has the same results, the foldable metamaterials frame with four cells is also tested by a Universal Testing Machine (UTM) (as shown in Fig. 5.11), and the testing results showed that it has the same compression properties with the one cell sample.

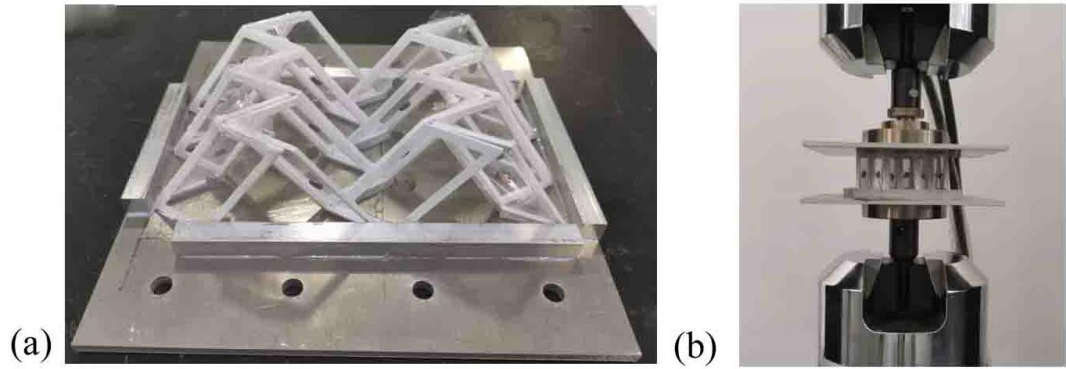


Fig. 5.11 The Compression testing of the foldable structures with several cells

Fig. 5.12 shows images of both samples from before (a) and after (b) compression testing, along with representative experimental load-extension curves (c). From these two curves, it is clear that the mechanical performance of the honeycomb structure is superior in terms of both stiffness and strength. As listed in Table 5.1, the modulus of the honeycomb structure was $117.67 \pm 19.67 \text{ MPa}$ while the modulus of the foldable metamaterials was $10.76 \pm 2.38 \text{ MPa}$. The compression strength of the two structures were $0.573 \pm 0.039 \text{ MPa}$ and $0.23 \pm 0.021 \text{ MPa}$ respectively. The poor performance of the foldable metamaterials in this case is attributed to the relatively soft PLA materials that make up the frame components. However, the ductile (4,5% failure strain) response of such a structure may still be of benefit for some applications.

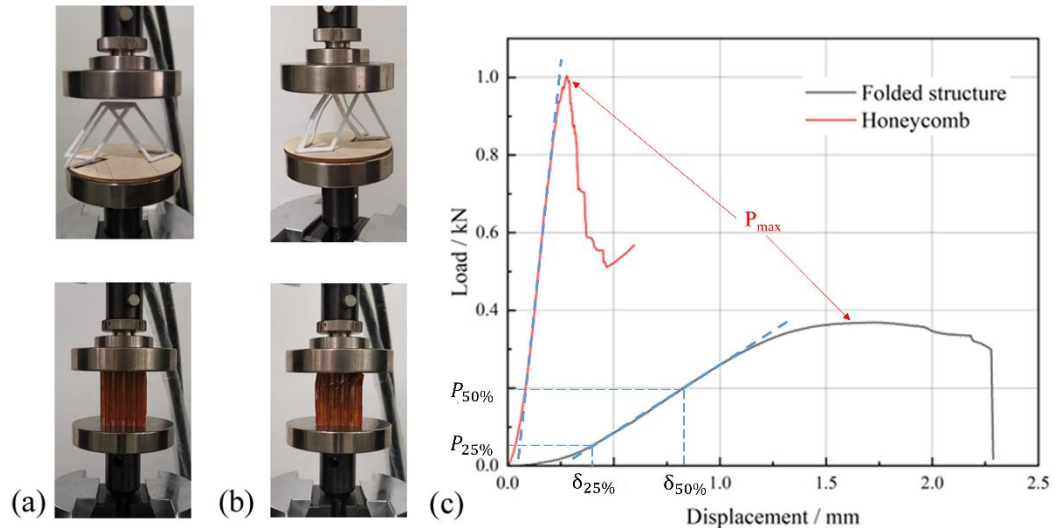


Fig. 5.12 Compression testing of the honeycomb and foldable structures: Images from the beginning (a) and end (b) of testing, along with the load-displacement curves of honeycomb and foldable structures (One group).

Fig. 5.13 and Fig. 5.14 show the foldable structures sample made by aluminum alloy and Carbon Fiber Reinforced Plastics (CFRP) respectively, the composites (bought from Well Advanced Materials Co., Ltd.) used T300 as the reinforced fiber and WP-R5600W3K as the matrix. A Stainless-steel plate with a triangle opening was used to fix the structure (As shown in Fig. 5.13(a)), the acrylic resin was used to bond the different frames together, Fig. 5.13(b) and Fig. 5.14(b) showed the CFRP and Al folded structure sample and Fig. 5.15 showed the one compressing testing results from three experiments. At last, the compressive strength and modulus of the Al foldable structure are 1.017 ± 0.14 MPa and 145.02 ± 13.15 MPa, the CFRP foldable structure is 3.34 ± 0.11 MPa and 233 ± 12.33 MPa which both are much larger than honeycomb structure. During the compression process, the structure showed bending deformation as the

parallelogram frame is connected at an oblique angle which explained the lower slope at the initial stage of the Load-Displacement curve. The initial failure of the Al foldable structure is because of the crack of the resin connection, after this, the structure can still bear the load of a large deformation by the plastic of the Al. When the CFRP foldable structure fails, the crack also first appears at the connection of the different parallelogram frame (the first drop in the Load-Displacement curve), and the structure is destroyed ultimately due to the fracture of the frame (the second drop in Load-Displacement curve).

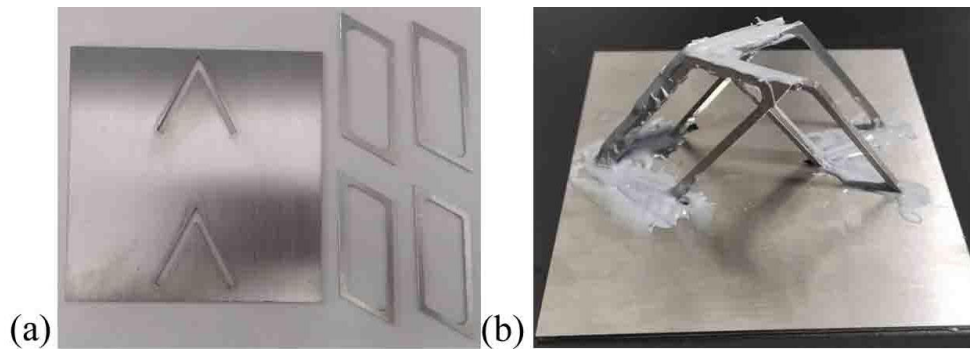


Fig. 5.13 Mechanical testing sample of Al sample: (a) Frame structure before assembly (b) Foldable structure

Table 5.1 shows the mechanical properties of the MPP-honeycomb structure and foldable structure made of Al and CFRP. Here, the weight of the foldable structure and honeycomb are obtained by weighting the testing sample while the weight of the MPP-Honeycomb structure is calculated through the density and volume of the structure. The MPP is assumed to be an aluminum alloy plate with an 8% perforation rate and 1mm thickness, with the density setting as 2.8g/cm^3 . Therefore, the weight of the micro perforated plate is 46.368g. The weight of the honeycomb is $4.20\pm 0.23\text{g}$, and the weight of the

CFRP foldable structure is $7.63 \pm 0.037\text{g}$ (with the 6mm diameter of the mass block). It can be found that although a honeycomb has a lighter weight, it needs to combine with a micro perforated plate to obtain sound absorption ability which would greatly increase its weight. This can be avoided by foldable structure because it mixes sound absorption structure and load-bearing structures together.

In conclusion, the CFRP foldable has much less weight than the traditional MPP-honeycomb structure while showing better mechanical properties. The strength and modulus are increased by 483% and 98%.

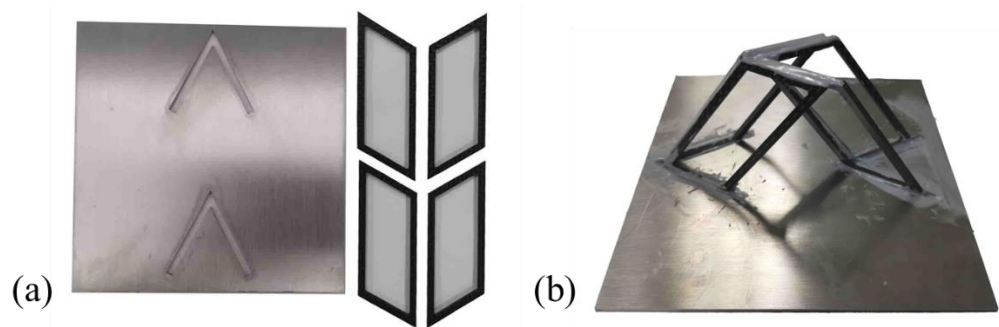


Fig. 5.14 Mechanical testing sample of CFRP sample: (a) Frame structure before assembly (b) Foldable structure.

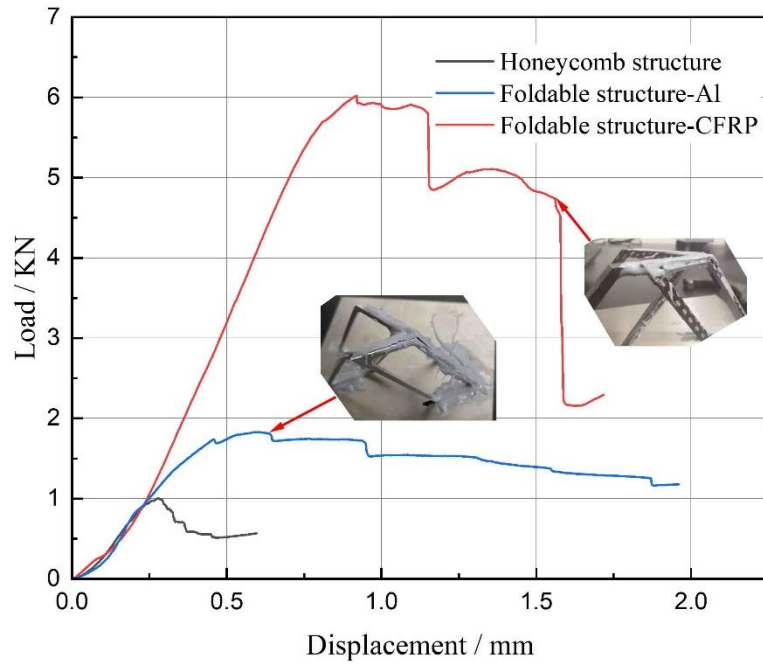


Fig. 5.15 Compressing testing results (One sample).

Table 5.1 Compression properties of honeycomb structure and foldable structure.

Mechanical properties	MPP-Honeycomb structure	Foldable metamaterials-Al	Foldable metamaterials -CFRP	Foldable metamaterials -PLA
Strength / MPa	0.57±0.04	1.02±0.14	3.34±0.11	0.23±0.021
Modulus / MPa	117.67±19.67	145.02±13.15	233.02±12.33	10.76±2.38
Weight / g	23.42±0.248	13.36±0.16	7.63±0.04	7.91±0.01

Fig.5.16 reprinted from the lightweight sound absorption structure work of Xiao et al. [232].

It can be found that the Chapter 5 work (foldable structure) is still in a high compression strength position with a low density when compared with other work in the structural field.

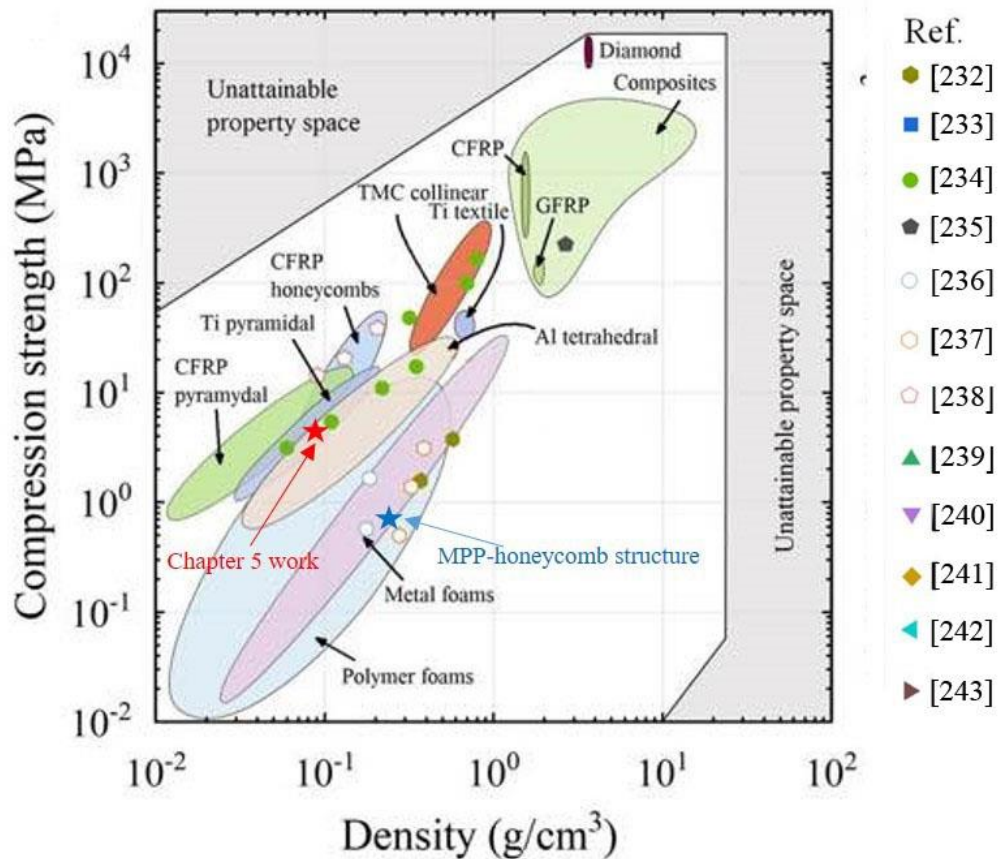


Fig. 5.16 Ashby charts displaying the properties of compression strength and density in this work and some latest references[233-244], reprinted from [232].

5.3 Conclusion

This research demonstrates the design and fabrication of a novel foldable PLA structure, prepared by 3D printing and a high performance structural CFRP alternative. The sound absorption performance was tested by an impedance tube method, showing that the sound absorption characteristics of the foldable PLA structure could be modified by changing the diameter of the mass blocks on a membrane within the folded frames. With the increase of the mass block diameter, the number of sound absorption peaks increased and shifted to lower frequencies. Meanwhile, a FE model accounting for fluid-structural interaction

was established to analyze the sound absorption characteristics of the structure. The simulated strain distribution results illustrated that resonance of the membrane was the main method for sound absorption in the structure. Furthermore, experimental compression and vibration isolation testing of both the foldable PLA structure and a reference honeycomb structure was performed. The testing results showed that the first resonant peak in the vibration isolation test decreased from 750 Hz to 350 Hz. At last, the material of the frame was changed to Al and CFRP to show the potential of the mechanical properties of the foldable metamaterials. The results showed that the modulus and strength of the foldable metamaterials can achieve 233.02 ± 12.33 MPa and 3.34 ± 0.11 MPa respectively when the material of foldable metamaterials is CFRP. Compared with the MPP-honeycomb structure, the compression strength and modulus of the CFRP-type foldable metamaterials are improved by 483% and 98% respectively while the weight is decreased by 67.4%.

However, it should be admitted that the foldable structure does not achieve a good sound absorption performance in general, especially in low frequency. From the test, it can be found that the diameter (weight) of the mass block will influence the sound absorption performance. However, we have not considered the effect of membrane tension stress on its sound absorption performance. Because the resonance of the membrane is the main method to absorb sound energy in this structure, the tension stress of the membrane will influence the sound absorption characteristic of the membrane a lot. Therefore, choosing an

appropriate tension stress is very important to achieve a good sound absorption performance and we assume this is the reason why foldable structure cannot show a good sound absorption ability. However, because we use the internal stress of the POF membrane, it is hard for us to change the tension stress under this condition. In the next step, the membrane of the foldable structure should be installed under a membrane tensioning device so that we can study the influence of the tension stress and design the best condition.

Chapter 6 Overall Summary of the Thesis and Future Plan

6.1 The Summary of the Research

At present, noise pollution has become a significant environmental risk, attracting increasing attention from researchers. The sound-absorbing materials typically lack mechanical characteristics such as lightweight and high-strength, as these properties are often mutually exclusive. However, in practical applications, the mechanical properties and weight of sound-absorbing materials are crucial factors that cannot be ignored. Therefore, this thesis focused on the integration of sound absorption and structural bearing, while maintaining the characteristics of light weight. Initially, this thesis optimizes the MPP-honeycomb structure, combining a hierarchical pore structure with the traditional MPP-honeycomb to enhance sound absorption without increasing weight. Subsequently, a woven fabric composite was designed to create a folded structure that serves both sound absorption and load-bearing purposes. Based on this, membrane-type acoustic metamaterials (AMs) was used as the panel of the folded structure to achieve the lightweight, high-strength, and high-efficiency sound absorption ability ultimately. Fig.6.1 shows the characteristics of these three works on sound absorption performance, structural properties, and simple manufacturing.

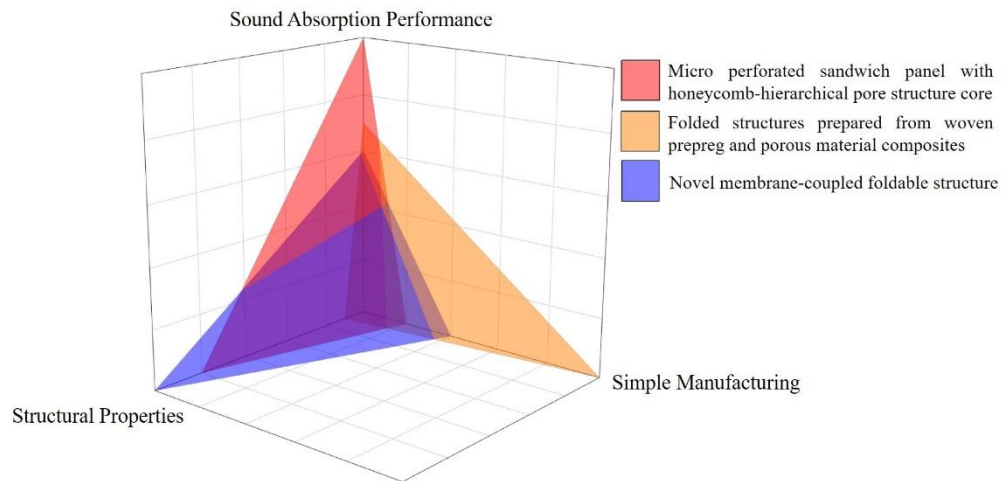


Fig. 6.1 The characteristics of three works.

The main achievements and innovations are as follows:

(1) A micro perforated sandwich panel with a honeycomb-hierarchical pore structure core has been developed. This structure combines a porous material with a hierarchical pore structure and a micro perforated sandwich panel with a honeycomb core together to achieve a lightweight broadband sound absorbing structure. Experimental results showed that the structure can absorb sound in the range of 200-6000Hz effectively, with an average sound absorption coefficient of 0.626 ± 0.028 . Theoretical and FEA models have been established to predictively calculate the sound absorption performance of such structures, showing agreement with experiment results (16.8% and 8.6% error respectively). Overall, this structure greatly increases the sound absorption ability on the basis of sacrificing the weight and adding manufacturing difficulties.

(2) A composite material composed of woven prepreg and ventilated felt has been designed and prepared. Then, the composite materials was processed

to form a folded structure and the sound absorption performance of the structure and materials were experimentally tested. The results showed that compared with the woven prepreg the composite materials can significantly improve the sound absorption coefficient of the wave troughs in the sound absorption coefficient curve. Folding the composite into a structure can further improve the wave troughs in the sound absorption curve. The experimental results showed that the folded structure can maintain the sound absorption coefficient over 0.4 in the range of 400-6300 Hz, realizing broadband sound absorption. Meanwhile, the corresponding theoretical model has been established according to the characteristics of the structure, and the calculation results showed good agreement with the experimental results. Lastly, according to the theoretical model, three key parameters in folded structure design have been analyzed. The results showed that increasing the thickness of the composite materials will shift the sound absorption curve to lower frequencies, increase the trough values, and reduce the peak values. The height of the whole structure will not affect the sound absorption ability but only the sound absorption characteristic of the structure. The folding angle of the folded structure does not significantly affect the sound absorption ability of the structure. In conclusion, these composite materials have the advantages of simple manufacturing and good sound absorption ability. However, the lack of load-bearing ability also limited its application in structural components.

(3) A novel foldable structure was designed and fabricated by 3D printing.

The sound absorption performance was tested by an impedance tube method, showing that the sound absorption characteristics of the structure could be modified by changing the diameter of the mass blocks. With the increase of the mass block diameter, the number of sound absorption peaks will increase and move to a lower frequency. Meanwhile, a FE model accounting for fluid-structural interaction was established to analyze the sound absorption characteristics of the structure. The simulated strain distribution results illustrated that resonance was the main method for sound absorption in the structure. Furthermore, experimental compression and vibration isolation testing both of the foldable structure and a reference honeycomb structure was performed. The results showed that the modulus and strength of the foldable structure were 233.02 ± 12.33 MPa and 3.34 ± 0.11 MPa respectively when the material of foldable structure is CFRP. At last, the foldable structure was compared with the honeycomb structure. The experimental results indicated that compared with the MPP-honeycomb structure, the compression strength and modulus of the foldable structure are improved by 483% and 98% respectively, and the first resonant peak in the vibration isolation test is decreased from 750 Hz to 350 Hz. In summary, all the tests can prove that the foldable structure has achieved a balance between lightweight, load-bearing, and sound absorption.

6.2 Future Works

It can be found that although the micro perforated sandwich panel with honeycomb-hierarchical pore structure core and membrane-coupled foldable

structure can achieve sound absorption and load bearing at the same time, both of them have some limitations. The hierarchical pore structure will increase the weight and the membrane-coupled foldable structure does not have an excellent sound absorption ability. Therefore, these works still have a distance between the practical applications. To fill up these shortages, potential research topics are listed below:

(1) Using the composite materials in Chapter 3 replaces the membrane metamaterials to achieve better sound absorption performance of the foldable structure in Chapter 4. It can be found that the sound absorption performance of the foldable structure in Chapter 4 is not well enough, mainly because the membrane metamaterials cannot absorb sound effectively in an inclined condition. Because of the composite in Chapter 3 has been proved that it can absorb sound well in inclined conditions. Using the composite may obtain a better sound absorption performance.

(2) Optimizing the membrane metamaterials. Optimizing the membrane metamaterials is another solution in order to improve the sound absorption performance of the foldable structure in Chapter 4. According to sound absorption mechanisms of membrane metamaterials, the position and weight are two main factors that influence the sound absorption effect. As the weight has been tested in Chapter 4, the position can be optimized for a better sound absorption performance. For instance, the mass of the membrane metamaterials can be changed to two half-round iron plates and bonded on the two sides of the

membrane.

(3) Foldable structure. Although Chapter 4 is named after the foldable structure, it can be found that most samples in Chapter 4 cannot be changed after they are fabricated. Only Fig. 5.2(c) showed a foldable structure that was connected by a hinge. However, the foldable structure cannot show a good mechanical performance because the connection by hinge needs to punch on the frame which will decrease the strength a lot. Therefore, if the hinge can be bonded on the frame rather than bolted connection, the structure can change the height at any time which will increase the application area of the structure a lot.

Appendix A The Matlab Program for the Theoretical Model in Chapter 3

% Determine the frequency range.

f=10:10:6300;

% Input the related parameters.

w=2*pi*f;

c=340;

p0=1.295;

P0=1.01*10^5;

n=1.85*10^-5;

d1=0.00015;

a=d1/2;

p2=0.97;

u=1.5;

v=2.84*10^-5;

r1=1.4;

l=0.05;

l2=5;

t=1;

d2=1.3;

d3=0.0010;

a3=d3/2; %

p3=0.07;

$$p4=0.0538;$$

% Calculating the acoustic impedance of the porous materials Z_3 .

$$k=d1*(w*p0/4/n).^0.5;$$

$$k22=d3*(w*p0/4/n).^0.5;$$

$$X1=1+(9+(k.^2)/2).^(-0.5)+(8.*n./(1i.*w*p0*a^2)).*(1+k.^2./32).^0.5;$$

$$X2=1+(9+(k22.^2)/2).^(-0.5)+(8.*n./(1i.*w*p0*a3^2)).*(1+k22.^2./32).^0.5;$$

$$K=P0.*(1+1i.*w*d1^2*(r1-1)/8/4/v);$$

$$K2=P0.*(1+1i.*w*d3^2*(r1-1)/8/4/v);$$

$$p1=p0.*X1*3./p2;$$

$$p22=p0.*X2*1./p4;$$

$$z3=-1i.*((p1.*K).^0.5).*cot(w.*1.*sqrt(p1./K));$$

% Calculating the acoustic impedance of the micro perforated plate Z_1 .

$$k2=d2*(w/4/u/1000).^0.5;$$

$$k3=d3*(w/4/u/1000).^0.5;$$

$$z1=(32*p0.*u.*t.*(1+k2.^2./32).^0.5./d2^2+1i.*w./1000.*p0.*t.*(1+1./(9+k2.^2./2).^0.5))./p3;$$

% Calculating the acoustic impedance of the porous materials with hierarchical structures Z_2 .

$$z11=-1i*p0*c*cot(w*5/c);$$

$$p23=1./(1./real(p22)+(1-p4).*1./real(p1))+1i*1./(1./imag(p22)+(1-p4).*1./imag(p1));$$

$$K23=1./(1./real(K2)+(1-p4).*1./real(K))+1i*1./(1./imag(K2)+(1-$$

```

p4).*1./imag(K));

z2=-1i.*((p23.*K23).^0.5).*cot(w.*1.*sqrt(p23./K23));

Z1X=real(z1);

Z2X=real(z2);

Z1Y=imag(z1);

Z2Y=imag(z2);

X=Z1X+Z2X;

Y=Z1Y+Z2Y;

% Calculating the sound absorption coefficient  $\alpha$ .

a0=4.*p0.*c.*X./(Y.^2+(X+p0*c).^2);

plot(f,a0);

```

Appendix B The Matlab Program for the Theoretical Model in Chapter 4

```
% Determine the frequency range.

f=10:10:6300;

% Input the related parameters.

w=2*pi*f;

c=340;

p0=1.295;

P0=1.01*10^5;

n=1.85*10^-5;

d1=0.00015;

a=d1/2;

p2=0.8;

u=1.5;

v=2.84*10^-5;

r1=1.4;

t=0.1;

d2=0.1;

p3=8.6;

% Calculating the acoustic impedance of the cavity  $Z_{c3}$ .

d3=0.0117;

zc3=-1i.*p0.*c.*cot(w.*d3./c);

% Calculating the acoustic impedance of the micro perforated plate  $Z_{m3}$ .
```

```

d4=0.1;

p5=8.6;

k2=d4*(w/4/u).^0.5;

t1=0.01;

zm3=(32*p0.*u.*t1.*(1+k2.^2./32).^0.5./d4^2+1i.*w.*p0.*t1.*(1+1./(9+k2.^2.
/2).^0.5))./p5;

z3=zm3+zc3;

% Calculating the acoustic impedance of the porous materials Zc2.

d0=0.000150;

l2=0.002;

p6=0.97;

k=d0*(w*p0/4/n).^0.5;

X1=1+(9+(k.^2)/2).^(-0.5)+(8.*n./(1i.*w*p0*a^2)).*(1+k.^2./32).^0.5;

p1=p0.*X1^3./p6;

K=P0.*(1+1i.*w.*d0^2.*(r1-1)/8/4/v);

z0=(p1.*K).^0.5;

zc2=1i.*z0.*(1i.*z0+z3.*cot(w.*l2.*sqrt(p1./K)))./(1i.*z0.*cot(w.*l2.*sqrt(p1./
K))-z3);

% Calculating the acoustic impedance of the micro perforated plate Zm2.

k2=d4*(w/4/u).^0.5;

zm2=(32*p0.*u.*t1.*(1+k2.^2./32).^0.5./d4^2+1i.*w.*p0.*t1.*(1+1./(9+k2.^2.
/2).^0.5))./p5;

```

```

z2=zm2+zc2;

% Calculating the acoustic impedance of the cavity Zc11.

k1=w/c;

D1=0.0363;

Z0=p0.*c;

zc11=Z0.*(z2.*cos(k1.*D1)+1i.*Z0.*sin(k1.*D1))./(Z0.*cos(k1.*D1)+1i.*z2.*
sin(k1.*D1));

% Calculating the acoustic impedance of the micro perforated plate Zx1.

k2=d2*(w/4/u).^0.5;

zx1=(32*p0.*u.*t.*(1+k2.^2./32).^0.5./d2^2+1i.*w.*p0.*t.*(1+1./(9+k2.^2./2).
^0.5))./p3;

zc12=zx1+zc11;

% Calculating the acoustic impedance of the porous materials Zc1.

l3=0.002;

k=d1*(w*p0/4/n).^0.5;

X1=1+(9+(k.^2)/2).^(-0.5)+(8.*n./(1i.*w*p0*a^2)).*(1+k.^2./32).^0.5;

p1=p0.*X1^3./p2;

K=P0.*(1+1i.*w*d1^2*(r1-1)/8/4/v);

z0=(p1.*K).^0.5;

zc1=1i.*z0.*(1i.*z0+zc12.*cot(w.*l3.*sqrt(p1./K)))./(1i.*z0.*cot(w.*l3.*sqrt(p
1./K))-zc12);

% Calculating the acoustic impedance of the micro perforated plate Zm1.

```

```

zm1=(32*p0.*u.*t.*(1+k2.^2./32).^0.5./d2^2+1i.*w.*p0.*t.*(1+1./(9+k2.^2./2)
.^0.5))./p3;

z1=zm1+zc1;

Z1X=real(z1);

Z1Y=imag(z1);

X=Z1X;

Y=Z1Y;

% Calculating the sound absorption coefficient  $\alpha$ .

a0=4.*p0.*c.*X./(Y.^2+(X+p0*c).^2);

plot(f,a0);

```

Appendix C The Publications During the PhD Period

1. **Chenhao Dong**, Zhao Liu, Xiaoling Liu, Robert Samuel Pierce, Xiaosu Yi, Sound absorption performance of folded structures prepared from woven prepreg and porous material composites, *Applied Acoustics*. Volume 212,2023,109591.
2. **Chenhao Dong**, Zhao Liu, Robert Pierce, Xiaoling Liu, Xiaosu Yi, Sound absorption performance of a micro perforated sandwich panel with honeycomb-hierarchical pore structure core, *Applied Acoustics*, Volume 203, 2023, 109200.
3. Chen D, Xiong JJ, Bai JB, **Dong CH**. Simplified analytical model to predict nonlinear mechanical responses of flexible composite sheet subjected to out-of-plane loading, *Mechanics of Advanced Materials and Structures*, 2023, 30(9): 1723–1736.
4. Zhao Liu, **Chenhao Dong**, Lu Tong, Chris Rudd, Xiaoling Liu, Xiaosu Yi, A pre-screening study of honeycomb sandwich structure filled with green materials for noise reduction, *Composites Part A: Applied Science and Manufacturing*, Volume 163, 2022, 107226.
5. Liu Z, Dong C, Tong L, Rudd C, Yi X, Liu X. Sound Absorption Performance of Ultralight Honeycomb Sandwich Panels Filled with “Network” Fibers—*Juncus effusus*. *Polymers*. 2024; 16(13):1953.

Conference

1. **Chenhao Dong**, Zhao Liu, Xiaoling Liu, Xiaosu Yi. Sound absorption performance of hierarchical pore structure prepared from carbonized cotton. Presented at the 11th International conference on Green Composites, November 2-4, 2022, Changwon, South Korea.

Reference

- [1] O. Hänninen, A.B. Knol, M. Jantunen, et al., Environmental Burden of Disease in Europe: Assessing Nine Risk Factors in Six Countries, *Environmental Health Perspectives*, 2014, 122(5): 439-446. doi:<https://doi.org/10.1289/ehp.1206154>
- [2] Ministry of ecology and environment of People's Republic of China. Annual report on prevention and control of noise pollution. China. 2022.
- [3] D. Maa, Noise control (Chinese), Beijing, China: Science Press, 1987.
- [4] E.M.M. van Kempen Elise, H. Kruize, C. Boshuizen Hendriek, et al., The association between noise exposure and blood pressure and ischemic heart disease: a meta-analysis, *Environmental health perspectives*, 2002, 110(3): 307-317. doi:10.1289/ehp.02110307
- [5] Y. Cai, S. Hodgson, M. Blangiardo, et al., Road traffic noise, air pollution and incident cardiovascular disease: A joint analysis of the HUNT, EPIC-Oxford and UK Biobank cohorts, *Environment International*, 2018, 114: 191-201. doi:<https://doi.org/10.1016/j.envint.2018.02.048>
- [6] C. Blume, S.F. Schoch, D. Vienneau, et al., Association of transportation noise with sleep during the first year of life: A longitudinal study, *Environmental Research*, 2022, 203: 111776. doi:<https://doi.org/10.1016/j.envres.2021.111776>
- [7] S. Stansfeld, C. Clark, Health Effects of Noise Exposure in Children, *Current Environmental Health Reports*, 2015, 2(2): 171-178. doi:10.1007/s40572-015-0044-1
- [8] C.M.T. Tiesler, M. Birk, E. Thiering, et al., Exposure to road traffic noise and children's behavioural problems and sleep disturbance: Results from the GINIplus and LISApplus studies, *Environmental Research*, 2013, 123: 1-8. doi:<https://doi.org/10.1016/j.envres.2013.01.009>

- [9] M. Khosravipour, M. Ghanbari Kakavandi, F. Gharagozlou, et al., Independent, modified, and interacting effects of long-term noise, extremely low-frequency electromagnetic fields, and shift work exposures on liver enzymes, *Environmental Pollution*, 2023, 333: 122036. doi:<https://doi.org/10.1016/j.envpol.2023.122036>
- [10] World Health Organization. World report on hearing. Geneva: WHO. 2021.
- [11] BS EN ISO 354: 2003 Acoustics - Measurement of sound absorption in a reverberation room; Geneva, Switzerland : ISO,2003.
- [12] BS EN ISO 10534-2. Acoustics-Determination of sound absorption coefficient and impedance in impedance tubes-Part 2: Transfer-function method; Geneva, Switzerland : ISO,2001.
- [13] X. Qiu, 5 - Acoustic testing and evaluation of textiles for buildings and office environments, in: L. Wang (Ed.), *Performance Testing of Textiles*, Woodhead Publishing, 2016, pp. 103-128.
- [14] F. Wang, Z. Chen, C. Wu, et al., Prediction on sound insulation properties of ultrafine glass wool mats with artificial neural networks, *Applied Acoustics*, 2019, 146: 164-171. doi:<https://doi.org/10.1016/j.apacoust.2018.11.018>
- [15] K. Miskinis, V. Dikavicius, A. Buska, et al., Influence of EPS, mineral wool and plaster layers on sound and thermal insulation of a wall: a case study, *Applied Acoustics*, 2018, 137: 62-68. doi:<https://doi.org/10.1016/j.apacoust.2018.03.001>
- [16] B. Mohammadi, A. Ershad-Langroudi, G. Moradi, et al., Mechanical and sound absorption properties of open-cell polyurethane foams modified with rock wool fiber, *Journal of Building Engineering*, 2022, 48: 103872. doi:<https://doi.org/10.1016/j.jobbe.2021.103872>
- [17] S.H. Baek, J.H. Kim, Polyurethane composite foams including silicone-acrylic particles for

- enhanced sound absorption via increased damping and frictions of sound waves, *Composites Science and Technology*, 2020, 198. doi:<https://doi.org/10.1016/j.compscitech.2020.108325>
- [18] M.J. Cops, J.G. McDaniel, E.A. Magliula, et al., Measurement and analysis of sound absorption by a composite foam, *Applied Acoustics*, 2020, 160. doi:<https://doi.org/10.1016/j.apacoust.2019.107138>
- [19] L. Shen, H. Zhang, Y. Lei, et al., Hierarchical pore structure based on cellulose nanofiber/melamine composite foam with enhanced sound absorption performance, *Carbohydrate Polymers*, 2021, 255: 117405. doi:<https://doi.org/10.1016/j.carbpol.2020.117405>
- [20] U. Berardi, G. Iannace, Acoustic characterization of natural fibers for sound absorption applications, *Building and Environment*, 2015, 94: 840-852. doi:<https://doi.org/10.1016/j.buildenv.2015.05.029>
- [21] D.D. Abdi, M. Monazzam, E. Taban, et al., Sound absorption performance of natural fiber composite from chrome shave and coffee silver skin, *Applied Acoustics*, 2021, 182: 108264. doi:<https://doi.org/10.1016/j.apacoust.2021.108264>
- [22] X. Liu, M. Liu, F. Xin, Sound absorption of a perforated panel backed with perforated porous material: Energy dissipation of Helmholtz resonator cavity, *Mechanical Systems and Signal Processing*, 2023, 185: 109762. doi:<https://doi.org/10.1016/j.ymssp.2022.109762>
- [23] A. Hosseinpour, A.A. Katbab, A. Ohadi, Improving the sound absorption of a highly deformable nanocomposite foam based on ethylene-propylene-diene-monomer (EPDM) infused with multi-walled carbon nanotubes (MWCNTs) to absorb low-frequency waves, *European Polymer Journal*, 2022, 178: 111522. doi:<https://doi.org/10.1016/j.eurpolymj.2022.111522>
- [24] J.A. Liu, W.B. Sun, Z.B. Zheng, et al., Enhancing compressive properties and sound

absorption characteristic of open-cell Mg foams through plasma electrolytic oxidation treatment, Journal of Materials Research and Technology, 2023.

doi:<https://doi.org/10.1016/j.jmrt.2023.05.210>

[25] J.W. Chua, X. Li, T. Li, et al., Customisable sound absorption properties of functionally graded metallic foams, Journal of Materials Science & Technology, 2022, 108: 196-207.

doi:<https://doi.org/10.1016/j.jmst.2021.07.056>

[26] P.S. Liu, H.B. Qing, H.L. Hou, Primary investigation on sound absorption performance of highly porous titanium foams, Materials & Design, 2015, 85: 275-281.

doi:<https://doi.org/10.1016/j.matdes.2015.06.118>

[27] K.C. Opiela, T.G. Zieliński, T. Dvorák, et al., Perforated closed-cell aluminium foam for acoustic absorption, Applied Acoustics, 2021, 174: 107706.

doi:<https://doi.org/10.1016/j.apacoust.2020.107706>

[28] H. Choe, J.H. Lee, J.H. Kim, Polyurethane composite foams including CaCO₃ fillers for enhanced sound absorption and compression properties, Composites Science and Technology, 2020, 194: 108153.

doi:<https://doi.org/10.1016/j.compscitech.2020.108153>

[29] R.E. Salino, R.E. Catai, A study of polyurethane waste composite (PUR) and recycled plasterboard sheet cores with polyurethane foam for acoustic absorption, Construction and Building Materials, 2023, 387: 131201.

doi:<https://doi.org/10.1016/j.conbuildmat.2023.131201>

[30] S. Kiddell, Y. Kazemi, J. Sorken, et al., Influence of Flash Graphene on the acoustic, thermal, and mechanical performance of flexible polyurethane foam, Polymer Testing, 2023, 119: 107919.

doi:<https://doi.org/10.1016/j.polymertesting.2022.107919>

[31] L. Cai, J. Tian, K. Feng, et al., Sound absorption model of foam glass-ceramics based on

- microstructure, *Journal of Non-Crystalline Solids*, 2023, 604: 122136.
doi:<https://doi.org/10.1016/j.jnoncrysol.2023.122136>
- [32] Z. Du, D. Yao, Y. Xia, et al., The sound absorption properties of highly porous silicon nitride ceramic foams, *Journal of Alloys and Compounds*, 2020, 820: 153067.
doi:<https://doi.org/10.1016/j.jallcom.2019.153067>
- [33] Z. Du, D. Yao, Y. Xia, et al., Highly porous silica foams prepared via direct foaming with mixed surfactants and their sound absorption characteristics, *Ceramics International*, 2020, 46(9): 12942-12947. doi:<https://doi.org/10.1016/j.ceramint.2020.02.063>
- [34] T.-C. Hung, J.-S. Huang, Y.-W. Wang, et al., Inorganic polymeric foam as a sound absorbing and insulating material, *Construction and Building Materials*, 2014, 50: 328-334.
doi:<https://doi.org/10.1016/j.conbuildmat.2013.09.042>
- [35] S. Ehsan Samaei, U. Berardi, H. Asilian Mahabadi, et al., Optimization and modeling of the sound absorption behavior of polyurethane composite foams reinforced with kenaf fiber, *Applied Acoustics*, 2023, 202: 109176. doi:<https://doi.org/10.1016/j.apacoust.2022.109176>
- [36] W. Zhang, X. Liu, F. Xin, Normal incidence sound absorption of an acoustic labyrinthine metal-fibers-based porous metamaterial at high temperature, *International Journal of Mechanical Sciences*, 2023, 237: 107821. doi:<https://doi.org/10.1016/j.ijmecsci.2022.107821>
- [37] S. Ren, Q. Ao, H. Meng, et al., A semi-analytical model for sound propagation in sintered fiber metals, *Composites Part B: Engineering*, 2017, 126: 17-26.
doi:<https://doi.org/10.1016/j.compositesb.2017.05.083>
- [38] J. Wang, Q. Ao, J. Ma, et al., Sound absorption performance of porous metal fiber materials with different structures, *Applied Acoustics*, 2019, 145: 431-438.

doi:<https://doi.org/10.1016/j.apacoust.2018.10.014>

[39] B. Mohammadi, A. Safaiyan, P. Habibi, et al., Evaluation of the acoustic performance of polyurethane foams embedded with rock wool fibers at low-frequency range; design and construction, *Applied Acoustics*, 2021, 182: 108223.

doi:<https://doi.org/10.1016/j.apacoust.2021.108223>

[40] S. Prabhakaran, V. Krishnaraj, M.S. kumar, et al., Sound and Vibration Damping Properties of Flax Fiber Reinforced Composites, *Procedia Engineering*, 2014, 97: 573-581.

doi:<https://doi.org/10.1016/j.proeng.2014.12.285>

[41] X. Liu, X. Xiong, J. Pang, et al., Airflow resistivity measurement and sound absorption performance analysis of sound-absorb cotton, *Applied Acoustics*, 2021, 179.

doi:<https://doi.org/10.1016/j.apacoust.2021.108060>

[42] C.-W. Kang, H. Kolya, E.-S. Jang, et al., Steam exploded wood cell walls reveals improved gas permeability and sound absorption capability, *Applied Acoustics*, 2021, 179.

doi:<https://doi.org/10.1016/j.apacoust.2021.108049>

[43] S. Salunkhe, C. Patil, C.M. Thakar, Exploring the potential of natural materials as eco-friendly sound absorbers, *Materials Today: Proceedings*, 2023.

doi:<https://doi.org/10.1016/j.matpr.2023.03.098>

[44] N.H. Bhingare, S. Prakash, An experimental and theoretical investigation of coconut coir material for sound absorption characteristics, *Materials Today: Proceedings*, 2021, 43: 1545-

1551. doi:<https://doi.org/10.1016/j.matpr.2020.09.401>

[45] A.J. Otaru, H.P. Morvan, A.R. Kennedy, Numerical modelling of the sound absorption spectra for bottleneck dominated porous metallic structures, *Applied Acoustics*, 2019, 151: 164-

171. doi:<https://doi.org/10.1016/j.apacoust.2019.03.014>

[46] M.J. Jafari, R.F. Madvari, T. Ebadzadeh, Optimized design and experimental validation of sound absorption coefficient performance in aluminium metal foam by spark plasma sintering, *Heliyon*, 2023, 9(6): e16428. doi:<https://doi.org/10.1016/j.heliyon.2023.e16428>

[47] L. Liang, H. Mi, W. Guo, et al., Estimation of sound absorption coefficient of composite structured aluminum foam by radial basis function neural network, *Applied Acoustics*, 2022, 185: 108414. doi:<https://doi.org/10.1016/j.apacoust.2021.108414>

[48] K. Hirozawa, Numerical study on the influence of fiber cross-sectional shapes on the sound absorption efficiency of fibrous porous materials, *Applied Acoustics*, 2020, 164. doi:<https://doi.org/10.1016/j.apacoust.2020.107222>

[49] P.H. Birgitta Berglund, R. F. Soames Job Sources and effects of low-frequency noise, 1996, 99(5). doi:<https://doi.org/10.1121/1.414863>

[50] J. Zhang, D. Yao, W. Peng, et al., Optimal design of lightweight acoustic metamaterials for low-frequency noise and vibration control of high-speed train composite floor, *Applied Acoustics*, 2022, 199: 109041. doi:<https://doi.org/10.1016/j.apacoust.2022.109041>

[51] H.E. Bass, L.C. Sutherland, A.J. Zuckerwar, et al., Atmospheric absorption of sound: Further developments, *Acoustical Society of America Journal*, 1995, 97: 680-683. doi:10.1121/1.412989

[52] Z. Du, D. Yao, Y. Xia, et al., The sound absorption properties of highly porous silicon nitride ceramic foams, *Journal of Alloys and Compounds*, 2020, 820. doi:<https://doi.org/10.1016/j.jallcom.2019.153067>

[53] J.H. Chen, P.S. Liu, J.X. Sun, Sound absorption performance of a lightweight ceramic foam,

Ceramics International, 2020, 46(14): 22699-22708.

doi:<https://doi.org/10.1016/j.ceramint.2020.06.033>

[54] L. Cao, X. Yu, X. Yin, et al., Hierarchically maze-like structured nanofiber aerogels for effective low-frequency sound absorption, *J Colloid Interface Sci*, 2021, 597: 21-28.

doi:<https://doi.org/10.1016/j.jcis.2021.03.172>

[55] L. Shen, H. Zhang, Y. Lei, et al., Hierarchical pore structure based on cellulose nanofiber/melamine composite foam with enhanced sound absorption performance, *Carbohydr Polym*, 2021, 255: 117405. doi:<https://doi.org/10.1016/j.carbpol.2020.117405>

[56] X. Cai, Y. Zhang, J. Yang, Tunable ultra low and broad acoustic absorption by controllable pyrolysis of fiber materials, *Materials Today Communications*, 2018, 16: 226-231.

doi:<https://doi.org/10.1016/j.mtcomm.2018.06.009>

[57] H. Zhang, H. Liu, H. Wu, et al., Microwave absorbing property of gelcasting SiC-Si₃N₄ ceramics with hierarchical pore structures, *Journal of the European Ceramic Society*, 2022, 42(4):

1249-1257. doi:<https://doi.org/10.1016/j.jeurceramsoc.2021.12.011>

[58] P. Zhou, J. Zhang, Z. Song, et al., Ordered mesoporous carbon with hierarchical pore structure for high-efficiency electromagnetic wave absorber under thin matching thickness,

Journal of Materials Research and Technology, 2023, 25: 1560-1569.

doi:<https://doi.org/10.1016/j.jmrt.2023.06.056>

[59] L. Yang, J.W. Chua, X. Li, et al., Superior broadband sound absorption in hierarchical ultralight graphene oxide aerogels achieved through emulsion freeze-casting, *Chemical Engineering Journal*, 2023, 469: 143896. doi:<https://doi.org/10.1016/j.cej.2023.143896>

doi:<https://doi.org/10.1016/j.cej.2023.143896>

[60] J.-H. Oh, H.R. Lee, S. Umrao, et al., Self-aligned and hierarchically porous graphene-

polyurethane foams for acoustic wave absorption, *Carbon*, 2019, 147: 510-518.

doi:<https://doi.org/10.1016/j.carbon.2019.03.025>

[61] P. Xu, J. Fang, H. He, et al., In situ growth of globular MnO₂ nanoflowers inside hierarchical porous mangosteen shells-derived carbon for efficient electromagnetic wave absorber, *Journal of Alloys and Compounds*, 2022, 903: 163826.

doi:<https://doi.org/10.1016/j.jallcom.2022.163826>

[62] Maa DY. Theory and design of microperforated panel sound-absorbing constructions. *Sci Sinica* 1975;18(1):55–71. doi:<https://doi.org/10.1360/ya1975-18-1-55>

[63] X. Wang, L. Ma, Y. Wang, et al., Design of multilayer sound-absorbing composites with excellent sound absorption properties at medium and low frequency via constructing variable section cavities, *Composite Structures*, 2021, 266.

doi:<https://doi.org/10.1016/j.compstruct.2021.113798>

[64] X. Liu, C. Yu, F. Xin, Gradually perforated porous materials backed with Helmholtz resonant cavity for broadband low-frequency sound absorption, *Composite Structures*, 2021, 263.

doi:<https://doi.org/10.1016/j.compstruct.2021.113647>

[65] L.B. Wang, C.Z. Ma, J.H. Wu, A thin meta-structure with multi-order resonance for underwater broadband sound absorption in low frequency, *Applied Acoustics*, 2021, 179.

doi:<https://doi.org/10.1016/j.apacoust.2021.108025>

[66] L. Zhao, T.R. Lin, A turned double-layer microperforated panel for low frequency sound absorption in enclosures with limited cavity space, *Applied Acoustics*, 2022, 188: 108594.

doi:<https://doi.org/10.1016/j.apacoust.2021.108594>

[67] I. Prasetiyo, I. Sihar, A.S. Sudarsono, Realization of a thin and broadband microperforated

panel (MPP) sound absorber, *Applied Acoustics*, 2021, 183: 108295.

doi:<https://doi.org/10.1016/j.apacoust.2021.108295>

[68] P. Cobo, C. de la Colina, E. Roibás-Millán, et al., A wideband triple-layer microperforated

panel sound absorber, *Composite Structures*, 2019, 226: 111226.

doi:<https://doi.org/10.1016/j.compstruct.2019.111226>

[69] M. Toyoda, D. Eto, Prediction of microperforated panel absorbers using the finite-difference

time-domain method, *Wave Motion*, 2019, 86: 110-124.

doi:<https://doi.org/10.1016/j.wavemoti.2019.01.006>

[70] C. Rui Liu, J. Hui Wu, Z. Yang, et al., Ultra-broadband acoustic absorption of a thin

microperforated panel metamaterial with multi-order resonance, *Composite Structures*, 2020,

246: 112366. doi:<https://doi.org/10.1016/j.compstruct.2020.112366>

[71] H. Meng, M.A. Galland, M. Ichchou, et al., Small perforations in corrugated sandwich panel

significantly enhance low frequency sound absorption and transmission loss, *Composite*

Structures, 2017, 182: 1-11. doi:<https://doi.org/10.1016/j.compstruct.2017.08.103>

[72] Y. Tang, W. He, F. Xin, et al., Nonlinear sound absorption of ultralight hybrid-cored

sandwich panels, *Mechanical Systems and Signal Processing*, 2020, 135.

doi:<https://doi.org/10.1016/j.ymssp.2019.106428>

[73] Y. Tang, F. Xin, T.J. Lu, Sound absorption of micro-perforated sandwich panel with

honeycomb-corrugation hybrid core at high temperatures, *Composite Structures*, 2019, 226.

doi:<https://doi.org/10.1016/j.compstruct.2019.111285>

[74] X. Peng, G. Liu, J. Li, et al., Compression property and energy absorption capacity of 4D-

printed deformable honeycomb structure, *Composite Structures*, 2023, 325: 117591.

doi:<https://doi.org/10.1016/j.compstruct.2023.117591>

[75] L. Guo, H. Wang, W. Li, et al., Multi-scale damage modeling and out-of-plane shear behavior of carbon/carbon honeycomb structure, *Thin-Walled Structures*, 2023, 192: 111103.

doi:<https://doi.org/10.1016/j.tws.2023.111103>

[76] Z. Dong, Z. Wang, J. Tian, et al., Investigation on tearing damage of CFRP circular cell honeycomb in end-face grinding, *Composite Structures*, 2023, 325: 117616.

doi:<https://doi.org/10.1016/j.compstruct.2023.117616>

[77] M. Boccaccio, F. Bucciarelli, G.P.M. Fierro, et al., Microperforated Panel and deep subwavelength Archimedean-inspired spiral cavities for multi-tonal and broadband sound absorption, *Applied Acoustics*, 2021, 176. doi:<https://doi.org/10.1016/j.apacoust.2020.107901>

[78] L. Fok, M. Ambati, X. Zhang, Acoustic Metamaterials, *MRS Bulletin*, 2008, 33(10): 931-934. doi:10.1557/mrs2008.202

[79] G. Ji, J. Huber, Recent progress in acoustic metamaterials and active piezoelectric acoustic metamaterials - A review, *Applied Materials Today*, 2022, 26: 101260.

doi:<https://doi.org/10.1016/j.apmt.2021.101260>

[80] C. Gazzola, S. Caverni, A. Corigliano, From mechanics to acoustics: Critical assessment of a robust metamaterial for acoustic insulation application, *Applied Acoustics*, 2021, 183: 108311.

doi:<https://doi.org/10.1016/j.apacoust.2021.108311>

[81] S. Qu, M. Yang, Y. Xu, et al., Reverberation time control by acoustic metamaterials in a small room, *Building and Environment*, 2023, 244: 110753.

doi:<https://doi.org/10.1016/j.buildenv.2023.110753>

[82] F. Zangeneh-Nejad, R. Fleury, Active times for acoustic metamaterials, *Reviews in Physics*,

2019, 4: 100031. doi:<https://doi.org/10.1016/j.revip.2019.100031>

[83] J. Mei, G. Ma, M. Yang, et al., Dark acoustic metamaterials as super absorbers for low-frequency sound, *Nature Communications*, 2012, 3(1): 756. doi:10.1038/ncomms1758

[84] J. Guo, Y. Fang, R. Qu, et al., Development and progress in acoustic phase-gradient metamaterials for wavefront modulation, *Materials Today*, 2023. doi:<https://doi.org/10.1016/j.mattod.2023.04.004>

[85] F. Yang, J.-S. Yang, Y. Wang, et al., Theoretical study on dispersion relations of chiral acoustic metamaterials considering mass-rotation, *European Journal of Mechanics - A/Solids*, 2023, 100: 105005. doi:<https://doi.org/10.1016/j.euromechsol.2023.105005>

[86] Z. Zhang, X. Wang, Z.Y. Liu, et al., A study of low frequency sound insulation mechanism of a perforated plate-type acoustic metamaterial, *Journal of Sound and Vibration*, 2023, 558: 117775. doi:<https://doi.org/10.1016/j.jsv.2023.117775>

[87] X. Zhang, Y. Li, Y. Wang, et al., Ultra-wide low-frequency bandgap design of acoustic metamaterial via multi-material topology optimization, *Composite Structures*, 2023, 306: 116584. doi:<https://doi.org/10.1016/j.compstruct.2022.116584>

[88] J. Wen, H. Shen, D. Yu, et al., Exploration of amphoteric and negative refraction imaging of acoustic sources via active metamaterials, *Physics Letters A*, 2013, 377(34): 2199-2206. doi:<https://doi.org/10.1016/j.physleta.2013.06.016>

[89] C. Wang, R. Li, Z. Zhu, et al., A PVC plasticization electrically active laminated metamaterial with tunable sound insulating performance, *Engineering Structures*, 2022, 269: 114777. doi:<https://doi.org/10.1016/j.engstruct.2022.114777>

[90] B. Xia, N. Chen, L. Xie, et al., Temperature-controlled tunable acoustic metamaterial with

active band gap and negative bulk modulus, *Applied Acoustics*, 2016, 112: 1-9.

doi:<https://doi.org/10.1016/j.apacoust.2016.05.005>

[91] G. Ji, J. Zhou, J. Huber, The evaluation of electrical circuits for adjusting sound transmission properties of piezoelectric metamaterials, *Mechanical Systems and Signal Processing*, 2023, 200:

110549. doi:<https://doi.org/10.1016/j.ymssp.2023.110549>

[92] S.-W. Fan, S.-D. Zhao, A.L. Chen, et al., Tunable Broadband Reflective Acoustic Metasurface, *Physical Review Applied*, 2019, 11(4): 044038.

doi:10.1103/PhysRevApplied.11.044038

[93] P. Wang, F. Casadei, S. Shan, et al., Harnessing Buckling to Design Tunable Locally Resonant Acoustic Metamaterials, *Physical Review Letters*, 2014, 113(1): 014301.

doi:10.1103/PhysRevLett.113.014301

[94] Z. Tian, C. Shen, J. Li, et al., Programmable Acoustic Metasurfaces, *Advanced Functional Materials*, 2019, 29(13): 1808489. doi:<https://doi.org/10.1002/adfm.201808489>

[95] J. He, Q. Liang, P. Lv, et al., Tunable broadband multi-function acoustic metasurface by nested resonant rings, *Applied Acoustics*, 2022, 197: 108957.

doi:<https://doi.org/10.1016/j.apacoust.2022.108957>

[96] S. Ning, Z. Yan, D. Chu, et al., Ultralow-frequency tunable acoustic metamaterials through tuning gauge pressure and gas temperature, *Extreme Mechanics Letters*, 2021, 44: 101218.

doi:<https://doi.org/10.1016/j.eml.2021.101218>

[97] W. Akl, A. Baz, Active control of the dynamic density of acoustic metamaterials, *Applied Acoustics*, 2021, 178: 108001. doi:<https://doi.org/10.1016/j.apacoust.2021.108001>

[98] G. Hu, L. Tang, X. Cui, On the modelling of membrane-coupled Helmholtz resonator and

- its application in acoustic metamaterial system, *Mechanical Systems and Signal Processing*, 2019, 132: 595-608. doi:<https://doi.org/10.1016/j.ymssp.2019.07.017>
- [99] G. Ciaburro, G. Iannace, Membrane-type acoustic metamaterial using cork sheets and attached masses based on reused materials, *Applied Acoustics*, 2022, 189: 108605. doi:<https://doi.org/10.1016/j.apacoust.2021.108605>
- [100] J.-Y. Jang, K. Song, Synergistic acoustic metamaterial for soundproofing: Combining membrane and locally resonant structure, *International Journal of Mechanical Sciences*, 2023, 256: 108500. doi:<https://doi.org/10.1016/j.ijmecsci.2023.108500>
- [101] Y. Xu, Y. Hong, M. Li, et al., Underwater low-frequency sound absorption performance and broadband absorption design of membrane-type acoustic metamaterials, *Applied Acoustics*, 2023, 214: 109676. doi:<https://doi.org/10.1016/j.apacoust.2023.109676>
- [102] L.Y.M. Sampaio, G.K. Rodrigues, J.A. Mosquera-Sánchez, et al., Membrane smart metamaterials for unidirectional wave propagation problems, *Journal of Sound and Vibration*, 2021, 512: 116374. doi:<https://doi.org/10.1016/j.jsv.2021.116374>
- [103] T. Xing, X. Gai, J. Zhao, et al., Low frequency sound absorption of adjustable membrane-type acoustic metamaterials, *Applied Acoustics*, 2022, 188: 108586. doi:<https://doi.org/10.1016/j.apacoust.2021.108586>
- [104] L.Y.M. Sampaio, P.C.M. Cerântola, L.P.R. de Oliveira, Lightweight decorated membranes as an aesthetic solution for sound insulation panels, *Journal of Sound and Vibration*, 2022, 532: 116971. doi:<https://doi.org/10.1016/j.jsv.2022.116971>
- [105] J.-P. Groby, W. Lauriks, T.E. Vigran, Total absorption peak by use of a rigid frame porous layer backed by a rigid multi-irregularities grating, *The Journal of the Acoustical Society of*

America, 2010, 127(5): 2865-2874. doi:10.1121/1.3337235

[106] Y. Fang, X. Zhang, J. Zhou, et al., Acoustic metaporous layer with composite structures for perfect and quasi-omnidirectional sound absorption, *Composite Structures*, 2019, 223. doi:<https://doi.org/10.1016/j.compstruct.2019.110948>

[107] N. Gao, J. Wu, K. Lu, et al., Hybrid composite meta-porous structure for improving and broadening sound absorption, *Mechanical Systems and Signal Processing*, 2021, 154. doi:<https://doi.org/10.1016/j.ymssp.2020.107504>

[108] J. Yang, J.S. Lee, Y.Y. Kim, Multiple slow waves in metaporous layers for broadband sound absorption, *Journal of Physics D: Applied Physics*, 2017, 50(1): 015301. doi:10.1088/1361-6463/50/1/015301

[109] L. Xiong, B. Nennig, Y. Aurégan, et al., Sound attenuation optimization using metaporous materials tuned on exceptional points, *The Journal of the Acoustical Society of America*, 2017, 142(4): 2288-2297. doi:10.1121/1.5007851

[110] X. Cai, Q. Guo, G. Hu, et al., Ultrathin low-frequency sound absorbing panels based on coplanar spiral tubes or coplanar Helmholtz resonators, *Applied Physics Letters*, 2014, 105(12). doi:10.1063/1.4895617

[111] H. Zou, Z. Xu, Y. Hu, et al., Reflected continuously tunable acoustic metasurface with rotatable space coiling-up structure, *Physics Letters A*, 2022, 426: 127891. doi:<https://doi.org/10.1016/j.physleta.2021.127891>

[112] L. Xiang, G. Wang, C. Zhu, Controlling sound transmission by space-coiling fractal acoustic metamaterials with broadband on the subwavelength scale, *Applied Acoustics*, 2022, 188: 108585. doi:<https://doi.org/10.1016/j.apacoust.2021.108585>

- [113] G.d.N. Almeida, E.F. Vergara, L.R. Barbosa, et al., Low-frequency sound absorption of a metamaterial with symmetrical-coiled-up spaces, *Applied Acoustics*, 2021, 172: 107593. doi:<https://doi.org/10.1016/j.apacoust.2020.107593>
- [114] R. Ghaffarivardavagh, J. Nikolajczyk, R. Glynn Holt, et al., Horn-like space-coiling metamaterials toward simultaneous phase and amplitude modulation, *Nature Communications*, 2018, 9(1): 1349. doi:10.1038/s41467-018-03839-z
- [115] W. Tang, C. Ren, S. Tong, et al., Sandwich-like space-coiling metasurfaces for weak-dispersion high-efficiency transmission, *Applied Physics Letters*, 2019, 115(13). doi:10.1063/1.5120494
- [116] J. Li, C. Shen, A. Díaz-Rubio, et al., Systematic design and experimental demonstration of bianisotropic metasurfaces for scattering-free manipulation of acoustic wavefronts, *Nature Communications*, 2018, 9(1): 1342. doi:10.1038/s41467-018-03778-9
- [117] C. Ding, H. Chen, S. Zhai, et al., The anomalous manipulation of acoustic waves based on planar metasurface with split hollow sphere, *Journal of Physics D: Applied Physics*, 2015, 48(4): 045303. doi:10.1088/0022-3727/48/4/045303
- [118] J. Guo, X. Zhang, Y. Fang, et al., Reflected wave manipulation by inhomogeneous impedance via varying-depth acoustic liners, *Journal of Applied Physics*, 2018, 123(17). doi:10.1063/1.5022127
- [119] J. Guo, J. Zhou, An ultrathin acoustic carpet cloak based on resonators with extended necks, *Journal of Physics D: Applied Physics*, 2020, 53(50): 505501. doi:10.1088/1361-6463/abac2e
- [120] F. Xin, X. Ma, X. Liu, et al., A multiscale theoretical approach for the sound absorption of slit-perforated double porosity materials, *Composite Structures*, 2019, 223.

doi:<https://doi.org/10.1016/j.compstruct.2019.110919>

[121] N. Gao, L. Tang, J. Deng, et al., Design, fabrication and sound absorption test of composite porous metamaterial with embedding I-plates into porous polyurethane sponge, *Applied Acoustics*, 2021, 175. doi:<https://doi.org/10.1016/j.apacoust.2020.107845>

[122] S. Yan, L. Yuan, C. Wang, et al., A modular design approach for porous green sound-absorbing concrete for the noise barrier on high-speed railway, *Journal of Building Engineering*, 2023, 77: 107543. doi:<https://doi.org/10.1016/j.jobbe.2023.107543>

[123] T. Yuan, X. Song, J. Xu, et al., Tunable acoustic composite metasurface based porous material for broadband sound absorption, *Composite Structures*, 2022, 298: 116014. doi:<https://doi.org/10.1016/j.compstruct.2022.116014>

[124] S. Ren, Y. Liu, W. Sun, et al., Broadband low-frequency sound absorbing metastructures composed of impedance matching coiled-up cavity and porous materials, *Applied Acoustics*, 2022, 200: 109061. doi:<https://doi.org/10.1016/j.apacoust.2022.109061>

[125] Y. Li, J. Yan, Y. Peng, Multiscale porous with coiled-up channel for low-frequency broadband sound absorption, *International Journal of Mechanical Sciences*, 2022, 232: 107622. doi:<https://doi.org/10.1016/j.ijmecsci.2022.107622>

[126] Y. Wang, Y. Wang, J. Xu, et al., Broadband low-frequency sound absorption by coiled-up space embedded in a porous layer, *Applied Acoustics*, 2021, 182: 108226. doi:<https://doi.org/10.1016/j.apacoust.2021.108226>

[127] H. Zhao, Y. Wang, D. Yu, et al., A double porosity material for low frequency sound absorption, *Composite Structures*, 2020, 239. doi:<https://doi.org/10.1016/j.compstruct.2020.111978>

- [128] M. Pereira, J. Carbajo, L. Godinho, et al., Improving the sound absorption behaviour of porous concrete using embedded resonant structures, *Journal of Building Engineering*, 2021, 35: 102015. doi:<https://doi.org/10.1016/j.jobe.2020.102015>
- [129] L. Cao, Q. Fu, Y. Si, et al., Porous materials for sound absorption, *Composites Communications*, 2018, 10: 25-35. doi:<https://doi.org/10.1016/j.coco.2018.05.001>
- [130] M. Toyoda, K. Sakagami, D. Takahashi, et al., Effect of a honeycomb on the sound absorption characteristics of panel-type absorbers, *Applied Acoustics*, 2011, 72(12): 943-948. doi:<https://doi.org/10.1016/j.apacoust.2011.05.017>
- [131] K. Hoshi, T. Hanyu, T. Okuzono, et al., Implementation experiment of a honeycomb-backed MPP sound absorber in a meeting room, *Applied Acoustics*, 2020, 157: 107000. doi:<https://doi.org/10.1016/j.apacoust.2019.107000>
- [132] S. Yan, J. Wu, J. Chen, et al., Optimization design and analysis of honeycomb micro-perforated plate broadband sound absorber, *Applied Acoustics*, 2022, 186: 108487. doi:<https://doi.org/10.1016/j.apacoust.2021.108487>
- [133] X. Chen, P. Liu, Z. Hou, et al., Implementation of acoustic demultiplexing with membrane-type metasurface in low frequency range, *Applied Physics Letters*, 2017, 110(16). doi:10.1063/1.4981898
- [134] F. Cotana, Experimental data and performance of new high sound insulation ventilating windows, *INTER-NOISE and NOISE-CON Congress and Conference Proceedings*, Institute of Noise Control Engineering, 1999, pp. 995-998.
- [135] D. Diab, D. Dragna, E. Salze, et al., Nonlinear broadband time-domain admittance boundary condition for duct acoustics. Application to perforated plate liners, *Journal of Sound*

and Vibration, 2022, 528: 116892. doi:<https://doi.org/10.1016/j.jsv.2022.116892>

[136] H.V. Fuchs, X. Zha, Acrylic-glass sound absorbers in the plenum of the deutscher bundestag, Applied Acoustics, 1997, 51(2): 211-217. doi:[https://doi.org/10.1016/S0003-682X\(96\)00064-3](https://doi.org/10.1016/S0003-682X(96)00064-3)

[137] G. Li, C.K. Mechefske, A comprehensive experimental study of micro-perforated panel acoustic absorbers in MRI scanners, Magnetic Resonance Materials in Physics, Biology and Medicine, 2010, 23(3): 177-185. doi:10.1007/s10334-010-0216-9

[138] S. Xie, D. Wang, Z. Feng, et al., Sound absorption performance of microperforated honeycomb metasurface panels with a combination of multiple orifice diameters, Applied Acoustics, 2020, 158. doi:<https://doi.org/10.1016/j.apacoust.2019.107046>

[139] N. Gao, H. Hou, Experimental investigation of sound absorption in a composite absorber, Theoretical and Applied Mechanics Letters, 2021. doi:<https://doi.org/10.1016/j.taml.2021.100221>

[140] J. Guo, X. Zhang, Y. Fang, et al., Wideband low-frequency sound absorption by inhomogeneous multi-layer resonators with extended necks, Composite Structures, 2021, 260. doi:<https://doi.org/10.1016/j.compstruct.2020.113538>

[141] Y. Jiang, C. Shen, H. Meng, et al., Design and optimization of micro-perforated ultralight sandwich structure with N-type hybrid core for broadband sound absorption, Applied Acoustics, 2023, 202: 109184. doi:<https://doi.org/10.1016/j.apacoust.2022.109184>

[142] H. Li, J. Wu, S. Yan, et al., Design and study of broadband sound absorbers with partition based on micro-perforated panel and Helmholtz resonator, Applied Acoustics, 2023, 205: 109262. doi:<https://doi.org/10.1016/j.apacoust.2023.109262>

- [143] J. Wang, G.J. Bennett, Multi-chamber micro-perforated panel absorbers optimised for high amplitude broadband absorption using a two-point impedance method, *Journal of Sound and Vibration*, 2023, 547: 117527. doi:<https://doi.org/10.1016/j.jsv.2022.117527>
- [144] Y. Wang, H. Yuan, Y. Wang, et al., A study on ultra-thin and ultra-broadband acoustic performance of micro-perforated plate coupled with coiled-up space structure, *Applied Acoustics*, 2022, 200: 109048. doi:<https://doi.org/10.1016/j.apacoust.2022.109048>
- [145] X. Zhang, L. Cheng, Broadband and low frequency sound absorption by Sonic black holes with Micro-perforated boundaries, *Journal of Sound and Vibration*, 2021, 512: 116401. doi:<https://doi.org/10.1016/j.jsv.2021.116401>
- [146] H.-S. Kim, P.-S. Ma, B.-K. Kim, et al., Sound transmission loss of multi-layered elastic micro-perforated plates in an impedance tube, *Applied Acoustics*, 2020, 166: 107348. doi:<https://doi.org/10.1016/j.apacoust.2020.107348>
- [147] J. Carbajo, J. Ramis, L. Godinho, et al., Perforated panel absorbers with micro-perforated partitions, *Applied Acoustics*, 2019, 149: 108-113. doi:<https://doi.org/10.1016/j.apacoust.2019.01.023>
- [148] X. Ma, D. Yurchenko, K. Chen, et al., Structural acoustic controlled active micro-perforated panel absorber for improving wide-band low frequency sound absorption, *Mechanical Systems and Signal Processing*, 2022, 178: 109295. doi:<https://doi.org/10.1016/j.ymssp.2022.109295>
- [149] X. Zhang, L. Cheng, Y. Liu, et al., Acoustic modelling and analyses of geometrically complex systems with Micro-perforated panels, *Journal of Sound and Vibration*, 2021, 499: 115995. doi:<https://doi.org/10.1016/j.jsv.2021.115995>

- [150] X. Zhang, J. Wu, Q. Mao, et al., Design of a honeycomb-microperforated panel with an adjustable sound absorption frequency, *Applied Acoustics*, 2020, 164: 107246. doi:<https://doi.org/10.1016/j.apacoust.2020.107246>
- [151] Z. Ren, Y. Cheng, M. Chen, et al., A compact multifunctional metastructure for Low-frequency broadband sound absorption and crash energy dissipation, *Materials & Design*, 2022, 215: 110462. doi:<https://doi.org/10.1016/j.matdes.2022.110462>
- [152] X. Yu, H. Fang, F. Cui, et al., Origami-inspired foldable sound barrier designs, *Journal of Sound and Vibration*, 2019, 442: 514-526. doi:<https://doi.org/10.1016/j.jsv.2018.11.025>
- [153] Z. Cai, X. Li, X. Gai, et al., An empirical model to predict sound absorption ability of woven fabrics, *Applied Acoustics*, 2020, 170. doi:<https://doi.org/10.1016/j.apacoust.2020.107483>
- [154] J. Chen, H. Li, Z. Yan, et al., Simulation, measurement and optimization of sound absorption in gradient impedance fiber-based composites, *Measurement*, 2023, 221: 113499. doi:<https://doi.org/10.1016/j.measurement.2023.113499>
- [155] W. He, X. Peng, F. Xin, et al., A microstructure-based model of transport parameters and sound absorption for woven fabrics, *Composites Science and Technology*, 2022, 227: 109607. doi:<https://doi.org/10.1016/j.compscitech.2022.109607>
- [156] X. Liu, J. Jiang, X. Tang, et al., Sound absorption of hollow polyester woven fabric with honeycomb weave, *Applied Acoustics*, 2021, 180: 108148. doi:<https://doi.org/10.1016/j.apacoust.2021.108148>
- [157] X.-L. Gai, Z.-N. Cai, T. Xing, et al., Experimental study on sound absorbing property of spatial absorber of non-woven fabric with micro-perforated plate-like structure, *Applied*

Acoustics, 2020, 160: 107156. doi:<https://doi.org/10.1016/j.apacoust.2019.107156>

[158] R. Atiénzar-Navarro, M. Bonet-Aracil, J. Gisbert-Payá, et al., Sound absorption of textile fabrics doped with microcapsules, *Applied Acoustics*, 2020, 164: 107285. doi:<https://doi.org/10.1016/j.apacoust.2020.107285>

[159] H. Li, N. Zhang, X. Fan, et al., Investigation of effective factors of woven structure fabrics for acoustic absorption, *Applied Acoustics*, 2020, 161: 107081. doi:<https://doi.org/10.1016/j.apacoust.2019.107081>

[160] I. Prasetyo, E. Muqowi, A. Putra, et al., Modelling sound absorption of tunable double layer woven fabrics, *Applied Acoustics*, 2020, 157: 107008. doi:<https://doi.org/10.1016/j.apacoust.2019.107008>

[161] M. Liu, A.I. Fernández, M. Segarra, Chapter 8 - Materials for Phase Change Material at High Temperature, in: L.F. Cabeza, N.H.S. Tay (Eds.), *High Temperature Thermal Storage Systems Using Phase Change Materials*, Academic Press, 2018, pp. 195-230.

[162] M. Madgule, C.G. Sreenivasa, A.V. Borgaonkar, Aluminium metal foam production methods, properties and applications- a review, *Materials Today: Proceedings*, 2023, 77: 673-679. doi:<https://doi.org/10.1016/j.matpr.2022.11.287>

[163] A. Changdar, S.S. Chakraborty, Laser processing of metal foam - A review, *Journal of Manufacturing Processes*, 2021, 61: 208-225. doi:<https://doi.org/10.1016/j.jmapro.2020.10.012>

[164] J. Shi, H. Du, Z. Chen, et al., Review of phase change heat transfer enhancement by metal foam, *Applied Thermal Engineering*, 2023, 219: 119427. doi:<https://doi.org/10.1016/j.applthermaleng.2022.119427>

[165] K. Kumar, S.B. Ingole, A. saeedjassim, et al., Aluminum-foam by powder metallurgy: A

review, *Materials Today: Proceedings*, 2023. doi:<https://doi.org/10.1016/j.matpr.2023.03.344>

[166] M.Y. Omar, C. Xiang, N. Gupta, et al., Data characterizing compressive properties of Al/Al₂O₃ syntactic foam core metal matrix sandwich, *Data in Brief*, 2015, 5: 522-527. doi:<https://doi.org/10.1016/j.dib.2015.09.046>

[167] M. Zhang, G. Tian, H. Yan, et al., Anticorrosive superhydrophobic high-entropy alloy coating on 3D iron foam for efficient oil/water separation, *Surface and Coatings Technology*, 2023, 468: 129756. doi:<https://doi.org/10.1016/j.surfcoat.2023.129756>

[168] J. Zhao, P. Yan, B. Snow, et al., Micro-structured copper and nickel metal foams for wastewater disinfection: proof-of-concept and scale-up, *Process Safety and Environmental Protection*, 2020, 142: 191-202. doi:<https://doi.org/10.1016/j.psep.2020.06.013>

[169] X. Chen, C. Yang, Y. Sun, et al., Water management and structure optimization study of nickel metal foam as flow distributors in proton exchange membrane fuel cell, *Applied Energy*, 2022, 309: 118448. doi:<https://doi.org/10.1016/j.apenergy.2021.118448>

[170] C. Kádár, P. Kubelka, A. Szlancsik, On the compressive properties of aluminum and magnesium syntactic foams: Experiment and simulation, *Materials Today Communications*, 2023, 35: 106060. doi:<https://doi.org/10.1016/j.mtcomm.2023.106060>

[171] S. Kim, D.G. Kim, M. Kim, et al., Analyses of impact energy-absorbing performance of open- and closed-cell Al foams using modified split Hopkinson pressure bar, *Journal of Alloys and Compounds*, 2023, 965: 171349. doi:<https://doi.org/10.1016/j.jallcom.2023.171349>

[172] A. Lomte, B. Sharma, M. Drouin, et al., Sound absorption and transmission loss properties of open-celled aluminum foams with stepwise relative density gradients, *Applied Acoustics*, 2022, 193: 108780. doi:<https://doi.org/10.1016/j.apacoust.2022.108780>

- [173] Y. Wang, F. Chen, X. Wang, et al., Micro-CT in the mechanical properties and energy absorption of closed-cell aluminium foam, *Materials Today Communications*, 2023, 37: 106962. doi:<https://doi.org/10.1016/j.mtcomm.2023.106962>
- [174] T. Wan, Y. Liu, C. Zhou, et al., Fabrication, properties, and applications of open-cell aluminum foams: A review, *Journal of Materials Science & Technology*, 2021, 62: 11-24. doi:<https://doi.org/10.1016/j.jmst.2020.05.039>
- [175] S. Kim, C.-W. Lee, A Review on Manufacturing and Application of Open-cell Metal Foam, *Procedia Materials Science*, 2014, 4: 305-309. doi:<https://doi.org/10.1016/j.mspro.2014.07.562>
- [176] C. Aimar, L. Orgéas, S. Rolland du Roscoat, et al., Fatigue mechanisms of a closed cell elastomeric foam: A mechanical and microstructural study using ex situ X-ray microtomography, *Polymer Testing*, 2023, 128: 108194. doi:<https://doi.org/10.1016/j.polymertesting.2023.108194>
- [177] T. Winchester, E. Kustra, I. Cormier, et al., Ballistic performance of integral body armor with closed-cell aluminum foam: A numerical study, *Forces in Mechanics*, 2023, 11: 100187. doi:<https://doi.org/10.1016/j.finmec.2023.100187>
- [178] I. Bensalem, A. Benhizia, Novel design of irregular closed-cell foams structures based on spherical particle inflation and evaluation of its compressive performance, *Thin-Walled Structures*, 2022, 181: 109991. doi:<https://doi.org/10.1016/j.tws.2022.109991>
- [179] F. Saleem, S. Li, S. Cui, et al., The strain rate and density dependence of the mechanical properties of closed-cell aluminum foam, *Materials Science and Engineering: A*, 2023, 884: 145568. doi:<https://doi.org/10.1016/j.msea.2023.145568>
- [180] M. Zhu, X. Wei, M. Zhang, et al., Adsorption characteristics of amphiphilic open-cell poly(butylene succinate) foams with ultrahigh porosity, *The Journal of Supercritical Fluids*, 2023,

200: 106002. doi:<https://doi.org/10.1016/j.supflu.2023.106002>

[181] J. Ru, B. Kong, Y. Liu, et al., Microstructure and sound absorption of porous copper prepared by resin curing and foaming method, *Materials Letters*, 2015, 139: 318-321.

doi:<https://doi.org/10.1016/j.matlet.2014.09.084>

[182] M.A. Navacerrada, P. Fernández, C. Díaz, et al., Thermal and acoustic properties of aluminium foams manufactured by the infiltration process, *Applied Acoustics*, 2013, 74(4): 496-

501. doi:<https://doi.org/10.1016/j.apacoust.2012.10.006>

[183] K. Huang, D. Yang, S. He, et al., Acoustic absorption properties of open-cell Al alloy foams with graded pore size, *Journal of Physics, D. Applied Physics: A Europhysics Journal*, 2011,

44(36): 365405-1-365405-6. doi:10.1088/0022-3727/44/36/365405

[184] X. Yu, Z. Lu, W. Zhai, Enhancing the flow resistance and sound absorption of open-cell metallic foams by creating partially-open windows, *Acta Materialia*, 2021, 206: 116666.

doi:<https://doi.org/10.1016/j.actamat.2021.116666>

[185] W. Zhai, X. Yu, X. Song, et al., Microstructure-based experimental and numerical investigations on the sound absorption property of open-cell metallic foams manufactured by a template replication technique, *Materials & Design*, 2018, 137: 108-116.

doi:<https://doi.org/10.1016/j.matdes.2017.10.016>

[186] J. Lee, I. Jung, Tuning sound absorbing properties of open cell polyurethane foam by impregnating graphene oxide, *Applied Acoustics*, 2019, 151: 10-21.

doi:<https://doi.org/10.1016/j.apacoust.2019.02.029>

[187] X.H. Yang, S.W. Ren, W.B. Wang, et al., A simplistic unit cell model for sound absorption of cellular foams with fully/semi-open cells, *Composites Science and Technology*, 2015, 118:

276-283. doi:<https://doi.org/10.1016/j.compscitech.2015.09.009>

[188] Y. Ren, K. Wang, B. Zhu, et al., Synthesis of ZnO micro-rods on the cell walls of open celled Al foam and their effect on the sound absorption behavior, *Materials Letters*, 2013, 91: 242-244. doi:<https://doi.org/10.1016/j.matlet.2012.10.012>

[189] Y. Li, Z. Li, F. Han, Air Flow Resistance and Sound Absorption Behavior of Open-celled Aluminum Foams with Spherical Cells, *Procedia Materials Science*, 2014, 4: 187-190. doi:<https://doi.org/10.1016/j.mspro.2014.07.591>

[190] J.A. Liu, W.B. Sun, Z.B. Zheng, et al., Enhancing compressive properties and sound absorption characteristic of open-cell Mg foams through plasma electrolytic oxidation treatment, *Journal of Materials Research and Technology*, 2023, 25: 1263-1272. doi:<https://doi.org/10.1016/j.jmrt.2023.05.210>

[191] Y. Ren, Z. Li, F. Han, Synthesis of Co₃O₄ Micro-needles on the Cell Walls and their Effect on the Sound Absorption Behavior of Open Cell Al Foam, *Procedia Materials Science*, 2014, 4: 191-195. doi:<https://doi.org/10.1016/j.mspro.2014.07.593>

[192] D.P. Papadopoulos, I.C. Konstantinidis, N. Papanastasiou, et al., Mechanical properties of Al metal foams, *Materials Letters*, 2004, 58(21): 2574-2578. doi:<https://doi.org/10.1016/j.matlet.2004.03.004>

[193] M.F. Ashby, A. Evans, N.A. Fleck, et al., *Metal foams: a design guide*: Butterworth-Heinemann, Oxford, UK, ISBN 0-7506-7219-6, Published 2000, Hardback, 251 pp., \$75.00, *Materials & Design*, 2002, 23(1): 119. doi:[https://doi.org/10.1016/S0261-3069\(01\)00049-8](https://doi.org/10.1016/S0261-3069(01)00049-8)

[194] M. Ercelik, M.S. Ismail, K.J. Hughes, et al., X-ray CT-based numerical investigation of nickel foam-based GDLs under compression, *International Journal of Hydrogen Energy*, 2023.

doi:<https://doi.org/10.1016/j.ijhydene.2023.07.001>

[195] C. Betts, D. Balint, J. Lin, In-situ Micro-tensile Testing and X-ray Micro-tomography based FE Modeling of Open-cell Metal Foam Struts and Sandwich Panels, *Procedia Materials Science*, 2014, 4: 197-202. doi:<https://doi.org/10.1016/j.mspro.2014.07.595>

[196] T. Xiao, L. Lu, W. Peng, et al., Numerical study of heat transfer and load-bearing performances of corrugated sandwich structure with open-cell metal foam, *International Journal of Heat and Mass Transfer*, 2023, 215: 124517. doi:<https://doi.org/10.1016/j.ijheatmasstransfer.2023.124517>

[197] D. Zhao, K.E. Matheson, B.R. Phung, et al., Investigating the effect of grain structure on compressive response of open-cell metal foam using high-fidelity crystal-plasticity modeling, *Materials Science and Engineering: A*, 2021, 812: 140847. doi:<https://doi.org/10.1016/j.msea.2021.140847>

[198] A. Jung, A.D. Pullen, W.G. Proud, Strain-rate effects in Ni/Al composite metal foams from quasi-static to low-velocity impact behaviour, *Composites Part A: Applied Science and Manufacturing*, 2016, 85: 1-11. doi:<https://doi.org/10.1016/j.compositesa.2016.02.031>

[199] ISO 11654 Acoustics - Sound absorbers for use in buildings - Rating of sound absorption; Geneva, Switzerland : ISO,1997.

[200] Y. Zhao, H. Min, N. Rong, Random incidence sound absorption of micro-perforated panel absorbers backed with parallel-arranged cavities of different depths, *Applied Acoustics*, 2024, 222: 110064. doi:<https://doi.org/10.1016/j.apacoust.2024.110064>

[201] M. Zheng, C. Chen, X. Li, Ultra-broadband and nonlinear robust sound absorption based on ultra-microperforated panel, *Journal of Sound and Vibration*, 2024, 575: 118262.

doi:<https://doi.org/10.1016/j.jsv.2024.118262>

[202] H. Gao, H. Liu, L. Liao, et al., A bifunctional hierarchical porous kaolinite geopolymer with good performance in thermal and sound insulation, *Construction and Building Materials*, 2020, 251: 118888. doi:<https://doi.org/10.1016/j.conbuildmat.2020.118888>

[203] Z.-J. Nie, J.-X. Wang, C.-Y. Huang, et al., Hierarchically and wood-like cyclodextrin aerogels with enhanced thermal insulation and wide spectrum acoustic absorption, *Chemical Engineering Journal*, 2022, 446: 137280. doi:<https://doi.org/10.1016/j.cej.2022.137280>

[204] Z. Wang, Y. Huang, X. Zhang, et al., Broadband underwater sound absorbing structure with gradient cavity shaped polyurethane composite array supported by carbon fiber honeycomb, *Journal of Sound and Vibration*, 2020, 479. doi:<https://doi.org/10.1016/j.jsv.2020.115375>

[205] G. Bezançon, O. Doutres, O. Umnova, et al., Thin metamaterial using acoustic black hole profiles for broadband sound absorption, *Applied Acoustics*, 2024, 216: 109744. doi:<https://doi.org/10.1016/j.apacoust.2023.109744>

[206] H. Zhang, P. Hao, H. Wu, et al., Sound absorbing properties of spiral metasurfaces inspired by micro-perforated plates, *Theoretical and Applied Mechanics Letters*, 2023, 13(3): 100437. doi:<https://doi.org/10.1016/j.taml.2023.100437>

[207] ISO 10534-1. Acoustics. Determination of sound absorption coefficient and impedance in impedance tubes. Part 1: Method using standing wave ratio; Geneva, Switzerland : ISO,1996.

[208] M.E. Delany, E.N. Bazley, Acoustical properties of fibrous absorbent materials, *Applied Acoustics*, 1970, 3(2): 105-116. doi:[https://doi.org/10.1016/0003-682X\(70\)90031-9](https://doi.org/10.1016/0003-682X(70)90031-9)

[209] I.B. Crandall, *Theory of vibrating systems and sound*. Van Nostrand, 1926.

[210] X. Olny, C. Boutin, Acoustic wave propagation in double porosity media, *The Journal of*

- the Acoustical Society of America, 2003, 114: 73-89. doi:<https://doi.org/10.1121/1.1534607>
- [211] D.A. Bies, C.H. Hansen, Flow resistance information for acoustical design, *Applied Acoustics*, 1980, 13(5): 357-391. doi:[https://doi.org/10.1016/0003-682X\(80\)90002-X](https://doi.org/10.1016/0003-682X(80)90002-X)
- [212] D. Mousanezhad, S. Kamrava, A. Vaziri, Origami-based Building Blocks for Modular Construction of Foldable Structures, *Scientific Reports*, 2017, 7(1): 14792. doi:10.1038/s41598-017-13654-z
- [213] Q. Ma, R. Rejab, J. Siregar, et al., A review of the recent trends on core structures and impact response of sandwich panels, *Journal of Composite Materials*, 2021, 55. doi:10.1177/0021998321990734
- [214] Y. Du, C. Song, J. Xiong, et al., Fabrication and mechanical behaviors of carbon fiber reinforced composite foldcore based on curved-crease origami, *Composites Science and Technology*, 2019, 174: 94-105. doi:<https://doi.org/10.1016/j.compscitech.2019.02.019>
- [215] X. Jin, H. Fang, X. Yu, et al., Reconfigurable origami-inspired window for tunable noise reduction and air ventilation, *Building and Environment*, 2023, 227: 109802. doi:<https://doi.org/10.1016/j.buildenv.2022.109802>
- [216] J.C. Ji, Q. Luo, K. Ye, Vibration control based metamaterials and origami structures: A state-of-the-art review, *Mechanical Systems and Signal Processing*, 2021, 161: 107945. doi:<https://doi.org/10.1016/j.ymsp.2021.107945>
- [217] H. Han, V. Sorokin, L. Tang, et al., Origami-based tunable mechanical memory metamaterial for vibration attenuation, *Mechanical Systems and Signal Processing*, 2023, 188: 110033. doi:<https://doi.org/10.1016/j.ymsp.2022.110033>
- [218] T. Jiang, Q. Han, C. Li, Topologically tunable local-resonant origami metamaterials for

wave transmission and impact mitigation, *Journal of Sound and Vibration*, 2023, 548: 117548.

doi:<https://doi.org/10.1016/j.jsv.2022.117548>

[219] P.P. Pratapa, P. Suryanarayana, G.H. Paulino, Bloch wave framework for structures with nonlocal interactions: Application to the design of origami acoustic metamaterials, *Journal of the Mechanics and Physics of Solids*, 2018, 118: 115-132.

doi:<https://doi.org/10.1016/j.jmps.2018.05.012>

[220] M. Wan, K. Yu, J. Gu, et al., 4D printed TMP origami metamaterials with programmable mechanical properties, *International Journal of Mechanical Sciences*, 2023, 250: 108275.

doi:<https://doi.org/10.1016/j.ijmecsci.2023.108275>

[221] T. Cambonie, E. Gourdon, Innovative origami-based solutions for enhanced quarter-wavelength resonators, *Journal of Sound and Vibration*, 2018, 434: 379-403.

doi:<https://doi.org/10.1016/j.jsv.2018.07.029>

[222] G. Wen, S. Zhang, H. Wang, et al., Origami-based acoustic metamaterial for tunable and broadband sound attenuation, *International Journal of Mechanical Sciences*, 2023, 239: 107872.

doi:<https://doi.org/10.1016/j.ijmecsci.2022.107872>

[223] Z. Wang, S. Yao, K. Liu, et al., Origami embedded honeycomb with three-axial comparable and improved energy absorption performance, *Thin-Walled Structures*, 2023, 193: 111295.

doi:<https://doi.org/10.1016/j.tws.2023.111295>

[224] Z. Cai, X. Li, X. Gai, et al., An empirical model to predict sound absorption ability of woven fabrics, *Applied Acoustics*, 2020, 170: 107483.

doi:<https://doi.org/10.1016/j.apacoust.2020.107483>

[225] L. Tong, D. Hu, L. Chao, et al., Development of hybrid breathing materials for sustainable

composite manufacturing, *Journal of Cleaner Production*, 2021, 321: 129028.

doi:<https://doi.org/10.1016/j.jclepro.2021.129028>

[226] H. Ruiz, P. Cobo, F. Jacobsen, Optimization of multiple-layer microperforated panels by simulated annealing, *Applied Acoustics*, 2011, 72(10): 772-776.

doi:<https://doi.org/10.1016/j.apacoust.2011.04.010>

[227] H.-Z. Li, X.-C. Liu, Q. Liu, et al., Sound insulation performance of double membrane-type acoustic metamaterials combined with a Helmholtz resonator, *Applied Acoustics*, 2023, 205:

109297. doi:<https://doi.org/10.1016/j.apacoust.2023.109297>

[228] C. Dong, Z. Liu, R. Pierce, et al., Sound absorption performance of a micro perforated sandwich panel with honeycomb-hierarchical pore structure core, *Applied Acoustics*, 2023, 203:

109200. doi:<https://doi.org/10.1016/j.apacoust.2022.109200>

[229] Z. Yang, J. Mei, M. Yang, et al., Membrane-Type Acoustic Metamaterial with Negative Dynamic Mass, *Physical Review Letters*, 2008, 101(20): 204301.

doi:10.1103/PhysRevLett.101.204301

[230] H.H. Huang, C.T. Sun, G.L. Huang, On the negative effective mass density in acoustic metamaterials, *International Journal of Engineering Science*, 2009, 47(4): 610-617.

doi:<https://doi.org/10.1016/j.ijengsci.2008.12.007>

[231] Y. Chen, G. Huang, X. Zhou, et al., Analytical coupled vibroacoustic modeling of membrane-type acoustic metamaterials: Membrane model, *The Journal of the Acoustical Society of America*, 2014, 136(3): 969-979. doi:10.1121/1.4892870

[232] Z. Xiao, P. Gao, X. He, et al., Lightweight cellular multifunctional metamaterials with superior low-frequency sound absorption, broadband energy harvesting and high load-bearing

capacity, *Materials & Design*, 2024, 241: 112912.

doi:<https://doi.org/10.1016/j.matdes.2024.112912>

[233] Z. Li, X. Li, J.W. Chua, et al., Architected lightweight, sound-absorbing, and mechanically efficient microlattice metamaterials by digital light processing 3D printing, *Virtual and Physical Prototyping*, 2023, 18(1): e2166851. doi:<https://doi.org/10.1080/17452759.2023.2166851>

[234] X. Li, X. Yu, M. Zhao, et al., Multi-level bioinspired microlattice with broadband sound-absorption capabilities and deformation-tolerant compressive response, *Advanced Functional Materials*, 2023, 33(2): 2210160. doi:<https://doi.org/10.1002/adfm.202210160>

[235] Z.C. Eckel, C. Zhou, J.H. Martin, et al., Additive manufacturing of polymer-derived ceramics, *Science*, 2016, 351(6268): 58-62. doi:10.1126/science.aad2688

[236] T. Yu, H. Hyer, Y. Sohn, et al., Structure-property relationship in high strength and lightweight AlSi10Mg microlattices fabricated by selective laser melting, *Materials & Design*, 2019, 182: 108062. doi:<https://doi.org/10.1016/j.matdes.2019.108062>

[237] Z.P. Sun, Y.B. Guo, V.P.W. Shim, Deformation and energy absorption characteristics of additively-manufactured polymeric lattice structures — Effects of cell topology and material anisotropy, *Thin-Walled Structures*, 2021, 169: 108420. doi:<https://doi.org/10.1016/j.tws.2021.108420>

[238] J. Song, W. Zhou, Y. Wang, et al., Octet-truss cellular materials for improved mechanical properties and specific energy absorption, *Materials & Design*, 2019, 173: 107773. doi:<https://doi.org/10.1016/j.matdes.2019.107773>

[239] X. Chen, G. Yu, Z. Wang, et al., Enhancing out-of-plane compressive performance of carbon fiber composite honeycombs, *Composite Structures*, 2021, 255: 112984.

doi:<https://doi.org/10.1016/j.compstruct.2020.112984>

[240] A. Aldoshan, S. Khanna, Effect of relative density on the dynamic compressive behavior of carbon nanotube reinforced aluminum foam, *Materials Science and Engineering: A*, 2017, 689: 17-24. doi:<https://doi.org/10.1016/j.msea.2017.01.100>

[241] X. Zhang, J. Yao, B. Liu, et al., Three-Dimensional High-Entropy Alloy–Polymer Composite Nanolattices That Overcome the Strength–Recoverability Trade-off, *Nano Letters*, 2018, 18(7): 4247-4256. doi:10.1021/acs.nanolett.8b01241

[242] L.R. Meza, S. Das, J.R. Greer, Strong, lightweight, and recoverable three-dimensional ceramic nanolattices, *Science*, 2014, 345(6202): 1322-1326. doi:doi:10.1126/science.1255908

[243] J. Mueller, J.R. Rane, K. Shea, et al., Architected Lattices with High Stiffness and Toughness via Multicore–Shell 3D Printing, *Advanced Materials*, 2018, 30(12): 1705001. doi:<https://doi.org/10.1002/adma.201705001>

[244] B.G. Compton, J.A. Lewis, 3D-printing of lightweight cellular composites, *Advanced materials*, 2014, 26(34): 5930-5935. doi:10.1002/adma.201401804